Politecnico di Torino

POLITECNICO DI TORINO

Department of Mechanical and Aerospace Engineering (DIMEAS)

Master's Degree in Biomedical Engineering

Master's Thesis

Design optimization for improved usability in a passive upper limb exoskeleton for industrial use based on Pneumatic Artificial Muscles

Supervisors:
Dr. Carlo de Benedictis
Prof. Carlo Ferraresi
Dr. Maria Paterna

Candidate:
Simona Gatto

A.Y. 2024/2025

Abstract

In the industrial field, overhead works are one of the leading causes of Work-related Musculoskeletal Disorders (WMSDs). These disorders not only pose a significant health risk to workers but, also, negatively impact industrial productivity. It has been observed that, in Europe, absenteeism rates in industries caused by WMSDs, exceed those due to the influenza virus. Both these aspects, in view of the advancements of Industry 4.0, represent an issue to which a solution must be found to ensure greater workers safety. A promising solution to mitigate these risks is provided by exoskeletons for industrial use, which are electromechanical devices worn by operators and designed around the shape and function of the human body. Their purpose is to assist workers by enhancing operational capacity and reducing physical effort. Since these devices must be worn in direct contact with the user, their development leads to significant challenges. Specifically, they must guarantee, first and foremost, the safety and comfort of the user, while simultaneously assisting movement without restricting it but rather supporting the worker during occupational tasks. In this scenario, passive exoskeletons for upper limbs come into play.

In particular, the prototype analysed in this master's thesis is a passive exoskeleton for industrial applications, which employs two Pneumatic Artificial Muscles, specifically two McKibben Muscles (MKMs), as energy storage elements. The particularity in the functioning of MKMs is linked to their ability to generate tensile forces when pressurized, which closely resemble the behavior of natural muscles. The exoskeleton under consideration operates by generating a support torque that counteracts the gravitational one; the latter is generated by both the load of the user's arm and by the presence of any additional tool in its hands. This mechanism leads to a reduction in load magnitude at the shoulder joint level and, consequently, to a lower incidence of injuries.

First, an evaluation has been conducted to assess the progress and the significant advancements made in exoskeleton technology over the past few decades, and then, the principles governing the operation of PAMs have been explained. Subsequently, the focus shifted to the core objective of the thesis, namely, to optimize and improve usability and efficiency of a former exoskeleton prototype. To this end, the prototype has been analysed, highlighting the adjustments made to the components with the aim of improving and optimizing the structure's usability. The structural behavior of the

exoskeleton, both in terms of stresses and displacements, has been tested, using Finite Element Methods, to evaluate its performance under typical working conditions. Ultimately, supplementary analyses have been conducted to estimate the entity of the loads exerted on the subject during the functioning of the device.

Table of Contents

List of Figures

List of Figures

List of Tables

Chapter 1

Introduction

Human performances are limited due to maximum muscle forces and the accumulation of fatigue, which results in a decrease in the ability to exert maximal force due to exercise. In the case of repeated daily exertion, degenerative processes can occur, and they could cause pain. This issue is relevant in the industrial environment where such exertions are frequent, in fact, it is possible to speak about Work-related Musculoskeletal Disorders (WMSDs). In fact, with the development of industrial science and technology forced posture movements of low-load, rapid rhythms and high repetition for long duration have become a primary feature of modern industry. Musculoskeletal imbalance emerges when fatigue outruns the worker's recovery system, which is followed by musculoskeletal disorders. Especially, overhead work is one of the major causes of musculoskeletal disorders [1][2][3]. An epidemiological study conducted in China has shown that one of the most common sites for WMSDs among workers is the shoulder [4]. Another study, also carried out in China, by Liang et al. [5], has analyzed the prevalence and severity of shoulder WMSDs in various industries. The study showed that, among the participants, about 35.5% felt the presence of WMSDs in the shoulder, and in some areas this percentage even reached peaks of 50%.

This issue not only represents a significant health risk for workers but, it is also critical for companies themselves. In fact, a study conducted by Liberty Mutual Insurance found that work-related musculoskeletal disorders are the most common and expensive type of injuries in the United States, with an economic impact of up to $2 billion per year in workers' compensation costs in the construction industry [6]. Similarly, in European industries, it has been estimated that work absenteeism is reported in more than 50% of employees affected by WMSDs, which is significantly higher than in workers infected by the influenza virus (10-12%). Furthermore, employees suffering from WMSDs are also absent from work for a longer period compared to workers with other health problems

[7]. With the purpose of limiting the risks, the National Institute for Occupational Safety and Health (NIOSH) recommends limits to prevent muscle fatigue, but an innovative resource to help workers is provided by exoskeletons.

Exoskeletons are electromechanical devices worn by operators and designed around the shape and function of the human body. They have a wide range of applications, and their specific role depends on the context in which they are used. Exoskeletons can work like *extenders*, amplifying the force of humans to improve physical performances such as increasing load-bearing capacity, reducing metabolic expenditure or enhancing the ability to run at higher speeds or for longer distances [8],[9]. These features of exoskeletons are, for example, mainly used in the military or even in the occupational sector. Also, they can be used in the rehabilitation sector with the purpose of assisting or correcting the patients' movements.

Exoskeletons can be used at the level of the upper limbs, at the level of the lower limbs or can also be full body, with the aim of reproducing or improving the behavior of the anatomical structure involved. The full-body class refers to the exoskeletons made to assist all the limbs, or most of the body. The upper body refers to the exoskeletons made for the upper limbs, and involving the chest, head, back, and/or shoulders. The lower body category refers to the exoskeletons made for the lower limbs: thighs, lower legs, and/or hips [10]. Exoskeletons are not only designed for full, upper or lower body, but can be also designed for specific body parts, for example, for specific joints. The percentages of diffusion for each exoskeleton type are shown in Fig.1 [10].

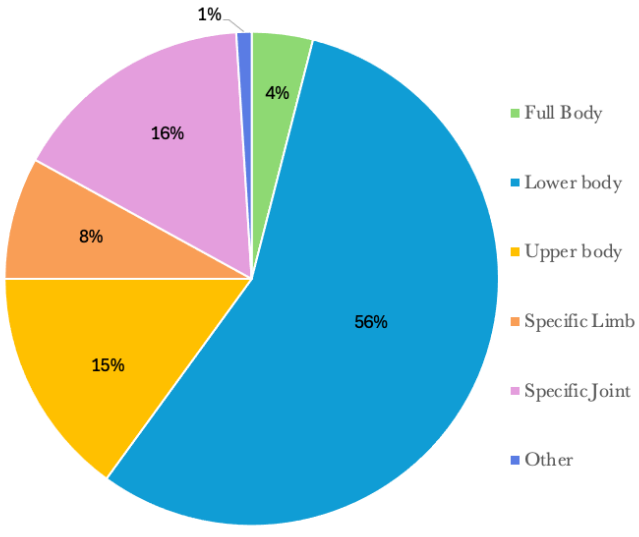

Figure 1: Exoskeleton Distribution by Body Area. Adapted from [10]

As shown in Fig.1, the lower body exoskeletons are the most widespread, with the 56% frequency, since are designed to help users with motility's problems that mostly occur in

the lower body. Nevertheless, upper body exoskeletons are used in many application areas and are imperative in the exoskeleton field [10].
Upper limb exoskeletons are generally anthropomorphic in nature and find application in industry, compensation of neuromuscular injuries, post-stroke rehabilitation, or for supporting disabled people in daily life [11] [12] [13] [14].
Regarding full body exoskeletons, however, their development has been limited due to the complexities in their design mechanical integration intricacies, and heavier weight. Full-body exoskeletons are usually used to amplify man's strength and are used, for example, to transfer most of the force the user would be subjected to the structure in order to increase the individual's natural capabilities [15].
An exoskeleton is required to replicate the kinematics and dynamics of human musculoskeletal structure and to thus support the limb's motion [16] which is challenging with the existing mechanisms and mode of actuation.
In the design phase of a limb exoskeleton, it is necessary to focus on the anatomy and the dynamics of the structure under consideration, as well as to assess the objective for which the exoskeleton will be employed.

1.1. Upper Limb Anatomy

The upper limb allows a wide range of movements to interact with the surrounding environment. The three most important joints are: shoulder, elbow and wrist.

1.1.1. Shoulder complex

The shoulder joint is the most complex joint of the human body because it includes five separate articulations: the sternoclavicular joint, the acromioclavicular joint, the coracoclavicular joint, the scapulothoracic joint and the glenohumeral joint. [17].

The Sternoclavicular joint, Fig.2, is a saddle-type synovial joint that links the clavicle with the trunk, specifically is constituted by the proximal end of the clavicle that articulates with the clavicular notch of the manubrium of the sternum. A fibrocartilaginous articular disc improves the fit of the articulating bone surfaces and serves as a shock absorber. The SC joint provides the major axis of rotation for movements of the clavicle and scapula. It allows several movements such as elevation/depression of the shoulder, protraction/retraction of the shoulder through

moving the shoulder girdle anteriorly and posteriorly and, also, rotation when the arm is raised over the head [17].

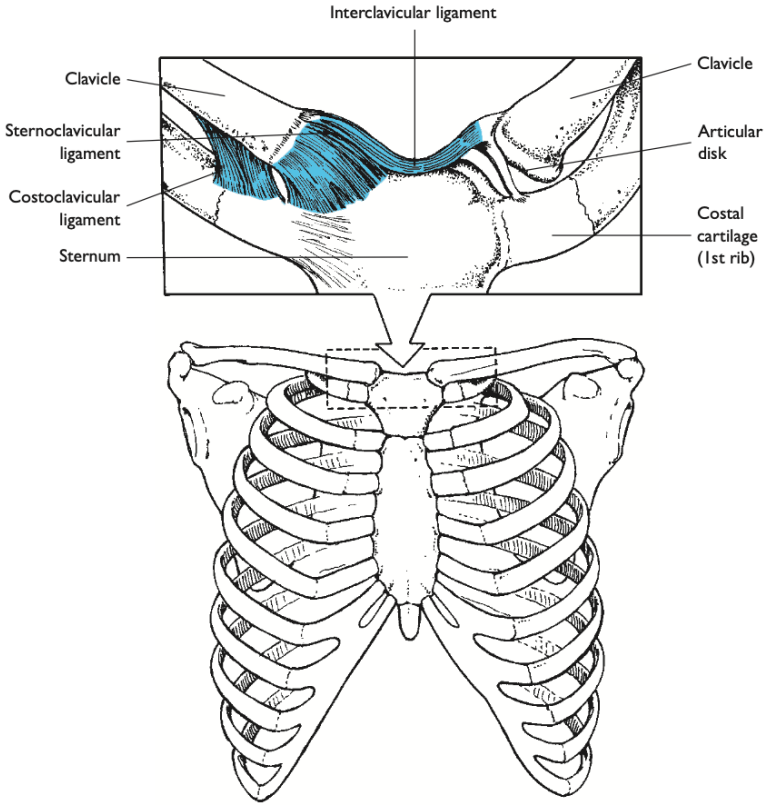

Figure 2: Sternoclavicular joint [17]

The Acromioclavicular joint, Fig.3, is the articulation between the clavicle and the acromion of the scapula. Particularly, it consists of the acromion process of the scapula and the distal end of the clavicle. It is classified as an irregular diarthrodial, although its structure permits limited movement in all three planes. It allows a gliding movement in the superior/inferior and anteroposterior planes, along with a small amount of axial rotation. The close-packed position of the acromioclavicular joint occurs when the humerus is abducted to 90° [17].

The Coracoclavicular joint, Fig.3, is a syndesmosis, which is a particular type of joint in which the joint cavity and the covering cartilage are missing, while the bone segments, which may be spaced apart, are held together by a membrane or ligaments. It is formed by the coracoid process of the scapula and the conoid tubercle of the clavicle that are bound together by the coracoclavicular ligament.
However, in some individuals the joint is more complete, and it presents a capsule and an articular cartilage [18].

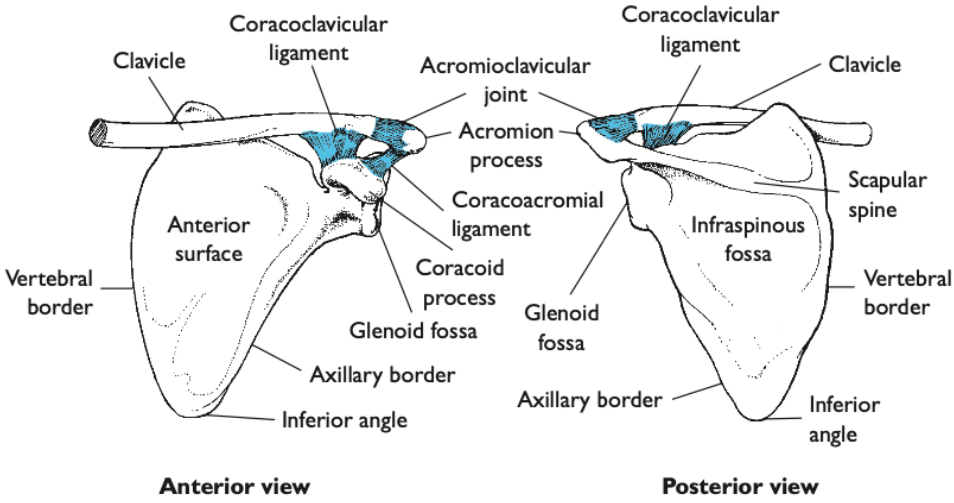

Figure 3: The acromioclavicular and coracoclavicular joint [17]

The Scapulothoracic joint includes the area between the anterior scapula and the thoracic wall. This is not usually considered as a true anatomic joint since it has none of the usual joint characteristics (union by fibrous, cartilaginous, or synovial tissues), in fact, is considered as a unit that collects the sternoclavicular and the acromioclavicular joints. The scapula can move both in sagittal and frontal planes with respect to the trunk and the muscles attaching to the scapula perform two functions: the first one is linked to the stabilization of the shoulder and the second one is associated with facilitating movements of the upper extremity through appropriate positioning of the glenohumeral joint. The movements within the scapulothoracic junction are described by three degrees of freedom; elevation-depression, protraction-retraction, external rotation-internal rotation.

The Glenohumeral joint, Fig.4, is a ball-and-socket joint that is located between the head of the humerus and the glenoid fossa of the scapula. It is reinforced by a wide range of ligaments, such as the glenohumeral, coracohumeral and coracoacromial ligaments, and rotator cuff muscles [19][20]. It is the most freely movable joint in the human body because the head of the humerus has three to four times the amount of surface area as the shallow glenoid fossa of the scapula, with which it articulates. The glenoid fossa is also less curved than the surface of the humeral head, enabling the humerus to move linearly across the surface of the glenoid fossa in addition to its extensive rotational capability [17]. Since it is a highly mobile structure, it needs to be stabilised by means of ligaments and tendons particularly the rotator cuff, which stabilizes the rotation of the humerus.

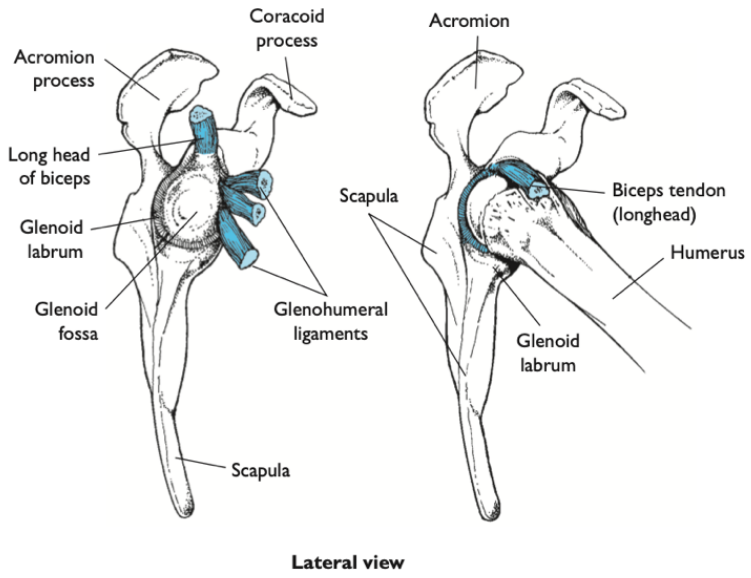

Figure 4: The glenohumeral joint [17]

The rotator cuff muscles, specifically, operate dynamically and enable the execution of a wide range of movement and, also, provide structural integrity. The movements performed by the shoulder are: abduction, adduction, flexion, extension, internal rotation and external rotation [21].

The combination of all the joints listed above forms the more complex shoulder joint, Fig.5 (a), that reflects the functioning of all the previous mentioned structures but the glenohumeral joint is typically considered the major shoulder joint [17].

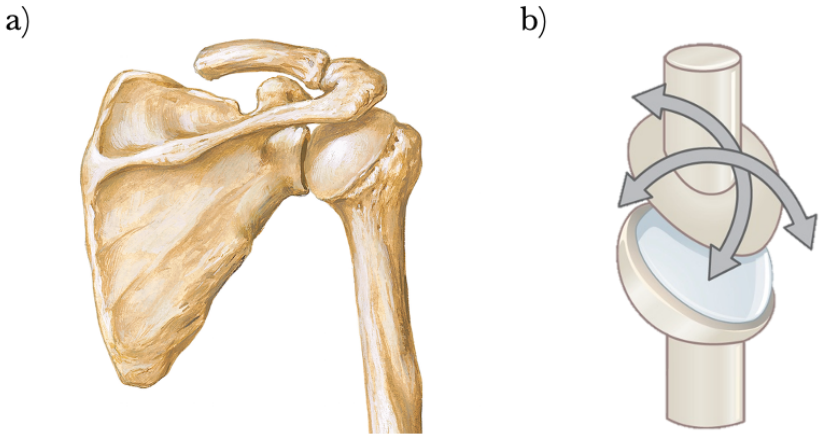

Figure 5: a) Shoulder joint posterior view [22]; b) Enarthrosis model [23]

1.1.2. The elbow joint

The elbow, Fig.6 (a), is a trochlear arthrosis and is a complex articulation consisting of two different joints: the humerus-ulnar, the humerus-radial and the proximal radioulnar joints. The radioulnar joints, in fact, are represented by the two points in which radius and ulna articulate in the forearm. These are located one near the elbow, the proximal one, and one near the wrist, the distal one and both these joints are responsible for pronation and supination of the forearm [17]. The elbow's joints are surrounded by a common joint capsule. The humeroulnar and the humeroradial joints are the ones that give the elbow its hinge characteristics since the rounded surfaces of the trochlea and capitulum of the humerus rotate against the concave surfaces of the trochlear notch of the ulna and the head of the radius. Specifically, the humeroradial joint is classified as a gliding joint bur the humeroulnar joint restricts motion to the sagittal plane, and this conjunction allows the flexion/extension movements. Stability in the frontal plane is mainly provided by the ulnar collateral ligament and the radial collateral ligament. As in the shoulder joint, the articular surfaces are covered by articular cartilage [20]. The movements performed by the elbow are flexion/extension and forearm supination/pronation.

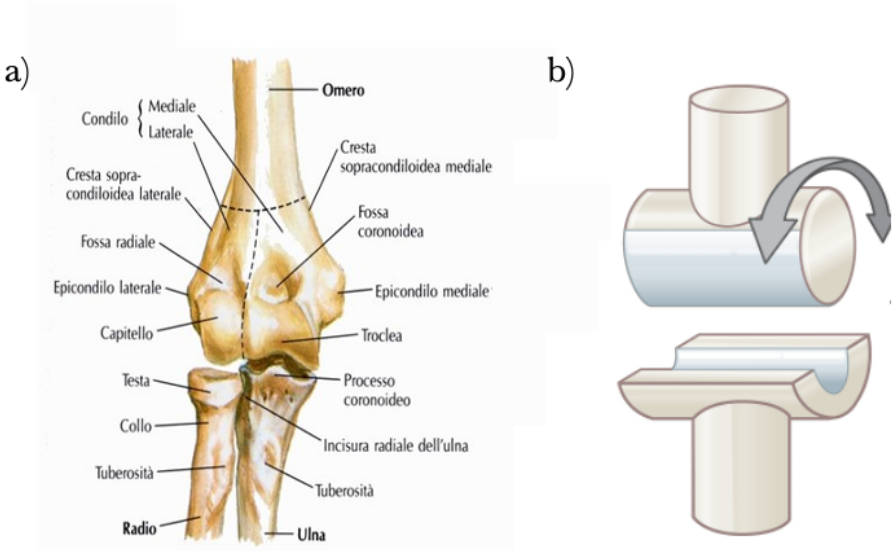

Figure 6: a) Elbow joint: front view [22]; b) Trochlear arthrosis model [23]

1.1.3. The wrist joint

The wrist, Fig.7 (a), is a synovial joint of the condylar type. The actual joint consists of ulna and radius that connect with two carpal bones, the scaphoid and lunate bone. A cartilaginous disc separates the distal head of the ulna from the lunate and triquetral bones and the radius. However, the radiocarpal joint and the distal radioulnar joint have two different joint capsules. The intercarpal joints are gliding joints that contribute little to wrist motion.
Since it is a condyloid articulation, its shape is ellipsoidal, so the wrist allows movements along the two axes and, in particular, it allows movements in sagittal plane and frontal plane. The movements that could occur are: flexion, extension, adduction and abduction [17].

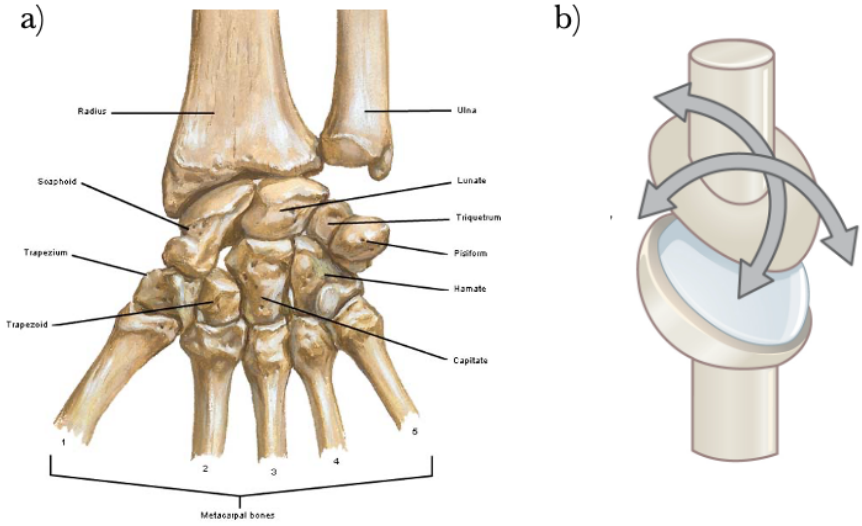

Figure 7: Wrist joint: front view [14]; b) Condyloid arthrosis model [15]

1.2. Biomechanical characterization

Proceeding with a biomechanical characterization of the above-mentioned joints, it is important to define the space in which joint movements are performed. As seen above, the shoulder, elbow and wrist joints are usually modelled respectively as: ball-and-socket joint, Fig. 5 (b), hinge joint, Fig.6 (b) and condyloid joint, Fig.7 (b).
From an anatomical point of view, three main planes are observed that are useful to describe the directions of the movements and these are: frontal, transverse and sagittal, Fig.8. Abduction and adduction movements occur in the frontal plane, flexion and

extension movements are performed in the sagittal plane while abduction, adduction, internal and external rotation occur in the transverse plane [20].

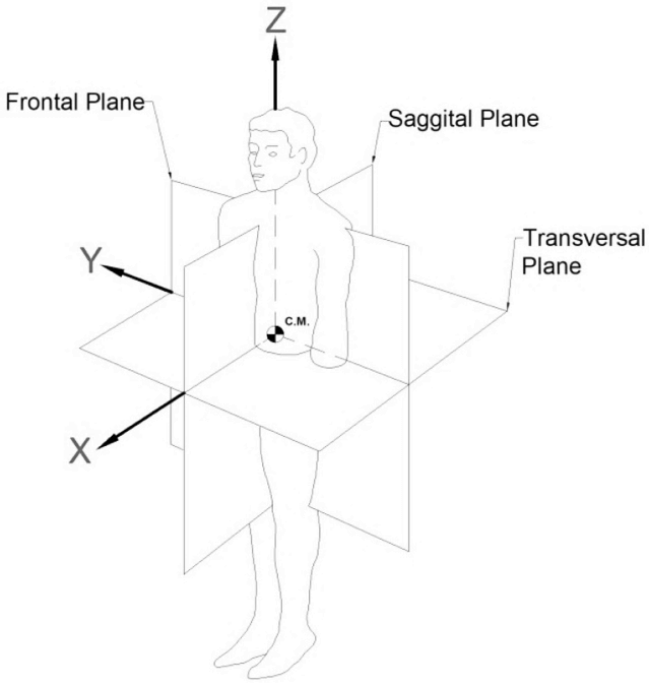

Figure 8: Anatomic coordinate planes [24]

To analyze and characterize the articulations, it is essential to identify a corresponding mechanical joint for each articulation that accurately represents the physiological movements occurring at the joints under examination. Consequently, it is crucial to associate each joint with its respective Degrees of Freedom (DOFs). Various kinematic models of the upper limb exist in the literature, differing in complexity, joint classification, and their mechanical equivalents. Each joint movement has physical limits that can be described in arcs of motion. If there is an articulation malfunctioning the arc of movement of the joint varies. The amount of movement expressed in degrees that a joint presents in each of the three planes of space is called Range of Motion (ROM) [24]. The normal and physiological ROM values, according to the Association for the Study of Osteosynthesis, for each of the joints of interest for this research are listed in Tab.1 with the relative joint movements, that are shown in Fig.9.

Table 1: ROM of upper limb joints

Articulation	Movement	Range (°)
Shoulder	Flexion	180°
	Extension	50°
	Abduction	180°
	Adduction	50°
	External Rotation	90°
	Internal Rotation	90°
Elbow	Flexion	140°
	Extension	0°-10°
	Forearm Pronation/Supination	80°
Wrist	Flexion	60°
	Extension	60°
	Radial Deviation	20°
	Ulnar Deviation	30°
	Pronation/Supination	90°

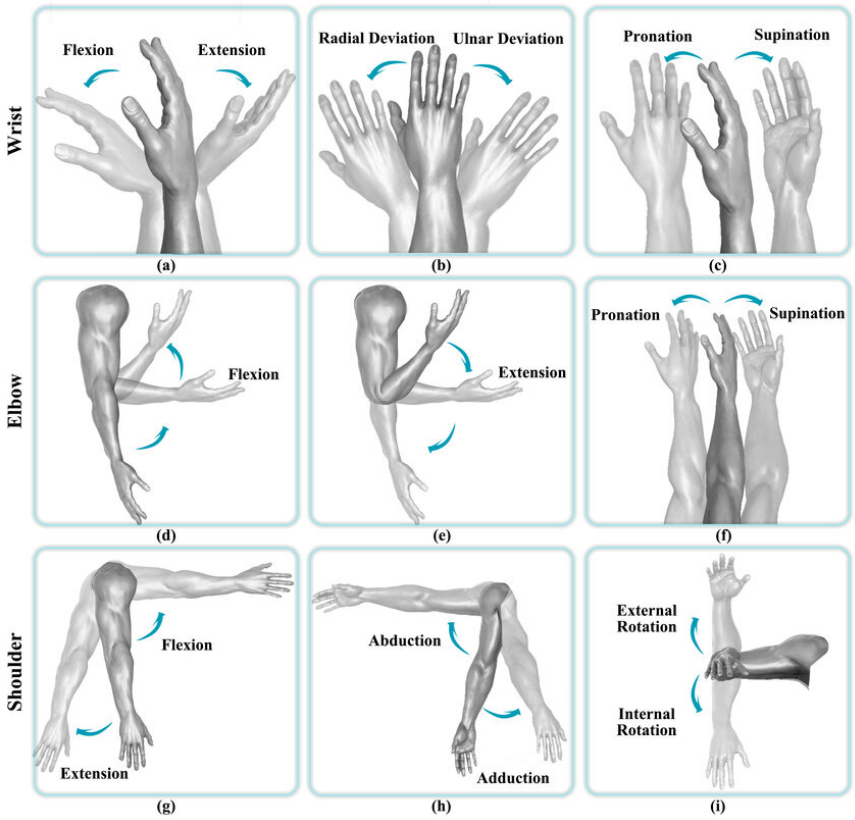

Figure 9: Upper limb movements [25]

It is important to underline that a correct modelling of the joints is essential, since it is necessary to reproduce the movements that the joints perform as accurately as possible. Therefore, understanding the movements of the anatomical articulations is crucial. When designing a structure that interacts with the joints and replicates their movements, proper alignment with the joint axes must be ensured to achieve natural redundancy [3].

1.2.1. Shoulder Joint Center (SJC)

The structure of exoskeletons resembles human arm anatomy, so the technical rotation axes must be aligned with the human rotational axes. This requirement is easier to fulfill in the case of simple joint, for example the elbow joint, but is difficult for the complex one, like the shoulder joint [26].
The shoulder, in fact, has a large ROM and, in addition, its behaviour is given by the interaction between four anatomical structures: the thorax, the scapula the humerus and the clavicle [27]. The shoulder consists of two spherical surfaces in contact, and it is characterized by a combination of large rotations and millimetric translations, due to the different radii of the contact surfaces [27][28][29]. The degree of complexity for modelling the shoulder joint depends, of course, on the specific application. In the case, however, of a structure that must be applied in contact with the human body and in which it is essential to obtain an alignment with the anatomical axes, modelling the shoulder as a ball-and-socket joint is too simplifying and could generate misalignments [26].
To produce arm elevation, the following movements must occur: the rotations of the humerus around the glenohumeral joint (GH joint), the rotation of the scapula around the acromioclavicular joint (AC joint) and the rotation of the clavicle around the sternoclavicular joint (SC joint). As consequence, the CGH-joint changes his position [26].
In general, it is complex to assess glenohumeral displacements with the majority of electromagnetic or optoelectronic instruments with skin markers. It is necessary to use intracortical instruments that, through the combined use of optoelectronic systems, have enough resolution to measure the entity of the displacements [30].
Many studies have been conducted to evaluate the displacements of the shoulder joint. Carignan et al. [31], for example, developed an empirical equation to determine the vertical displacement of the GH joint. Self-adapting device models have also been developed, for example by Li et al. [32], which can autonomously adapt to the movement of the GH joint centre.

Another model was developed by Nef and Riener [26][33], who worked on creating a general model capable of predicting the movement of the CGH joint (Center of Glenohumeral Joint), or SJC. For this research, some simplifications have been made: the individuals with the same body size do have the same CGH-joint movement pattern, the training does not influence the CGH-joint movement pattern, the subjects do the movements spontaneous and without conscious control. The aim of this study was to find the variation of the position, in x and y directions, of the CGH-joint considering different arm elevation angles (θ_1), as shown in Fig.10.

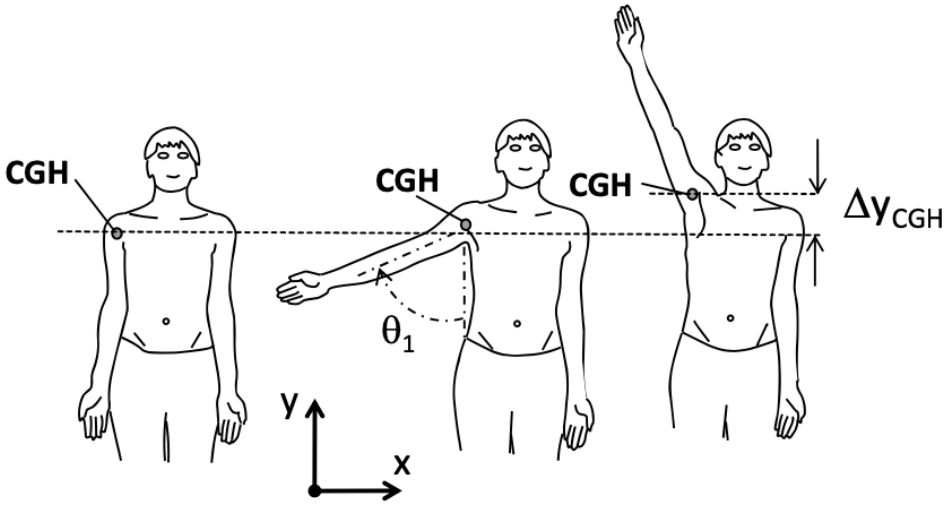

Figure 10: Location of the CGH-joint [26]

For evaluating the value of the displacement Nef and Riener, have developed a mathematical model based upon Eq.1:

$$\begin{pmatrix} x_{CGH} \\ y_{CGH} \end{pmatrix} = \begin{pmatrix} -l_c \cos(\alpha - 90) + l_s \sin(\beta + \alpha) \\ l_c \sin(\alpha - 90) + l_s \cos(\beta + \alpha) \end{pmatrix} \frac{\mathrm{h}}{\mathrm{h_{ref}}} \quad (1)$$

In which:

- l_c is the length of the clavicle;
- l_s is the distance between the centre of the acromioclavicular joint and the glenohumeral joint;
- α is the angle of the sternoclavicular joint;
- β is the angle of the acromioclavicular joint;
- h is the body size of the subject;
- h_{ref} is the body size from a recent subject.

In the specific case of the research, h_{ref} has been chosen equal to 170 cm and for this specific value the results of displacement obtained are the ones shown in Fig.11 [33].

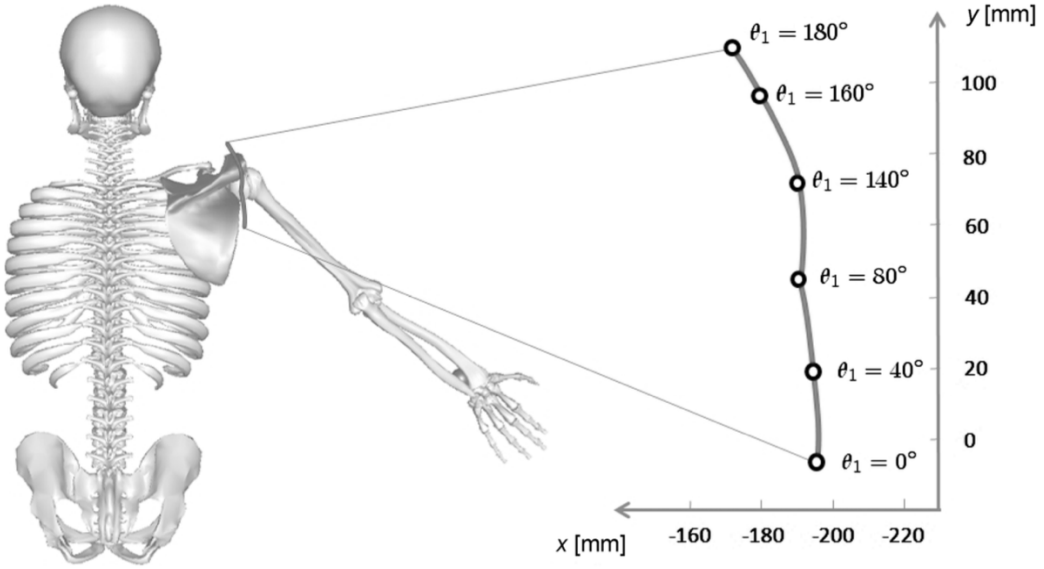

Figure 11: Results of CGH-joint displacement for a subject 170 cm tall [33]

It can be noticed that, while the entity of the x_{CGH} displacement is limited, the entity of the y_{CGH} is consistently bigger.
From these results it is therefore possible to understand that the magnitude of the CGH-joint displacement is relevant in the vertical direction in comparison to the medial one.

1.2.2. Upper Limb schematization

As previously mentioned, the modelling of the other articulations of the upper limb is certainly easier than modelling the shoulder. In biomechanical modeling of the forearm, it is typically simplified as a single segment, where the wrist and elbow are approximated as hinge joints, allowing only flexion and extension. If, however, a more detailed treatment is required, that also takes prone supination into account, then it becomes more complex to construct a model that best reproduces the anatomical reality. One model, developed by Fick, consists of two L-shaped elements connected by two spherical joints representing the humeroradial joint and the distal radioulnar joint. However, this model generates an adduction movement of the hand that is not realistic so, to solve this limitation, it was proposed to add a translational DOF between radius and ulna, at the proximal radioulnar joint [34].

The majority of models propose a schematisation of the upper limb with a number of DOF between 5 and 7. An example of a 6 DOF scheme is illustrated in Fig.12.

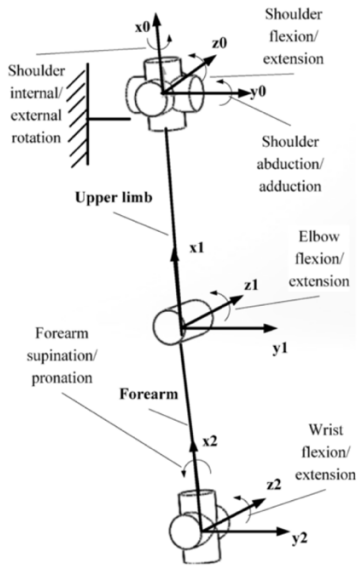

Figure 12: 6-DOF upper limb model [35]

In this model, the joints have been designed to allow, at the shoulder level, both internal/external rotation, whose axis coincides with the x-axis, the abduction/adduction mechanism, which occurs around the y-axis and, finally, the flexion/extension movement, with respect to the z-axis. At the elbow level, flexion/extension is allowed and finally at the wrist level the joint allows both flexion/extension and pronation/supination of the forearm.
Obviously, in the case of an upper limb exoskeleton, where it is essential to consider the alignment between the axes of the exoskeleton and the anatomical axes, this schematisation is not sufficiently detailed. In fact, considering what has been said before about the displacement of the shoulder centre during the arm elevation, 2 more DOF should be added at the shoulder to model the translations.

Chapter 2

Exoskeletons

2.1. History of exoskeletons - State of the Art

For the design of an exoskeleton, it is necessary to create a structure that is as biomimetic as possible. It must therefore seek to replicate the anatomical structures by adapting itself as best as possible to the field of application in which it has to be used. As shown in Fig.13, the first idea of exoskeleton date back to the 19th century when Yagn designed the first system that, connected to the body, should help the user. Specifically, it was an "apparatus to facilitate walking and running". The system was composed by springs and had a unique design to redistribute the energy given by the user while moving. Another invention was created following Yagn's principle at the beginning of the 20th century by Kelle. The structure was smaller respect to the one created by Yagn but, at the same time, more functionally limited [10].

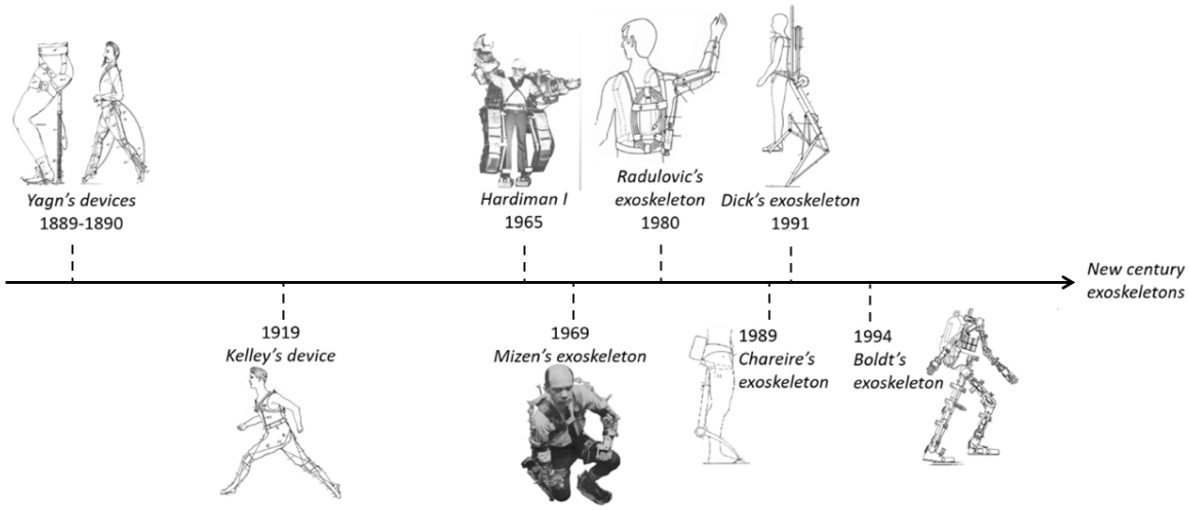

Figure 13: Evolution of exoskeletons timeline. Adapted from [10]

The first real prototype of exoskeleton called *Hardiman* only appeared in the 1960, Fig.14 (a). The latter was developed for military purposes and was powered by hydraulic actuators [36].

a)

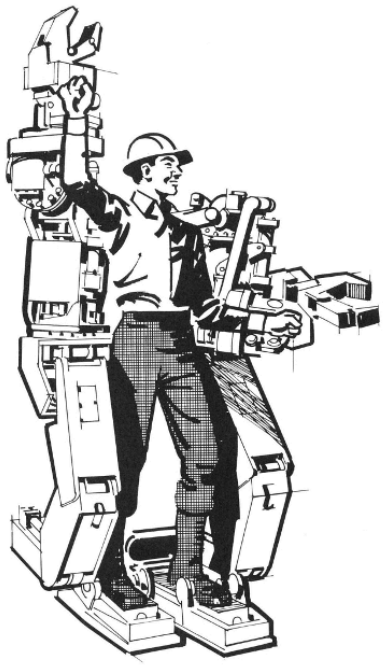

b)

SYSTEM SPECIFICATION

• Size		
	Height	72"
	Width (at hips)	39"
	Fore & Aft	29"
• Weight		1500 lbs.
• Lift Capability		1500 lbs.
• Power Requirements		
	Hydraulic	25 HP @ 3000 psi
	Electric	± 15 V D.C. - 3 amps
• Walking Speed		2.5 ft./sec.
• Reach		
	Vertical	72"
	Horizontal	36"
• Number of Joints		
	Hand (2 Joints)	Thumb Tip Flex
		Thumb Flex
	Arm (7 Joints)	Wrist Flex
		Forearm Rotate
		Elbow Flex
		Upper Arm Rotate
		Shoulder Flex
		Back Flex
		Arm Abduction - Arm Adduction
	Leg (4 Joints)	Hip Abduction - Arm Adduction
		Hip Flex
		Knee Flex
		Ankle Flex
	Foot (2 Joints)	Ankle Inversion
		Foot Rotate
	Total - 15 per side x 2 = 30 Joints	
• Type of Controls		
	Hand	Hydromechanical Rate Control with Force Feedback.
	Arm	Electrohydraulic Bilateral Servo Control. Force Feedback Ratio 25:1.
	Leg and Foot	Electrohydraulic Unilateral Servo. Indirect Force Feedback.

Figure 14: (a) Hardiman exoskeleton; (b) System specification

The prototype consisted of two structures, the inner one had to, following human movement, drive hydraulic actuators to move the outer exoskeleton. The principal utility of Hardiman was to carry heavy loads [37]. The device was never actually commercialized but always remained a prototype because the weight and the complexity were too high. The specifications of the systems are shown in Fig. 14 (b). The biggest problem with the design of Hardiman was that the hydraulic system required pumps and bladders that occupied almost a room [16].

The 60s marked a turning point in the exoskeleton development, in fact, since Hardiman's development, several prototypes have been developed in the last century.

About the new century's exoskeletons, one of the first one to be commercialised, in 2008, was HAL (Hybrid Assisted Limb), Fig.15, that was developed at the University of Tsukuba. It is a total body exoskeleton, which aim is to assist people with disabilities or to support people in industrial o sanitary field. This exoskeleton is powered by a 15 kg battery. The structure detects muscle myoelectrical signals on the skin surface below the hip and above the knee and these signals are sent to a computer which controls electric motors applied at the hips and at the knees of the exoskeleton for amplifying the muscle strength. The exoskeleton also uses potentiometers for measuring the joint angles, force

sensors for measuring the ground reaction forces and a gyroscope and accelerometer for measuring the torso angle [38].

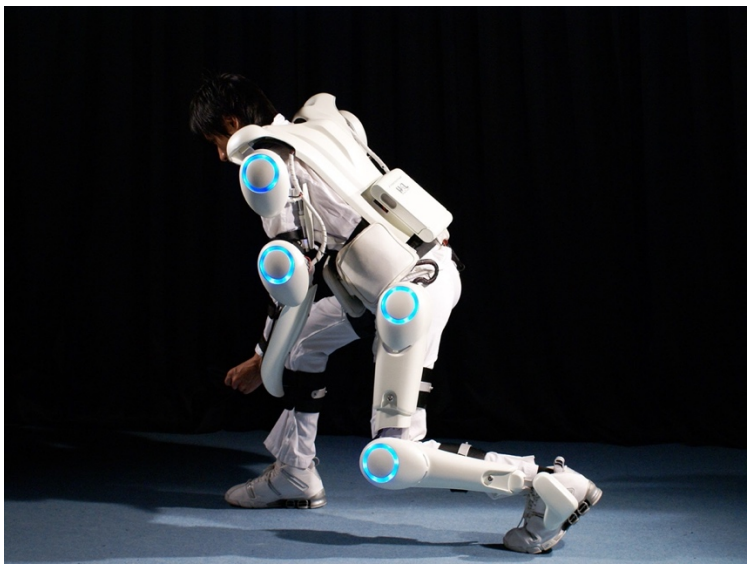

Figure 15: HAL exoskeleton

Another innovative exoskeleton that has been commercialized was the one produced by Kazerooni, which consisted of a manipulator that allows the man to extend his own force while retaining control of the action by the user. This system, unlike Hardiman, does not use a master-slave system, in fact, in this case, the user directly transmits the mechanical power, in addition to the information signals, and no actuators are needed to reflect the force back to the man. The operator therefore feels less of the load on the extender, but is still near the structure, whereas with a master-slave system, the operator could also be in a remote position. The undoubted advantage of Kazerooni's prototype is greater fluidity and smoothness of movement [39]. Thus developed one of the earliest examples of Physical Human–Robot Interaction (pHRI). The evaluation of pHRI is still one of the most relevant aspects in the design of an exoskeleton.
In particular, the interaction between man and exoskeleton is mainly influenced by three factors: the mechanisms, which are designed considering the anatomy, the actuation and transmission modes, which must consider compliance/rigidity, and finally the choice of control method, which is also relevant for pHRI [16].

2.2. Upper limb exoskeletons

The development and growth of research in the field of upper limb exoskeletons make it necessary to carry out a classification with the purpose of analyzing the main

characteristics that differentiate the various models, an example of classification is reported in Fig.16.

Upper Limb Exoskeletons	**Field of Application**	• Military • Clinical • Research • Industrial • Civilian • Other fields
	Applied Limb segment	• Shoulder • Elbow • Wrist • Hand • Finger
	Type of Actuation	• Electrical Motors • Pneumatic Actuators • Hydraulic Actuators • Shape Memory Alloy • Ultrasonic Motors
	Power Transmission Method	• Gear drives • Cable/Wire drives • Linkages • Belt drives
	Link configuration	• Serial • Parallel • Hybrid

Figure 16: Classification of exoskeleton robot systems. Adapted from[10] [40].

Also, the number of DOFs can be considered as a partitioning element, since the various exoskeletons present a different degree of complexity depending on the number of joints they support; single joint exoskeletons support a single articulation and are therefore usually simpler and lighter, while multi joint exoskeletons, as the term itself implies, support multiple articulations and therefore have a greater degree of complexity together with more advanced and often bulkier structures. The research has shown that both single and multi-joint exoskeletons have advantages, so the best choice depends on the specific application.
In the following paragraphs, the two major categories of classification, namely the fields of application and types of actuations, will be discussed in more detail.

2.2.1. Fields of Application

The fields of application for upper limb exoskeletons are extremely varied, including motion-assistance, military, medical rehabilitation, manufacturing. The main purpose of the exoskeleton depends precisely on the sector in which it will be employed; in

general, the main control strategies concern assistance, correction and resistance. Assistance is provided when the operator needs support during the performance of a strenuous action and therefore the exoskeleton must provide the necessary force to support the operator or even perform the task completely. Correction, on the other hand, is mainly provided in rehabilitation, where the exoskeleton recognizes an incorrect movement executed by the subject and must correct it, so that the patient learns the correct motion. Resistance, finally, is mainly used if the subject exhibits tremors that need to be stopped [41].

In the rehabilitation sector, exoskeletons are particularly useful for the treatment of patients with physical paralysis as a result of stroke or other diseases such as Amyotrophic Lateral Sclerosis (ALS). An example of an exoskeleton used in rehabilitation is the ALEx-RS (Arm Light Exoskeleton Rehab Station), Fig.17, by Wearable Robotics. It's a 6-degree-of-freedom exoskeleton, designed for stroke patients that allows the user a series of movements of the upper limbs that mimic natural motions thanks to a cable transmission system. Specifically, the exoskeleton consists of four active sensorised joints that allow abduction-adduction, flexion-extension, rotation of the shoulder and flexion-extension of the elbow. There are, also, two passive sensorised joints that allow forearm prone-supination and wrist flexion-extension.

Figure 17: Alex-RS exoskeleton

It also features biomarkers that allow continuous assessment of movement to track performance and customise treatment on a patient-specific basis. In addition, it is possible to set up a 'mirror' operation by which the paralyzed limb can copy the movements of the healthy limb [42]. In particular, the usefulness of Alex-RS was tested through a study conducted on 18 healthy patients and it was seen that the use of the exoskeleton increased the individuals' proprioception, where proprioception refers to the

awareness of the positions of the body segments and their respective movements in the surrounding space. From the results of the performed study, in fact, it was observed how the exoskeleton in question, and, in general, how the use of exoskeletons, can in some way help in the understanding and evaluating the proprioception of deficits, which in a clinical context, and particularly in rehabilitation, is certainly fundamental [43].
In the industrial context, exoskeletons usually aim to help the worker and thus limit Work-Related Musculoskeletal Disorders. For this reason, exoskeletons in the industrial context are aimed to support the stooped working postures, the static holding of a load and the dynamic lifting (or lowering) of a weight. Despite the growing interest in exoskeletons over the last few decades, large-scale implementation in industry is still far off because many are, even, on an experimental basis and thus prototypes in some cases have not yet been introduced to the market.
To the above, it must be added that, especially in an industrial context, the introduction of exoskeletons implies safety standards to be followed so that the worker is not exposed to risk. Despite this, even today, there are no international safety standards for the industrial application of exoskeletons, unlike those used for personal care which are regulated by the ISO13482 standard, and this represents a significant obstacle to their adoption [44].
An example of upper limb exoskeleton that has been designed for the industrial sector is the AGADEXO Shoulder, Fig.18. This exoskeleton is aimed at reducing worker fatigue during work phases. It can lift up to 10 kg, making it an important aid for the worker and a valuable ally in preventing musculoskeletal disorders. In particular, its technology is specifically promising since it has intelligent sensors that activate the device when its help is needed, thereby also reducing energy consumption [45].

Figure 18: AGADEXO Shoulder

2.2.2. Type of Actuation

A fundamental characteristic for classifying exoskeletons relates to the different types of actuation systems. Specifically, two major categories can be defined, which are active and passive exoskeletons. An active exoskeleton uses one or more actuators that augment the human's power and help in actuating the human joints. A strictly passive system does not use any type of actuator, but rather uses materials, springs or dampers with the ability to store energy harvested by human motion and to use this as required to support a posture or a motion [44]. A more accurate subdivision can be made into four different types of actuations: electric, hydraulic, pneumatic and other types of actuations.

When designing an exoskeleton, choosing the most suitable actuation system is important because there are so many variables to consider, including: power/mass ratio, power/volume ratio, stress, strain, steady-state efficiency, power consumption, bandwidth, auxiliary transmission system, auxiliary power supply equipment, and ease control procedures [46].

As can be seen in Fig. 19, most of the devices currently in use employ an electric motor as actuation. This is because they undoubtedly have advantages such as fast operation through the using of high-speed motors, high precision and great controllability. The ideal characteristics an actuator should have, for the context of use in an exoskeleton, are: reduced weight, high operating bandwidth, production of precise movements and providing a high amount of torque [3].

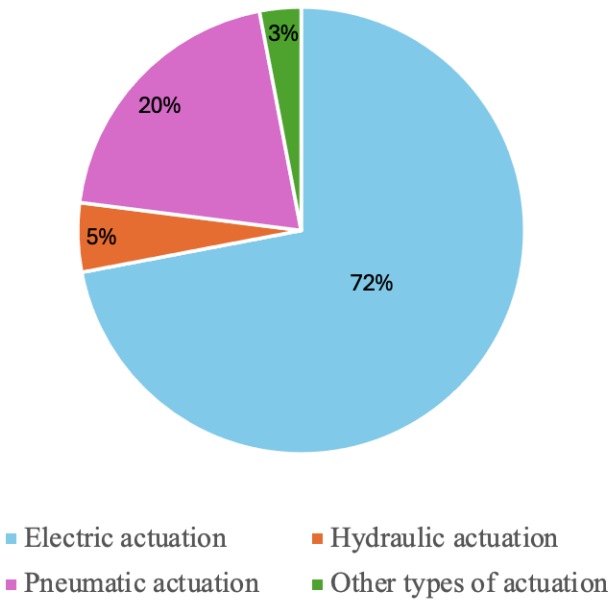

Figure 19: Usage of actuation method for upper limb exoskeleton systems. Adapted from [40].

Hydraulic actuators utilize pressurized fluid to transmit power to a joint, offering significant potential due to their ability to generate higher mechanical torque compared to electric and pneumatic actuators. However, they also present several drawbacks, such as the complexity of maintenance, needed to prevent leaks. Additionally, hydraulic systems require substantial space because of the need for a complex apparatus, including compressors and cooling systems, as well as the accommodation of pipes and oil lines. Moreover, these systems tend to be heavy and produce considerable noise [3], [46], [47].
Pneumatic actuators use pressurised air to produce an output force. For their supply, either special compressors or compressed air containers are required. Compared to hydraulic actuators, pneumatic ones are lighter and cheaper. In addition, they offer a clean, non-flammable alternative actuating device. Some of their main advantages, compared to electric actuators, are their smaller size and their lower impedances due to their inherent compliance, which softens the applied force and thus makes this type of actuator excellent for the rehabilitation field [48]. However, the biggest drawbacks are their limited precision and accuracy, but, the most important disadvantage, is that the operational bandwidth is relatively low (5 Hz) which limit the rate at which they can respond to command signals [3].
Since the presence of a flexible component is therefore a positive aspect for the exoskeleton, flexible joints have also been designed to lower the impedance of the structure and, also, improve the pHRI. These flexible joints can be either fixed compliance, called SEA (Series Elastic Actuators), or variable compliance.
SEAs reduce inertia and interface with the user to provide precise and stable force control, thereby improving the safety of the subject, but at the same time present the risk of generating unexpected reaction forces due to the release of elastic energy. Furthermore, some studies show that, due to the constant stiffness, the energy efficiency of the robotic device is generally low and can only be improved when the behaviour of the trajectory of the robotic joint matches the natural frequency of the system.
In order to overcome these limitations, in recent years, fixed compliance joints with non-linear behaviour have been developed, which allow for greater autonomy in the choice of parameters and can therefore be best adapted to specific conditions [47], [49]. In Tab.2 are schematized the features of the three most common actuation systems and, also, their advantages and disadvantages. With regard to the other types of actuations they include shape memory alloy, that use the property of nickel-titanium alloy to change shape in response to temperature, or piezoelectric motors.
Piezoelectric materials are not widely used because they are difficult to produce and rather expensive [46]. In an attempt to combine the advantages of active and passive

exoskeletons, new hybrid exoskeletons have therefore recently been developed which feature actuation technologies that combine active and passive elements.
For example, the above-mentioned AGADEXO shoulder is an example of a hybrid exoskeleton, in fact, it uses an elastic mechanism, as passive component, and an electric motor, as active component, which optimizes the device's energy consumption. At the same time, it aims to improve on the problems of active exoskeletons in terms of cost and weight.

Table 2: Features of most common actuation systems [46]

	Electric motors	*Pneumatic actuators*	*Hydraulic actuators*
Power to Weight	~1/10 hydraulics ratio	Between hydraulic and electric	Excellent
Power to Volume	~1/5 hydraulics ratio	Between hydraulic and electric	Excellent
Load Holding	Power required	No power required	No power required
Bandwidth	Very high	~1/5 hydraulics ratio	High performances in the 50 to 100 Hz
Power supply & Power consumption	Batteries	Compressor and accumulators – high power consumption	Compressor and accumulators – very high power consumption
Auxiliary system	Transmission needed	To transmit power a wide wiring is needed	To transmit power a wide wiring is needed
Noise	Silent	Noisy	Noisy
Maintenance	Un-necessary	Frequent	Frequent
Environment	Indoor/ outdoor	Indoor-supply system can be external Outdoor – supply system has to be carried	Indoor-supply system can be external Outdoor – supply system has to be carried
Use	Rehabilitation and power augmentation	Rehabilitation and power augmentation	Rehabilitation and power augmentation

2.2.3. Passive Exoskeletons

Passive exoskeletons base their functioning into the storing of human kinetic energy to transform it in mechanical energy. Later the mechanical energy will be converted back into kinetic energy for assisting the wearer [50]. Passive exoskeletons have the advantages of being much lighter than active exoskeletons as they do not need an actuator and, furthermore, are more flexible and have the possibility to work in remote locations for long hours. At the same time, however, they present the big disadvantage that their support to the human worker is limited as the required energy is harvested

through human muscles at different times. In last decades the diffusion of passive exoskeleton has particularly increased due to their ability to support various industries where workers are required to perform tasks with their upper limbs, such as production lines, masonry, carpentry, and fruit or vegetable harvesting. Passive shoulder exoskeletons, in particular, are frequently designed to assist with overhead tasks by compensating for gravitational forces [51]. The typical structure of a passive exoskeleton is made of a rigid frame, usually aluminum or carbon fiber and a passive element like an elastic fabric material or a spring damper system that has the role of providing the assistive force [51].

Another advantage that makes the use of passive exoskeletons easier than the use of active exoskeletons is linked to the maintenance. This aspect has not been particularly investigated in literature but since passive exoskeletons use simple mechanical elements certainly have more advantages than active ones.

Due to the many advantages previously mentioned passive upper arm exoskeletons have often been tested in industrial environment, and it has been observed that their use is linked to a potential efficiency [52]. Particularly, the research conducted by Hyun et al., [53], has highlighted the requirements for an upper exoskeleton in industrial field that are:

- to allow a range of movement of the upper arm as large as possible to not impeding the worker's shoulder range of motion;
- to not use an external power source so as to design a passive upper arm exoskeleton since it is difficult to manage regular battery replacement;
- to choose light materials so as the device not to be burdensome for workers' bodies
- to guarantee endurance, robustness and maintainability for long term usage.

Following these requirements Hyun et al. developed a passive upper limb exoskeleton, Hyundai Vest Exoskeleton (H-VEX), which functioning is linked to a multi-linkage based spring-energy dissipation mechanism, shown in Fig. 20. This mechanism allows the generation of an assistive torque dissipated by spring-energy according to the elevation angle of the exoskeletal upper arm. The spring energy is generated during arm lowering, involving an increase of Ls , while is dissipated during arm elevating which involves a decreasing of L_s .

In this way, when the upper limb is in a resting position there is no assistive torque, but when the user has to flex the shoulder and thus raise the arm, the support torque is increased. If, on the other hand, the user has to extend the shoulder and thus lower the

limb, the support torque decreases because the user will be facilitated in performing the operation by the gravitational torque [53].

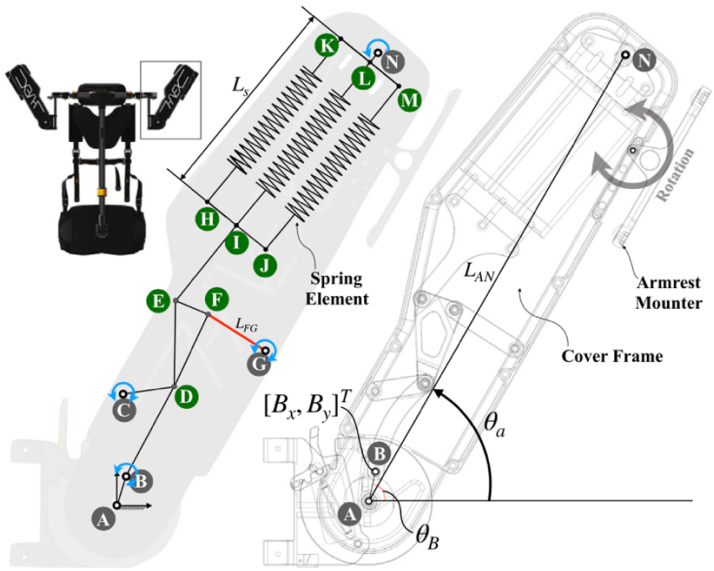

Figure 20: H-VEX functioning mechanism [53]

The H-VEX can be worn like a backpack since it presents shoulder and waist strip and, also, the weight is equal to 2.5kg that is way lower in comparison with other products developed for similar purposes [53].

2.3. Pneumatic Artificial Muscles

As mentioned earlier, pneumatic actuators are an important resource due to their low weight and high compliance characteristics. This makes them excellent candidates for use in industry. In particular, their high compliance permits smooth movements, unlike other types of actuators, since their compliance can be easily controlled by modulating the operating pressure.

All these characteristics make them perfectly suitable for use in the field of exoskeletons, because they facilitate human-machine interactions. The types of pneumatic actuators are disparate including cylinders, bellows, pneumatic motors and also Pneumatic Artificial Muscles (PAMs). The latter have an inverse function to the more classic bellows in that, unlike the former, they tend to contract when inflated. In particular, the force they exert depends not only on the pressures but also on the inflated state they are in, hence their behavior is similar to the one of springs. They have a very low weight due to the fact that the external structure is made of a membrane, but despite this they still

manage to produce the same energy as a cylinder since they operate at the same pressures and volumes [54].

The first prototype of artificial muscles dates back to 1930, the year in which Garasiev, a Russian inventor, first proposed fluidic artificial muscles whose operation was based on various liquid-based actuators. They had elastic behaviour but used a liquid and not a gas because it was easier to control since it was incompressible and had less hysteresis than simple compressed air. Instead, the most widely used artificial pneumatic muscle models currently in use, which exploit McKibben's model, were developed around twenty years later [55]. In 1950s, the American physicist J.L. McKibben developed the first artificial pneumatic muscle used in orthotic appliances for polio patients. They are made of a long tube of synthetic or natural rubber that is wrapped in an artificial net, such as Kevlar, which can be angled at various predetermined angles. The rubber coating surrounds the fibers and protects them, and, in addition, the two ends are secured with metal fittings that allow the transfer of mechanical power to the load. In fact, the PAM when pressurised to predetermined pressure levels, converts pneumatic power into a traction force. This occurs because when compressed air is insufflated inside the PAM it tends to expand radially, with a consequent axial contraction, resulting in a decrease in length, while when the air is forced out of the tube it behaves elastically and regains its original shape. The schematization of the phases of functioning is shown in Fig.21. The forces generated by this type of actuator are not linear with respect to contraction (stroke) and motions are unidirectional [54], [56].

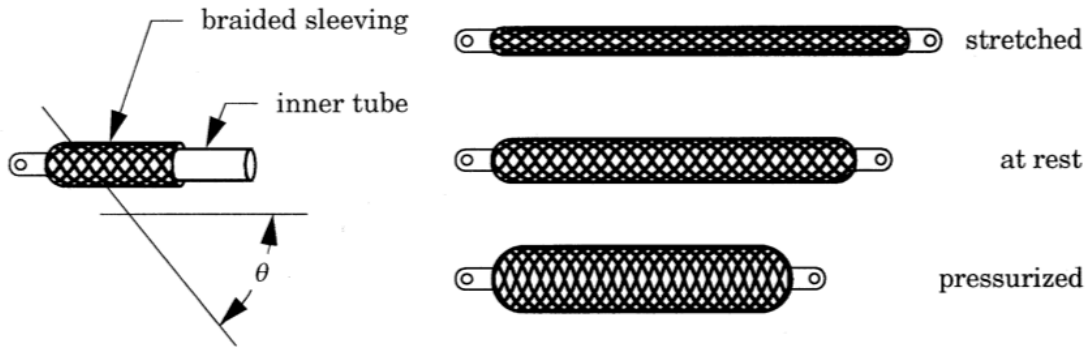

Figure 21: Schematisation of the components of a McKibben muscle [54]

PAMs are used in applications in which they have to mimic the behaviour of muscles, as they exhibit linear contractile behaviour with a monotonically decreasing load-contraction relationship, a feature that is also common in most skeletal muscles.

Furthermore, both have to be set up antagonistically in order to get bidirectional motion and both are able to control joint compliance. Nevertheless there are many differences between PAM and skeletal muscle in fact these latter do not change volume during contraction, have modular structure because are made of microscopic contractile systems, are organized in units whose activation depends on the level of external load, come in fast and slow types depending on the need of sustained action and speed, have integrated multiple force and strain sensors, have energy stored in them and running through them that can serve as energy source [54].

2.3.1. PAM models

As shown in Fig.22, there are several PAM models that differ in geometry or fiber orientation but are characterized by similar basic functioning.
The McKibben Muscle or Braided Muscle, Fig.22 (a), are cylindrical and the fibers are orientated helically around the longitudinal axis of the muscle with respect to a θ angle (which can be either $+\theta$ or $-\theta$) called the pitch angle or braid angle or weave angle. When pressurized the tube presses laterally against the sleeve. Thereby the internal pressure is balanced by braid fiber tension due to fiber curvature about the tube. Fiber tension is integrated at the braid's end points to balance an external load. Therefore, it is necessary that there is a pressure connection between inner tube and braided sleeving, and, for this reason, they cannot be used in under pressure because otherwise it would not be possible to transfer a sufficient amount of work to the terminals [54].

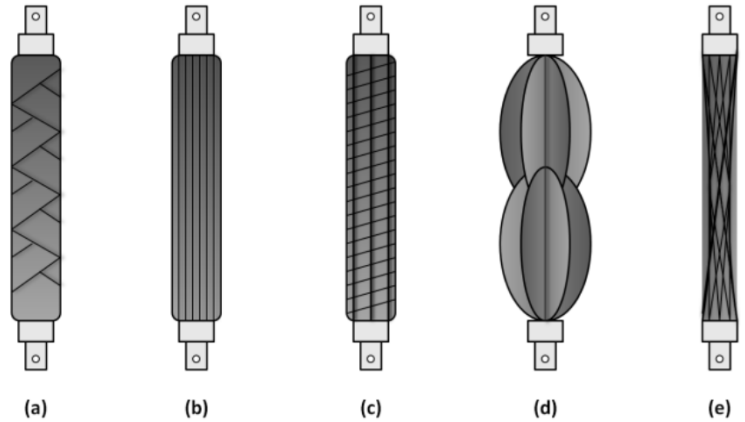

Figure 22: Various types of PAMs: (a) McKibben Muscle/Braided Muscle, (b) Pleated Muscle, (c) Yarlott Netted Muscle, (d) ROMAC Muscle and (e) Paynter Hyperboloid Muscle [56]

The value of the pitch angle modifies the volume of the McKibben muscle following the relation:

$$V=\frac{L_s^3}{4\pi N^2}\cos\theta\sin^2\theta \quad (2)$$

Where:

- Ls is the length of each strand
- N is the number of encirclements the braid makes around the tube

The maximum volume is obtained when the value of the angle is 54.7°, over this value the muscle shell is not stable since it would buckle. When the muscle stretches the angle decreases to a lower limit, which is determined by fiber thickness, the amount or density of fibers, the number of encirclements and the diameter of the end fittings. The value of the developed tension is also influenced by the friction generated between the strands and the sheath and between the strands themselves and, also, by the internal deformation of the tube. In particular, both friction and non-elastic deformation determine both a hysteresis in the force curve and the occurrence of a threshold pressure that must be exceeded for the diaphragm to deform [54]. The latter represent the two major disadvantages of the McKibben muscle, in addition to the fact that the behaviour of the muscle shows variations when it is at high or low temperatures [57].

The Pleated Muscle, Fig.22 (b), has a pleated membrane in the axial direction and, when it expands, it unfolds these pleats, so it produces no frictional force and therefore little energy is needed to expand the membrane [54].

The Yarlott Netted Muscle, Fig.22 (c), unlike braided muscle, has larger holes, and for this reason if the membrane is stretchable, it will only be able to withstand low pressure levels. For this, a retractor-type membrane is usually used [54].

The ROMAC Muscle (Robotic ACtuator Muscle), Fig.22 (d), consists of a polylobed bladder harnessed by a wire netting and closed at either ends by fitting. The bladder is made of a sheath, that is characterized by its high tensile stiffness, its flexibility and its fluid-tightness. The netting or harness is comprised of non- stretchable flexible tension links, which are joined at nodes so as to form four-sided diamond shaped apertures in the network. It shows less hysteresis and a little threshold pressure, compared to the braided ones, due to the absence of friction and the thin membrane [54].

The Paynter Hyperboloid Muscle, Fig.22 (e), is made of a membrane that, when is in its fully elongated state, has the shape of a hyperboloid of revolution. The elastomeric membrane is embedded by a sleeve of inextensible, flexible threads that are anchored to the end fittings. With the actuator at its longest, these threads run in straight lines from end to end, thus defining the hyperboloid surface. The muscle can be powered both pneumatically and hydraulically [54].

2.3.2. PAM Applications

The sector in which PAMs are mostly used is the robotic field, due to their similarity to the behaviour of muscles. Thanks to their use, it has been possible to recreate biologically inspired robots that mimic the morphology and physiology of humans and animals.
An example of these robots is the Shadow Biped Walker, a humanoid robot that uses twenty-eight PAMs, or Airic's robotic arm, developed by Festo AG & Co. The latter uses thirty PAMs to recreate the behaviour of muscles and bones using piezoelectric valves [56]. Another area in which PAMs have great application is the medical field, both for the rehabilitation therapy of patients suffering from degenerative muscle diseases and for neurological injuries that impair movement capabilities. For example, they have been used for robotic motion-support orthoses by exploiting the operation of PAMs through antagonistic pairs. And finally, their operation is also exploited in the industrial sector due to their ease of installation and can be used, for example, to drive industrial machinery[56].

Chapter 3

Analysis of the exoskeleton prototype

The exoskeleton under consideration, Fig.23, is a passive upper limb exoskeleton that is designed for industrial use, so its main function is to allow the user to hold the arms in an overhead position, in presence or absence of tools in the hand, without straining the shoulder joint and reducing the muscular load to a level that avoids the occurrence of WMSDs. In particular, the exoskeleton implements two PAMs whose role is to generate a torque, called support torque, which must compensate, as much as possible, for the gravitational torque acting on the shoulder joint.

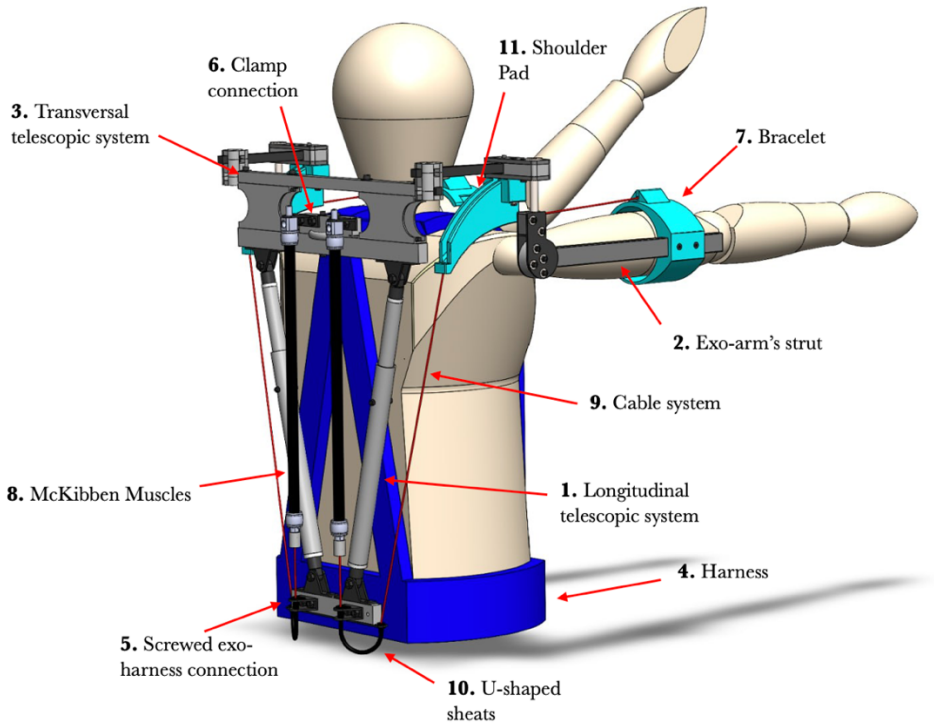

Figure 23: Exoskeleton structure

The prototype allows a shoulder flexion angle between 70° and 135°, as the angle is limited by a mechanical limit switch, while the abduction angle is limited to 30°. The total weight of the structure is approximately 5.5 kg.

The structure, shown in Fig.23, can be adjusted according to the height of the user, since in the back frame there are two telescopic tubes, (1), which allow the length regulation in the longitudinal direction. The prototype can be used by individuals between 160 cm and 175 cm tall, since the adjustable range of the longitudinal telescopic system is between 460 mm and 500 mm.

Similarly, thanks to a screw system, the useful length of the exoskeleton arm's strut, (2), can be also varied. In particular, the useful length of the exo arm can be modified between 180 mm and 260 mm.

Finally, there is the possibility of adjustment of the prototype in accordance with the distance between the shoulders, the biacromial distance, of the user. Thanks to a square telescopic bar, (3), the distance between the two shoulder pads can be varied so that the transversal distance can be changed from 370 mm to 410 mm.

A commercial harness (4), specifically the Portwest FP14, is used to anchor the exoskeleton structure to the user. The harness is equipped with a waist belt to which the rear part of the structure is screwed, (5), while the upper part of the harness is connected by a clamp, (6), which is inserted into a specific slot in the back frame.

Another particularly relevant point of interface between the user and the exoskeleton is the bracelet, (7). This one connects to the arm at the distal part of the humerus, i.e. just above the elbow joint, and thus supports, when the prototype is in operation, the user's limb, and eventually the presence of a working tool.

The functionality of the exoskeleton is based on two PAMs, specifically two McKibben muscles, (8), which support the user during the functioning thanks to a cable system, (9), which acts as a transmission system, as it connects the lower extremity of each PAM to the bracelet. The cable is guided as it passes through a sheath, (10), and then arrives to the shoulder pad, (11), and then is fixed onto the bracelet.

In the following paragraphs, the main components of the exoskeleton are described in more detail and are categorized according to the main sections: the back frame, the shoulder pad and the exo arm.

3.1. The Back Frame

The back frame, Fig. 24, represents the most crucial part for operational effectiveness of the prototype. In fact, we can identify the PAMs which are the focal point of the operation of the structure, but also two of the adjustment mechanisms that allow the prototype to adapt according to the anthropometric characteristics of the user.

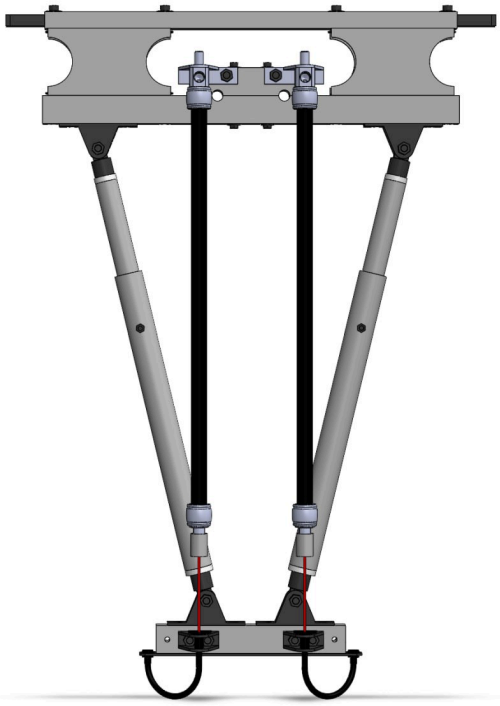

Figure 24: Back Frame

Beginning with the PAMs, they are, specifically, two MKMs manufactured by FESTO S.p.A (DMSP-10-350N-RM-CM), which have a nominal length of 350 mm. They are connected to the back frame in the upper part, by means of an L-shaped plate, while at the bottom they are not constrained since are connected to two cables (Braided climax - 200daN, OCKERT, Germany). These two cables are directed towards the fixed passing points on the lower part of the frame and then run upwards via two high-density polyethylene-coated steel sheaths.

The other key elements of the back frame are the devices that allow the back frame to be adjusted. Two telescopic bars, Fig.25 (a), with a circular cross-section, allow the length of the frame to be adjusted by means of screws that can be inserted into different predefined cavities to adapt to different user heights. They are connected to the frame

by means of two round tube end caps (NDL.T-20x1-1.5-M8 and NDL.T-25x1-1.5-2-M8, ELESA, Italy) and two articulated fork mounts equipped with flat eye terminals at both the top and bottom. These are connected, in the lower part, to a bar which acts as connecting element to the harness since it is screwed onto the belt.
The other adjustment system, instead, consists of a square-section telescopic rod, Fig. 25 (b). The latter allows the distance between the two shoulder pads to be adjusted according to the user's biacromial distance. Operation is based on the sliding of two square bars, which are fixed by two pins each that are inserted into the appropriate holes. Each square telescopic rod is then connected to an angle joint that represents the connecting element between the back frame and the exo arm. In fact, in the angle joint are inserted both the inner bar of the telescopic system for the setting of the biacromial distance and also the bar of the exo arm, that will be described in the next paragraph.

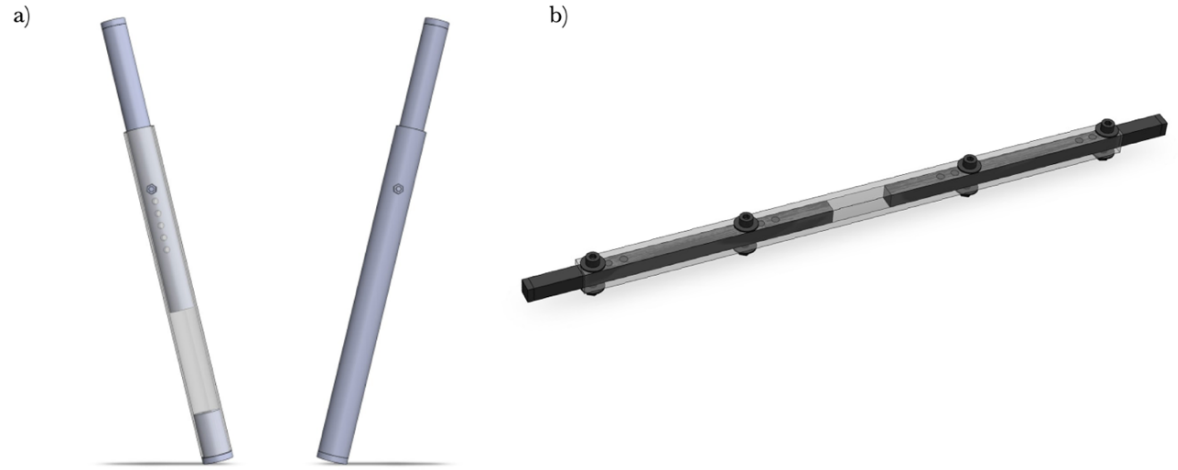

Figure 25: Back frame regulating elements: a) section and full view of the telescopic bars for setting the longitudinal length of the prototype; b) section view of the telescopic bar for setting the biacromial distance.

3.2. The Exoskeleton Arm

The second relevant compartment of the prototype is the exo-arm, Fig.26. Proceeding from the back frame towards the bracelet, firstly there is a bar which is inserted at one end into the previously mentioned angular joint, while, at the other end, it is inserted into a rectangular joint that represents the connecting element. The rectangular joint, in fact, connects three main components, namely, the bar, mentioned earlier, the shoulder pad and a pin.

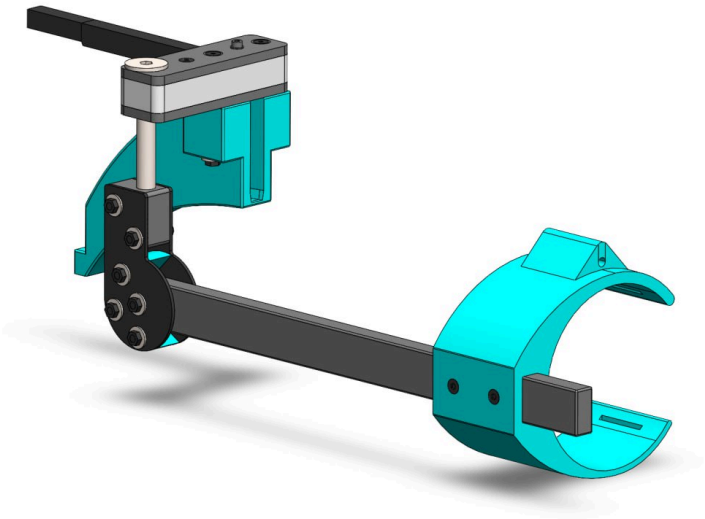

Figure 26: Exoskeleton arm

In the rectangular joint there are various connectors, shown in Fig.27, such as: two M4 countersunk screws, (1,2), which connect the shoulder pad to the joint, a further M4 countersunk screw, (3), which holds the pieces of the joint together, an M3 screw, (4), into which the bar is inserted and, finally, an M10 pin, (5), which is connected to another joint into which the strut will be inserted.

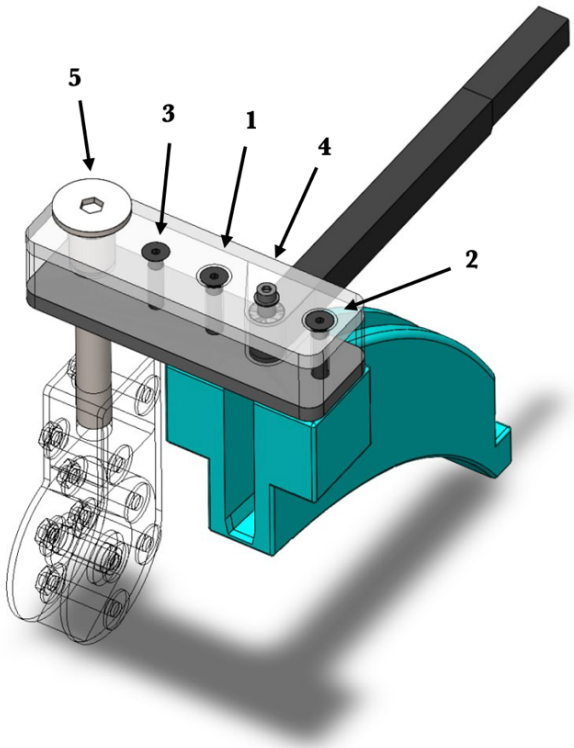

Figure 27: The connecting joint

In particular, the connection between the rod and the joint, Fig. 27 (4), is crucial as the rod has a circular hole that fits into a bushing and thus allows the abduction and adduction movements of the shoulder. As can be seen in the figure, there is also a notch in the joint that limits the ROM of the exo-arm.
Pursuing the analysis of the exo-arm the M10 pin is inserted into an additional joint, Fig.28, that connects also with the strut.

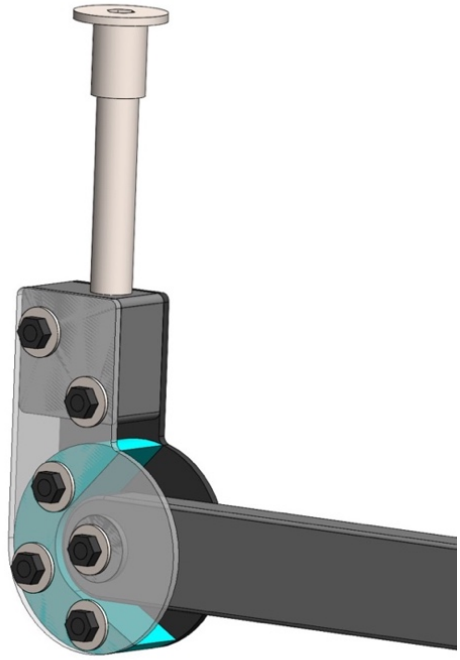

Figure 28: Section view of the joint and the PLA insert

This joint consists of two metal plates that are separated by a PLA insert that has been specifically designed to allow flexion-extension movement and act as a mechanical stop, in fact, it limits the shoulder abduction to 30°. The strut has a circular end, that is positioned at the interface with the PLA insert to allow the abduction movement. The strut and the other elements in the joint are secured by using six M4 bolts. The importance of the specific alignments of these two joints will be discussed in more detail in section 3.4.
The strut, Fig.29, is the last adjustment element and it consists of an aluminum rod on which the PLA cuff is hinged and whose position can be adjusted by means of two M4 screws that fit into specific holes inside the bar. The position of the cuff can be modified to suit the user's specific anthropometric measurements. The upper part of the cuff also has a hole into which is inserted the cable, which is the transmission element for the

force generated by the PAMs. The cable insert allows the cable to remain aligned with the user's arm to prevent misalignment.

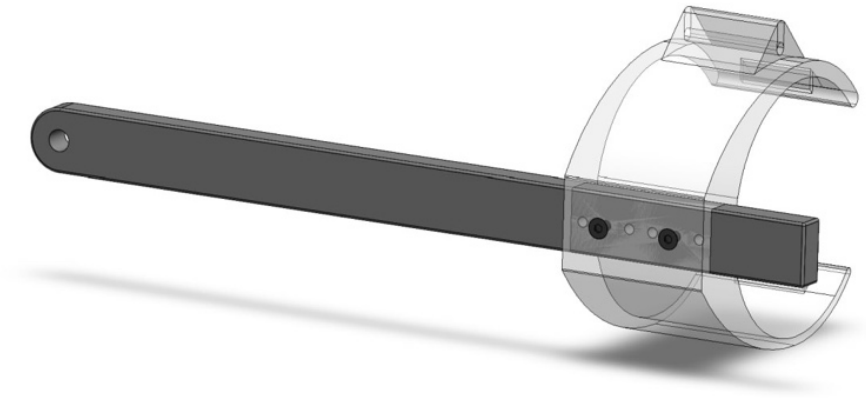

Figure 29: Strut and regulation system

3.3. The Shoulder Pad

The shoulder pad represents a fundamental element for the functioning of the prototype because it is the element on which the cable, that connects each PAM to its respective cuff, rests. For this reason, in fact, it is essential to design the profile of the shoulder pad so that it properly directs the forces involved. The profile of the shoulder pad must also be modelled so that it does not impact the user's shoulder as this would generate discomfort. Another fundamental characteristic that the shoulder pad must respect is to be above the SJC, as otherwise the cable would also be below the SJC and this would generate a torque, leading to a forced abduction of the user's limb. The shoulder pad must also be centered with respect to the SJC so as not to generate unwanted forces or misalignments and to allow a proper alignment for producing natural redundancy.

3.3.1. Shoulder Pad profile

To comply with all the previously mentioned characteristics, a graphical method was chosen as the method for designing the shoulder pad profile. Designed with a progressively larger radius, the profile achieves the necessity of increasing the PAM pulling force when the angle of elevation of the arm increases and, also, to allow the

equilibrium between the torque due to the gravity and the torque generated by the PAMs.

In Fig.30 there is a schematization of the shoulder pad's quantities involved:

- r is the lever arm of the tension force F_{mu} with respect to the shoulder joint;
- b is the distance between the position of the attachment point of the wire onto the bracelet and the final point of the shoulder pad, called Z;
- T is the tangency point of the wire onto the shoulder pad;
- θ_1 is the elevation angle of the upper arm;
- c_0 is the distance between the bracelet and the shoulder joint.

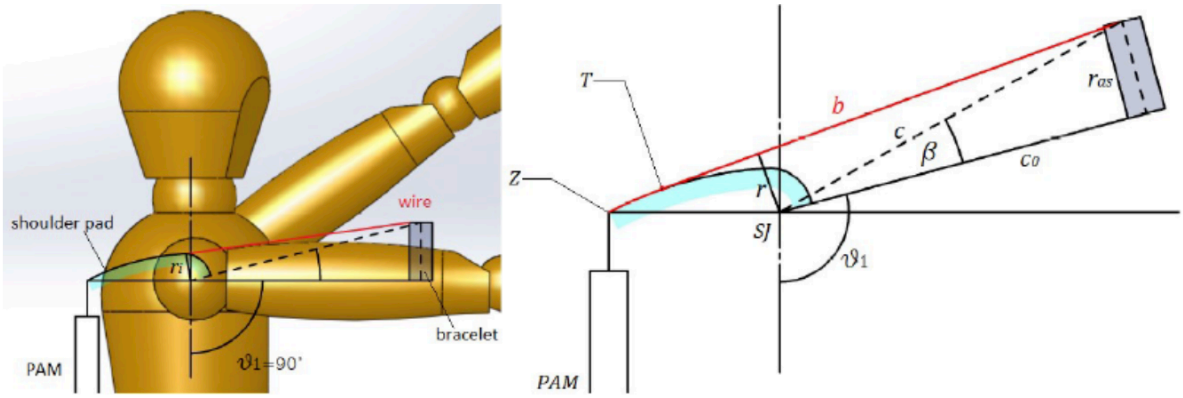

Figure 30: Shoulder pad functioning scheme

Specifically, an initial value of the shoulder pad radius, that is the radius at which the arm is flexed at an angle equal to 90°, was therefore set. With the aim of ensuring that the profile of the shoulder pad does not impact the user's shoulder, a minimum threshold was set equal to the distance between the SJC and the acromion, since the acromion is the bone that forms the peak of the human complex shoulder. The distance of the acromion with respect to the shoulder joint was obtained from literature [58], and is equal to 0.0345 m. In addition, however, it is also necessary that the shoulder pad does not exceed the position of the eyes in relation to the shoulder, therefore, it was necessary to take this specification into account when choosing the maximum initial value of the shoulder pad radius. Based on this specification, r_i=0.045m was set as the initial value.

On the other hand, regarding the choice of the final radius value i.e., the value of the radius of the profile when the arm is at its final position, meaning at an angle of 135°, it was fixed that the values of r_f should be between 0.065m and 0.075m since exceeding this range risked producing a profile that was too bulky for the shoulder pad. After determining the value of r_i, the value of r_f was chosen by interaction so as to maintain the final output torque as high as possible. The value of r_f equal to 0.07 shown the best

results as it gives the lowest RMS (Root Mean Square) value between the gravitational and the support torque.

Therefore, once the values of r_i and r_f were fixed, the profile of the shoulder pad was obtained graphically. Data were interpolated with circular interpolation so as to obtain the perfect curvature that would allow tangency with the cable. The coordinates of the tangency points, the contraction values of the MKMs, and the lever arms at the initial, final, and two intermediate positions were also obtained from CAD to finally interpolate with a fourth-degree polynomial.

The final profile of the shoulder pad is shown in Fig.31.

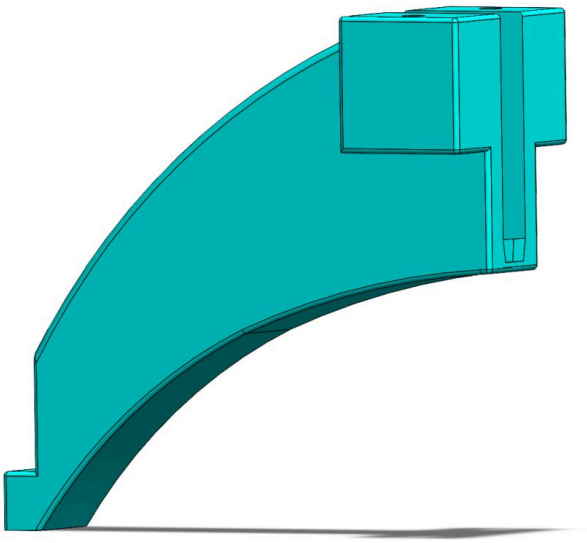

Figure 31: Shoulder pad profile

3.3.2. Shoulder Pad mechanism

The shoulder pad transmission mechanism has been chosen since it has shown the most promising results. Other mechanisms have been analyzed including a pulley-based transmission and a cam-based transmission.

The parameter that was evaluated to choose the most promising transmission method was the root mean square value (E) expressed by the following equation:

$$E = \sqrt{\frac{1}{N} \cdot \sum_{i=1}^{N} (M_{MKM_{(\theta 1)}} - M_{g_{(\theta 1)}})^2} \quad (3)$$

In the previous equation, the terms that figure are:

- M_g represents the gravitational torque
- M_{MKM} represents the support torque
- N is the number of samples.

In particular, the criterion used for the choice was to minimize E, since more the assistive torque equals the gravitational torque, the less effort the user has to make. The mechanisms that were evaluated for the choice of the most promising system were tested both in the weightless condition and in the condition in which the operator is holding a weight of 1 or 2 kg in the hand. To evaluate the shoulder pad mechanism, different levels of pressure, initial contraction ratio and McKibben muscle length were tested in order to find the best combination that would minimize the root mean square value between gravitational torque and support torque. The values that were seen to provide the best performance were 2% for the contraction ratio and 35 cm for the length of the McKibben muscle. Finally, by adjusting the pressure levels according to the weight applied on the operator's hand, low E levels were obtained.
The results of the analyses carried out with the three different transmission mechanisms show that the mechanism using the shoulder pad allows it to adapt its functioning during the working period by adjusting the feed pressure. By contrast, this is not possible in the case of the cam or pulley-based transmission, which, on the other hand, worsen their behaviour when the gravitational torque increases. Furthermore, the exoskeleton structure using the shoulder pad as the transmission method is less bulky. Although it is not the best mechanism from the point of view of working range, however, for the reasons mentioned above, it turned out to be the most promising mechanism among those examined and, for this reason, it was chosen as transmission mechanism.

3.4. The Kinematic chain

The exoskeleton is composed of a kinematic chain with 2 DOFs since it allows the shoulder's movements of abduction and flexion-extension. This type of kinematic chain is favorable from the point of view of bulk and simplicity, but at the same time the problem of misalignment remains. To limit the problem of misalignments it's necessary to obtain the alignment between the SJC and the ExoJC, i.e. the joint center of the exoskeleton.
It is therefore necessary that when the exoskeleton is put on and the shoulder is flexed at 90°, the two centers coincide. The difficulty with the need for this alignment is linked to the fact that SJC moves, as discussed in section 1.2.1, while ExoJC remains fixed. In

fact, when the user raises his arm then the SJC rises but ExoJC does not, this results in the bracelet moving along the subject's arm and this cause the generation of shear stresses between the bracelet and the user's arm. Moreover, it is not perfectly known the exact position of the shoulder joint center. To understand the reach of the shear stress and the approximations linked to the not perfect match between the SJC and the ExoJC it has been evaluated the consequences of the misalignment. It was achieved that in most working conditions the support torque is higher than 50% and the shear force does not reach excessive values.

The two joints described previously, in section 3.2, are fundamental since they must comply with the requirements of the exoskeleton. They represent a vertical and a horizontal hinge joint and, to function effectively, they must be arranged into a specific configuration where the two rotational axes are orthogonal to each other when the shoulder flexion is equal to 90°, Fig.32.

Additionally, they should be aligned as closely as possible with the anatomical axes of the shoulder to ensure accurate and natural movement, minimizing strain on the joint structure and optimizing biomechanical efficiency.

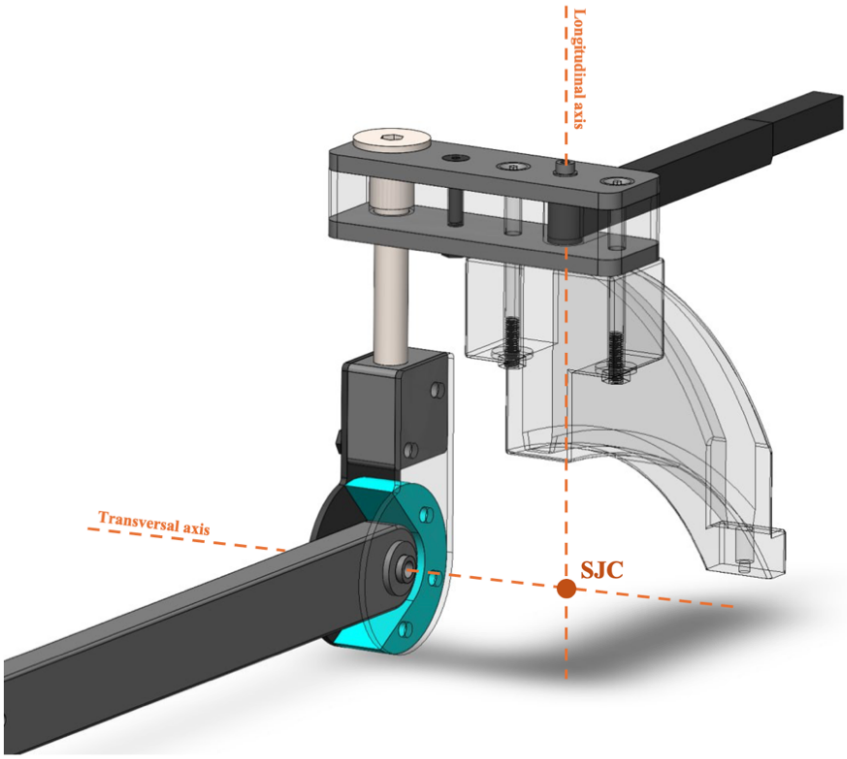

Figure 32: Joint axes

3.5. Materials

The shoulder pad, the bracelet and the two inserts placed into the connecting joints of each exo arm were obtained through 3D printing and are made of PLA. Most of the other parts of the exoskeleton are made of aluminum (EN AW-6060 T6), i.e. the strut of the exo arm of the telescopic bars and the upper part of the back frame. The rest of the components are made of stainless steel (AISI 304 X5CrNi18-10), i.e. the fork supports in the back frame, the inner rods of the transverse telescopic system, the metallic surfaces of the horizontal hinge joint.
The choice of the best material to use for each component was made taking into account the mechanical properties required for each component. For example, steel was chosen over aluminum for parts that are subject to greater stress and therefore require greater strength. On the other hand, aluminum is preferred for parts that are not subjected to excessive stress, as it has the great advantage of being lighter than steel.

3.6. Exoskeleton functioning

As mentioned above, the prototype's functioning is based on two PAMs, each with a cable at its lower end. These two cables are directed towards the lower part of the frame and then ascend via two high density polyethylene coated steel sheaths which direct the cable towards the upper part of the exoskeleton and bring it up to the shoulder pad. The cable is then inserted into a groove in the shoulder pad, which changes the direction of the cable so that it runs parallel to the wearer's limb. From there, the cable passes through a special wire tensioner that allows both the length of the cable to be adjusted, based on the anthropometric measurements of the subject's limb, and also the tensioning of the cable itself.
Before the subject can, actually, wear the exoskeleton, it must be adjusted based on the subject's height, subacromial distance and arm length. at this point it is then possible to put on the exoskeleton by fastening the harness correctly. When the exoskeleton is worn, it is necessary to verify the correct reciprocal positioning between the exoskeleton and the subject so that, either no misalignment is created that would hinder the proper functioning of the structure, or that no errors are produced that could hinder its safety. Indeed, it is important to check that when the shoulder is flexed at 90° the ExoJC is almost aligned with the SJC.
The MKMs are then pressurized, causing them to replicate the functioning described in the previous chapter. As a result, the muscles increase their transverse dimension and

shorten. Since they are connected to the frame at the top through a fixed attachment, their contraction pulls the cable to which they are connected at the bottom. The cable, therefore, having been tensioned by means of the cable tensioner and being subjected to traction, will produce a torque that will be exerted at the level of the exoskeleton arm that will counteract the gravitational force.

3.7. Limitations of the Prototype

The results of the prototype were seen to be promising in the test phase, but despite this, there were some components that showed the need for improvement or modification of some parts of the structure that can made the prototype more efficient and functional. These most significant limitations of the prototype include:

- the need to make the structure's adjustment systems simpler and faster so that it would be easier to modify the reciprocal distances based on the user's anthropometric measurements;

- the anchoring systems of the structure, including the harness, requiring a solution that is simpler, lighter, and easier to wear than the current design;

- the PAM pressurization system that does not allow the user to pressurize the PAMs individually;

- the disengagement mechanism for the artificial muscles and the wire length adjustment system, ensuring that the user can easily lower their arms when below 90°.

- the necessity of reducing the overall weight of the structure.

Chapter 4

The pressurization system

As above mentioned, the pressurization system of the actual prototype has shown some limitations linked to the impossibility for the user to pressurize, himself, the pneumatic artificial muscles. This is due to the fact that the PAMs are placed in the back frame of the structure and therefore the valves, that allow pressurizations of the muscles, are not accessible by the user himself. This problem is especially evident in the case where, after wearing the frame, the user has to pressurize the PAMs, or in the case where some leakage occurs in the system due, for example, to the valve not being screwed in correctly, and it is therefore necessary to re-pressurize, in order to return to the required pressure level and also in the case in which the pressure level has to be changed to modulate the action level according to the working task requirements. Hence the need to find a way to allow the user greater autonomy in pressurizing the artificial muscle. However, before evaluating the insertion of a pneumatic circuit that can solve the current limitation of the exoskeleton, it is important to know how the PAM works, and therefore to evaluate mathematical models that can predict the artificial muscle's behaviour.

4.1. PAM mathematical schematization

Several models have been developed to describe the functioning of PAMs based mainly on geometry, to characterise the static performance of the muscle. The models are used to find the static characteristic of the PAM, i.e. the relation between the muscle force F and the muscle contraction, under the effect of a constant muscle pressure, neglecting the time factor.

4.1.1. Chou and Hannford model

In particular, one of the most widely used is the Chou and Hannford model [59], which can be applied under the assumptions of:

- cylindrical actuator
- threads in the sheath are inextensible and always in contact with the outside diameter of the latex bladder
- frictional forces between the tubing and the sheath and between the fibres of the sheath are negligible
- latex tubing forces are negligible.

Under these conditions, the PAM can be modelled as in Fig. 33, where:
- L is the length of the cylinder;
- b is the thread length;
- D is the diameter;
- n is the number of threads turns;
- θ is defined as the angle of the threads with the longitudinal axis.

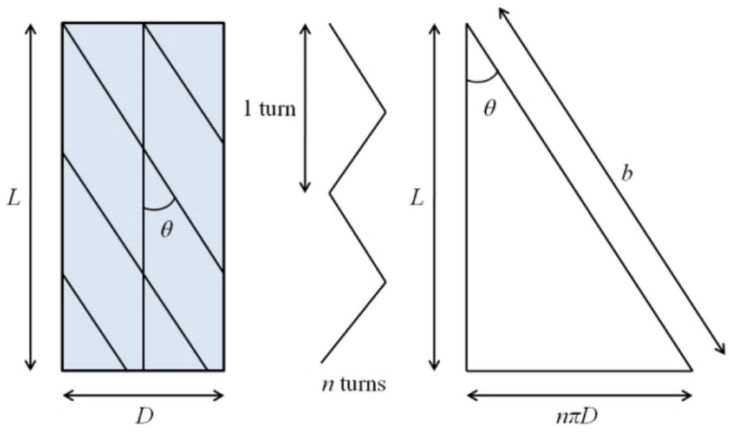

Figure 33: PAM schematization [56]

The resultant force equation that is derived through this model is given by the following equation:

$$F = P'b^2\left(3cos^2(q-1)\right)(4pn^2) \quad (4)$$

in which P' is the gauge relative pressure [56].

4.1.2. Tondu and Lopez model

Another widely used geometrical model for PAM is the one of Tondu and Lopez [60], that simplifies PAM model considering a geometrical description similar to the one of Chou and Hannford, assuming inextensibility of the mesh material, and considering angle changes during the alteration of the PAM's length.
Starting from these assumptions the following mathematical modeling approach can be derived, based on the theorem of virtual work:

$$F(\varepsilon, P) = \pi r_0^2 \cdot P[\alpha(1-\varepsilon)^2 - b] \quad (5)$$

Where:

- l is the length of the muscle;
- P is the pressure;
- r_0 is the nominal inner radius;
- θ_0 is the initial angle between the membrane fibers and the muscle axis;
- $\alpha = 3/tan^2\theta_0$;
- $b = 1/sin^2\theta_0$;
- $\varepsilon = (l_0 - l)/l_0$ with $0 \leq \varepsilon \leq \varepsilon_{max}$.

However, this model has been seen to overestimate the actual maximum contraction, and this is due to the fact that it assumes that the muscle is a continuous cylindrical shape. In reality, however, the muscle, when contracting, takes on a conical shape at both ends and, thus, its active part decreases. In order to overcome the limitation of this model, an empirical factor *k* was included to take into account the deformation and the resulting change in the shape of the PAM and, in this way, the equation assumes the form:

$$F(\varepsilon, P) = \pi r_0^2 \cdot P[\alpha(1-k\varepsilon)^2 - b] \quad (6)$$

4.1.3. Sarosi and Fabulya models

Since in the case of the prototype under consideration, the McKibben muscles used are DMSP-10-350N-RM-CM produced by Festo, then it is important to consider the analysis of four different mathematical models for PAMs produced by FESTO carried out by Tóthová and Pitel'[61]. According to this article, the best approximations were obtained using the equations formulated by Sarosi and Fabulya that approximate the static characteristics of a McKibben PAM and are based on an exponential function [61] [62]. The equations were developed in order to overcome the limitations of the precedent equations by Tondu and Lopez, since it was seen in some research, [63][64], that there were significant differences between the theoretical and experimental results. To eliminate these differences, the following two equations were developed:

$$F(p,\kappa) = (a_1 \cdot p + a_2) \cdot e^{a_3 \cdot \kappa} + a_4 \cdot p \cdot \kappa + a_5 \cdot p + a_6 \qquad (7)$$

$$F(p,\kappa) = (p + a_1) \cdot e^{a_2 \cdot \kappa} + a_3 \cdot p \cdot \kappa + a_4 \cdot p + a_5 \qquad (8)$$

In the previous equations, κ is the muscle contraction and a_i in which i=1,…,6 are six unknown coefficients which values are found using Matlab Curve Fitting Toolbox.
The difference between the equations (6) and (7) is that, the first one can be used with high accuracy for different Fluidic Muscle independently from length and diameter under different values of pressure while, the second one, can be only used with high accuracy for Fluidic Muscle with inner diameter of 20 mm [65].The approximations based on the exponential function has shown, together with the method based on the maximum force, the best results and that's why these two approximations are recommended for using in modeling of pneumatic actuators based on artificial muscle [66] .

4.2. The new pneumatic connection

The new system has been developed in order to overcome the previous limitations linked with the previous pressurization system. The new pressurization system, shown in Fig. 34, exploits two quick-connect couplings that allow the threaded end of the PAMs to be connected at one end, while the other end allows the insertion of a pipe.

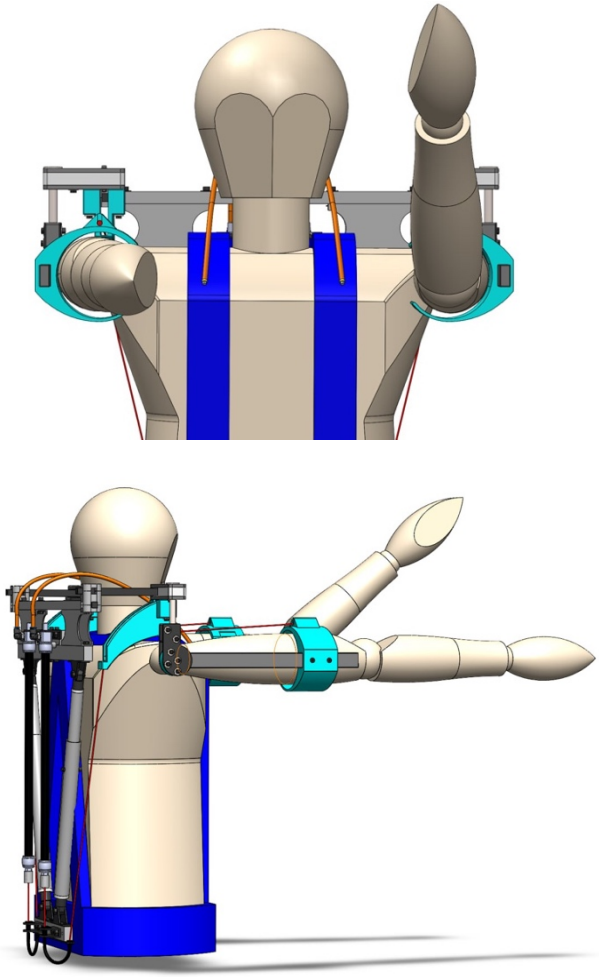

Figure 34: Frontal and lateral view of the new pneumatic system

The fittings used are FESTO L-fittings, which have the possibility of connecting to the threaded end of the PAM, also manufactured by FESTO, via a G1/8 connection, while at the other end they allow the insertion of a 6mm diameter tube. The length of the tube has been chosen to allow it to rise from the height at which the PAM fittings are positioned up to the shoulder and then curve to reach the chest area and then fix to the structure at the level of the harness shoulder straps.
It is essential that the tube at the level of the bend, that is generated above the shoulder, does not generate bottlenecks that would impede the correct functioning of the system, and it is also crucial that the bend is not too bulky so that it does not create obstacles for the user. It is also important that the pneumatic system is well fixed to the harness because, otherwise, during the pressurization of the system, there would be a risk that the structure would impact with the subject's face.

4.3. PAM static characterization

Before evaluating the performance of the new pressurization system, it is necessary to carry out the characterization of the PAM. Particularly, it has been carried out a static isotonic characterization, since, during the functioning of the exoskeleton, the pressure inside the artificial muscles doesn't change, except for a small amount of pressure losses that can be considered negligible. To carry out this test, it was necessary to build a test bench, which is depicted in Fig.35. In order to characterize the muscle, the PAM, (1), was fixed at the upper end, so that the end was constrained, while a plate and a linear load cell, (2), were connected in series at the lower end. In parallel to the PAM, a linear potentiometer, (3), was inserted, also constrained at the upper end, while the plunger component rested on the above-mentioned plate. In the set-up, a pressure gauge, (4), was also used, which was connected to the muscle, to assess pressure values, and in addition, a digital multimeter, (5), was connected to the linear displacement sensor for the purpose of reading the voltage output and deriving the corresponding displacement value from the plunger. During the experiment, several loads of 10 kg each were used, (6), up to a total of 60 kg, to assess the elongation of the muscle under the effect of the weight force. For each value of weight applied, several tests were carried out, varying the pressure level between 0 and 8 bar, in steps of 1 bar, thus creating cycles of pressure increase and decrease for each value of load applied.

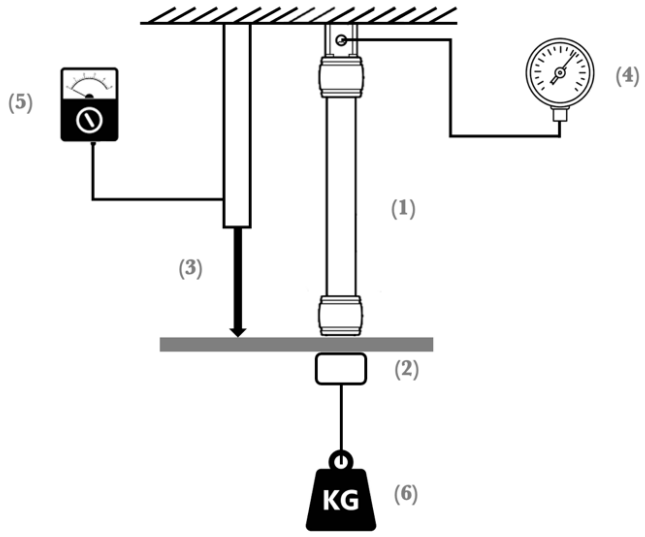

Figure 35: Static characterization set up

The aim is to evaluate the change in length of the PAM when the supplied force varies, with the purpose of determining the relationship between the force of the McKibben muscle and the percent shortening. Obviously, applied pressure values depended on the load connected to the PAM, in order to avoid harmful conditions. Indeed, the Festo guide of the fluidic muscle specifies that, for a PAM with a 10 mm diameter, the maximum possible pretensioning of the nominal length is equal to 3% while the maximum possible contraction of the nominal length is equal to 25% [67]. The characteristic curves, specific for Festo DMSP 10, are shown in the figure below, Fig. 36, where in the axes are reported the percentage of contraction, h, and the force, F. In addition, the vertical red line shows the maximum possible pretensioning and each curve represent the force developed for each pressure level.

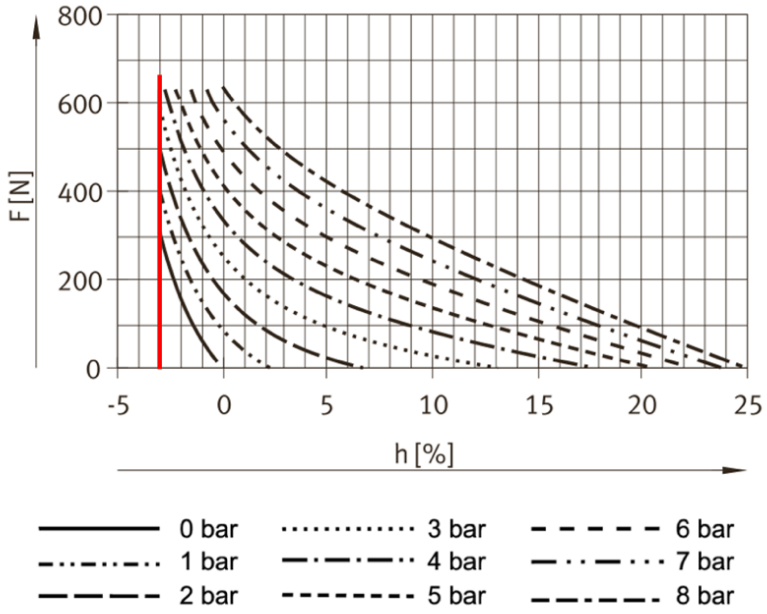

Figure 36: Characteristic curves for Festo DMSP 10 [67]

The data obtained from the experiment are shown in Table 4 and Table 5 which show, respectively, the values obtained during the increase and decrease cycles.

Table 3: Static characterization increase cycle

		Weight (kg)						
		0	10	20	30	40	50	60
Pressure (bar)	0	0.00	-	-	-	-	-	-
	1	1.72	0.06	-	-	-	-	-
	2	5.77	1.29	-	-	-	-	-
	3	12.35	4.61	2.52	-	-	-	-
	4	17.45	9.34	4.55	2.21	-	-	-
	5	20.70	13.88	7.86	3.87	1.66	-	-
	6	22.97	16.83	11.43	6.57	3.01	1.00	-
	7	24.51	19.17	14.25	9.34	5.47	2.30	-
	8	25.55	20.89	16.71	12.10	7.86	3.80	1.30

Table 4: Static characterization decrease cycle

		Weight (kg)						
		0	10	20	30	40	50	60
Pressure (bar)	0	0.43	-	-	-	-	-	-
	1	4.18	0.12	-	-	-	-	-
	2	10.87	2.46	-	-	-	-	-
	3	16.77	7.13	2.58	-	-	-	-
	4	20.21	12.16	5.96	2.27	-	-	-
	5	22.42	15.23	9.77	4.79	1.66	-	-
	6	23.96	18.12	12.72	7.80	3.56	1.30	-
	7	25.00	19.90	15.17	10.38	5.96	2.60	-
	8	25.55	20.89	16.71	12.10	7.86	3.80	1.30

From this data, it was possible to develop the curves showing the relationship between force and percentage shortening, that are shown in Fig.37.

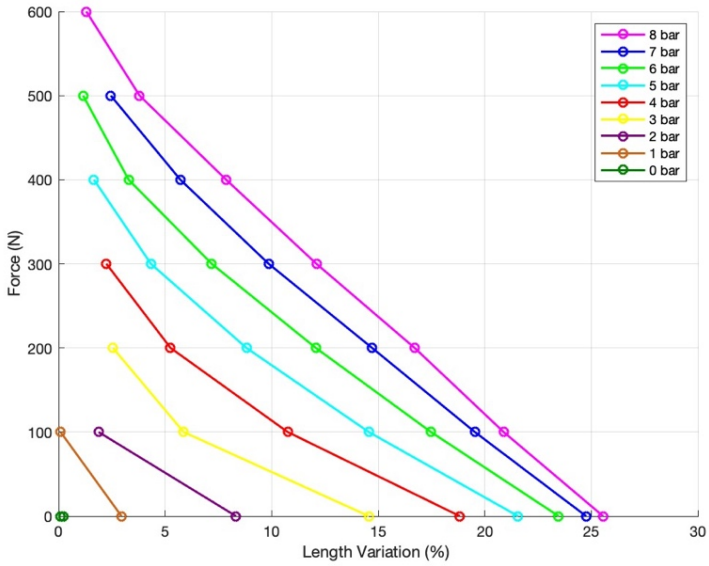

Figure 37: PAM characterization curves

It was also possible, through Eq.7, to find the six a_i coefficients using Matlab Curve Fitting Toolbox, that are reported in the following table.

Table 5: Coefficients obtained from static characterization

a_1	0.0179
a_2	111.2
a_3	-0.3097
a_4	-0.02455
a_5	0.8375
a_6	-126

4.4. Leakage test

Since the new pressurization system implies the addition of certain connecting elements that could affect the pressure tightness of the PAMs, it is advisable to assess whether there are any leaks between the connecting elements. In order to check the efficiency of the new system, a test bench was implemented. The setting for the experiment,

illustrated in Fig. 38, has the PAM, (1), with the upper end constrained, while the lower end is fixed to a support that is free to move in the vertical direction. In this way, by increasing the pressure with which the PAM is fed, the lower end is free to move upwards. The Festo L-connector is screwed to the pneumatic connection of the PAM, into which a 6 mm diameter tube is inserted, which in turn, is inserted into a T-connector. At the other two ends of the T-connector, two more 6-mm diameter tubes are inserted, one of which is linked to the pressure sensor, (2), while at the other end, a barbed nipple is inserted, into which the valve is screwed, (3). A digital multimeter, (4), was also used in order to read the voltage output of the pressure sensor and derive the corresponding pressure value.

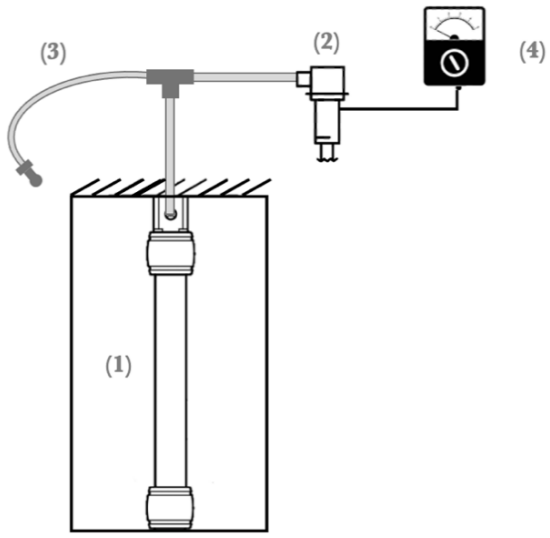

Figure 38: Leak test set up

The purpose of the experiment is to assess the tightness of the system, i.e. to monitor pressure levels over a range of time, which may coincide with that of uninterrupted use of the exoskeleton. For this, the system was tested three times, each with a different pressure level (4, 6 and 8 bar). For each pressure, the system was monitored for three hours, with the pressure level being tracked every 30 minutes. Specifically, the system was manually pressurized, by means of a pump through the valve, at the desired pressure level, and changes in the pressure value were evaluated via the voltage output of the pressure sensor. Prior to the test, the pressure sensor was characterized in order to know the input-output characteristic of the sensor. For characterizing the sensor, an ascent and descent cycle, from 0 to 9 bar, was carried out and the corresponding voltage level was evaluated, in steps of 1 bar. The result of the characterization can be seen in the graph shown in Fig. 39. The data obtained from the leak test are reported in Tab.6.

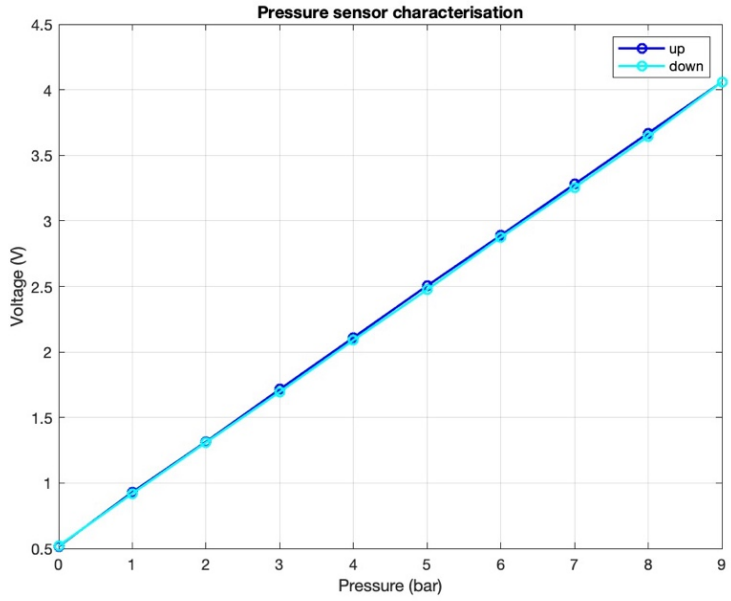

Figure 39: Pressure sensor characterization

Table 6: Leak test results

		Volt	bar
4 bar	t0=0	2.130	4.051
	t=30'	2.120	4.025
	t=1h	2.110	4.000
	t=1h 30'	2.110	4.000
	t=2h	2.110	4.000
	t=2h 30'	2.100	3.975
	t=3h	2.100	3.975
6 bar	t0=0	2.880	5.974
	t=30'	2.860	5.922
	t=1h	2.850	5.896
	t=1h 30'	2.840	5.870
	t=2h	2.840	5.870
	t=2h 30'	2.840	5.870
	t=3h	2.840	5.870
8 bar	t0=0	3.650	7.949
	t=30'	3.630	7.897
	t=1h	3.630	7.897
	t=1h 30'	3.620	7.872
	t=2h	3.620	7.872
	t=2h 30'	3.610	7.846
	t=3h	3.610	7.846

As evident from the data in the table, the pressure losses are extremely low, indicating that their impact on the overall system performance is negligible. In particular, the percentage pressure variation in the three cases is equal to:

- 1.88% for 4 bar;
- 1.74% for 6 bar;
- 1.3% for 8 bar.

In all three cases, it can be noticed that there is a greater loss of pressure in the first half hour than in the subsequent time intervals as the pressure tends to stabilize after the PAM is pressurised.

Chapter 5

Exo Arm modifications

The adjustment elements constitute another limitation of the prototype structure. This is due to the fact that all the adjustment systems rely on the presence of screws, which slows down the time it takes to adjust the structure based on the anthropometric measurements of the subject. For this reason, an attempt was made to modify the adjustment elements in order to find an alternative that would allow for easier adjustment. Naturally, to validate the structure, it was necessary to carry out FEM (Finite Element Method) analyses. The aim of the FEM simulation is both to evaluate the stresses acting on the structure, in order to ensure that the structure does not exceed the specified yield strength limits for each material, and to verify the displacements to which the structure is subjected.

5.1. New bracelet and adjustment system

There are two modifications that have been carried out on the bracelet. The first, as mentioned above, concerns the modification of the adjustment system. It was decided to replace the two screws, previously seen, with a spring-actuated indexing plunger produced by Elesa® (Monza, Italy). This plunger in fact has the undoubted advantage of faster adjustment. In this way to change the position of the bracelet on the strut, it is no longer necessary to unscrew the screws from the frame, which otherwise causes the deterioration of the PLA cuff due to continuous screwing. Plungers, in fact, have a threaded part that connects to the cuff, while the remaining part of the mechanism is retractable. When the plunger is pulled, the retractable part lifts up and allows the cuff to move, while, when the plunger is released, the retractable part returns to its stop

position retracting back into the frame. In order to connect the threaded part of the plunger to the bracelet, PLA inserts were also added to prevent the plastic material from deteriorating due to the contact with the metal material. The bracelet circumference has been modified aiming to create a less restrictive structure. It has been decided to create an only half-circumference section so that the rest of the structure is adjustable with a strap with hook-and-loop fastener. In this way the structure is more adaptable to users with different arm circumferences

5.2. FEM Analysis

After realizing the CAD structures in SolidWorks® 2023, a FEM analysis has been performed. Firstly, the materials that compose the structure have been set, then the connectors have been established, and, finally, the loads and the constraints have been defined. SolidWorks Simulation tool has been used to perform the FEM analysis.
The model has been tested under the worst load conditions in order to have a greater safety margin. The conditions that were simulated correspond to use by a 1.7 m tall subject, weighing 70 kg, holding a 2 kg object in his right hand. Furthermore, it was assumed that the arm is extended, and the flexion angle is 90°, while the abduction angle is 0°. Furthermore, given the presence of the tool in the right hand while the left arm is in unloaded condition, two different levels of feed pressure have been set in the two PAMs. Respectively 4.3 bar, for the left arm, and 7.7 bar for the right arm, since it has been evaluated that these two pressures are the best supply pressures for the arm in unloaded condition and the arm with the presence of 2 kg in the user's hand. The contraction ratio has been set equal to 2%. In the following sections only the right exo-arm will be considered since represents the most stressed case.

5.2.1. FEM Materials

The materials used for the exo-arm components, Fig.40, are mainly:

- PLA: used for the filling of the horizontal (1) and the vertical (2) hinge joints, for the bracelet (3) and for the shoulder pad (4);
- Stainless steel DIN.14301 X5CrNi18-10 (or AISI 304): used for the bar (5) that connects to the angular joint and for the external components of the horizontal (6) and vertical hinge joints (7);
- Aluminum EN AW-6060-T6: used for the strut (8);

- Alloy steel 8.8: used for all the connectors as well as for the connection pin between the horizontal and the vertical hinge joints;
- Brass: used for the insert for PLA located inside the bracelet;
- Stainless steel X10CrNiS18-9 (or AISI 303): for the spacer bushing and also for the metallic part of the indexing plunger.

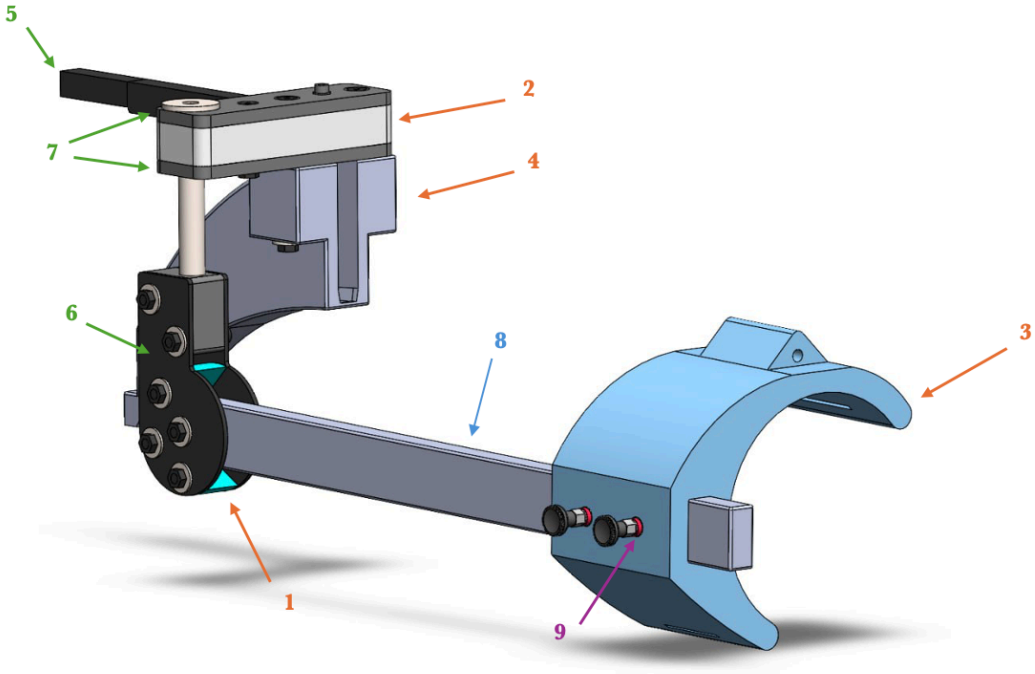

Figure 40: CAD structure of the Exo-Arm: in orange the PLA components; in green the AISI 304 components; in blue the aluminum component; in purple the AISI 303 components.

All materials, except PLA, have been modelled as isotropic. In contrast, an orthotropic model has been used to characterise PLA, as the mechanical properties depend on the direction of printing, and, in particular, are greater along the mold direction. In Tab.7 all the mechanical characteristics of the above-mentioned materials are listed, in particular, E represents the elastic modulus, ν is the Poisson's coefficient, G is the shear modulus, Sy is the yield strength and Sut is the ultimate tensile strength.

Table 7: FEM materials and their mechanical characteristics

	E (MPa)	ν	G (MPa)	Sy (MPa)	Sut (MPa)
PLA (printing direction)	2904.2	0.292	723.34	56	56
PLA (other directions)	2597.5	0.299	1010	35	35
AISI 304	200000	0.28	79000	400	600
EN AW-6060-T6	66000	0.33	25000	230	230
Alloy steel 8.8	210000	0.3	80000	640	800
Brass	100000	0.33	38000	239	300
AISI 303	193000	0.29	77000	580	740

5.2.2. Loads, connectors and constraints

Subsequently, load and constraints have been applied to the structure and also the connector have been modelled, as shown in Fig.41.

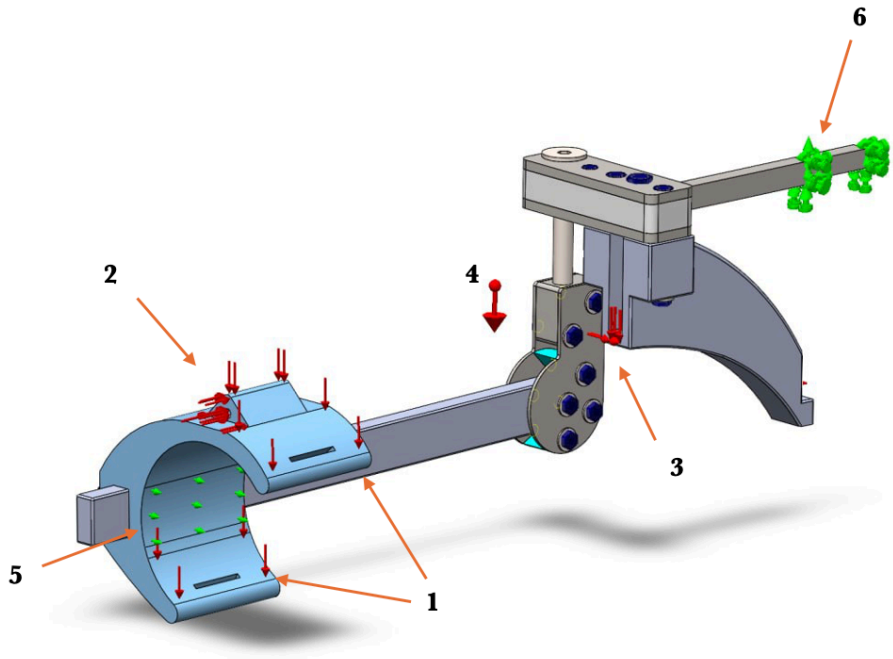

Figure 41:Exo-Arm modelling with loads, constraints and connectors

The reference axes are oriented with the x-axis in the anteroposterior direction, the y-axis in the craniocaudal direction and the z-axis in the mid-lateral direction.
The loads, represented in Fig.41 by the red arrows, were applied in the form of pressures. The load magnitudes have been evaluated considering the contributions of the force exerted by the MKM and also the weight of the arm and of the eventual presence of tools in the hand. The user arm has been simplified as a rigid link with mass concentrated in the center of mass.
The loads applied to the structure are located:

- On the surface of the bracelet (1). The force simulates the interaction force between the user and the bracelet and is linked both to the arm's weight and muscular action. It is equal to -0.023 MPa and acts in the y direction;
- On the upper part of the bracelet onto the cable attachment location (2). The force represents the traction force of the cable. It is directed both in the x-direction, and is equal to -2.579 MPa, and in the y direction, with a magnitude of 0.149 MPa;
- On the inner surface of the shoulder pad in which the cable lays (3). Similarly, the previous force, it is due to the cable traction force, and has three components, 0.51 MPa in the x-direction, -0.491 MPa in the y-direction, and -0.106 MPa in the z-direction.

The gravitational load has also been applied to the center of gravity of the structure (4).

The constraints, represented by the green arrows in Fig.41, are applied as follows:

- On the inner surface of the bracelet (5), at the connection with the strut. This represents the force applied to the bracelet by the arm of the user, which maintains the value of the abduction angle. It is modelled as a constraint in the z-direction;
- At the connection point between the bar and the angular joint (6), which represents the link between the exo-arm and the back frame. Since it is a fixed geometry, it is constrained in all three directions.

With regard to the connectors, they are all class 8.8, and for each one, has been defined a certain preload value based on the dimension of the connector.

Finally, the structure has been discretized using a tetrahedral mesh, as shown in Fig.42.

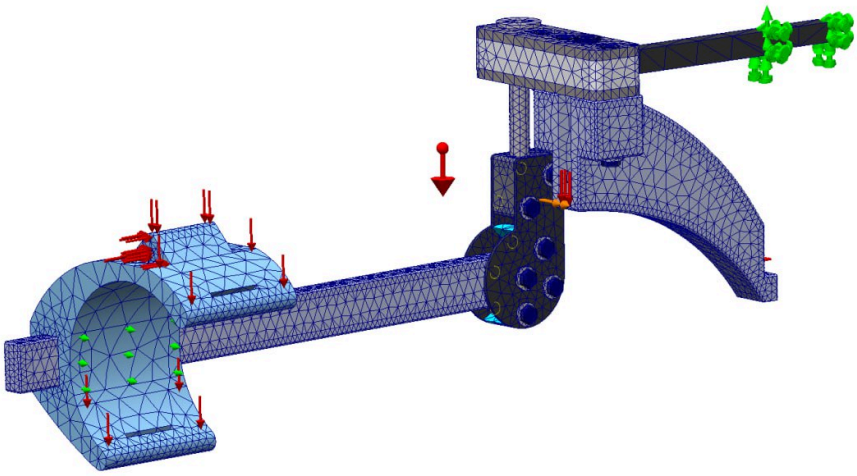

Figure 42: Exo-arm mesh

5.3. Simulation results

The results of the simulation will be discussed in terms of stress and displacement. Regarding the stress on the structure, shown in Fig.43, the component with the highest values is the M10 pin. Nevertheless, the stress values remain below the yield strength that is equal to 640 MPa.

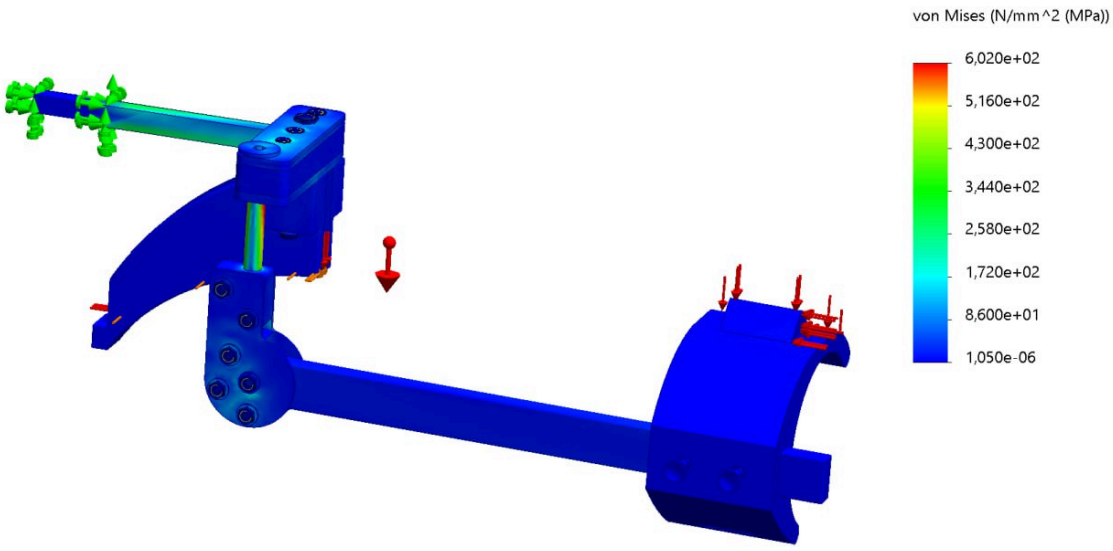

Figure 43: Exo-arm Von Mises stresses

In the indexing plunger, which represent the most significant modification compared to the previous structure, the maximum value of the Von Mises stress is much lower than the yield strength, as shown in Fig.44, so it withstands the loads of the structure.

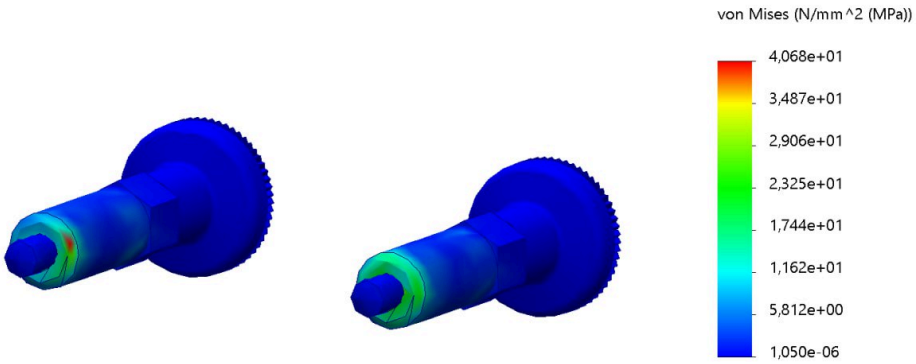

Figure 44: Indexing plungers Von Mises stresses

The distribution of the displacements in the three different directions are shown in Fig. 45, where the URES, i.e. the resultant displacement, is also displayed Fig. 45 (a).
The overall behaviour of the structure, as can be seen from the displacement values in the y-direction, is characterized by a downward displacement affecting both the cuff and the strut, while the shoulder pad tends to move inwards, as can be seen from the displacement values in the z-direction.

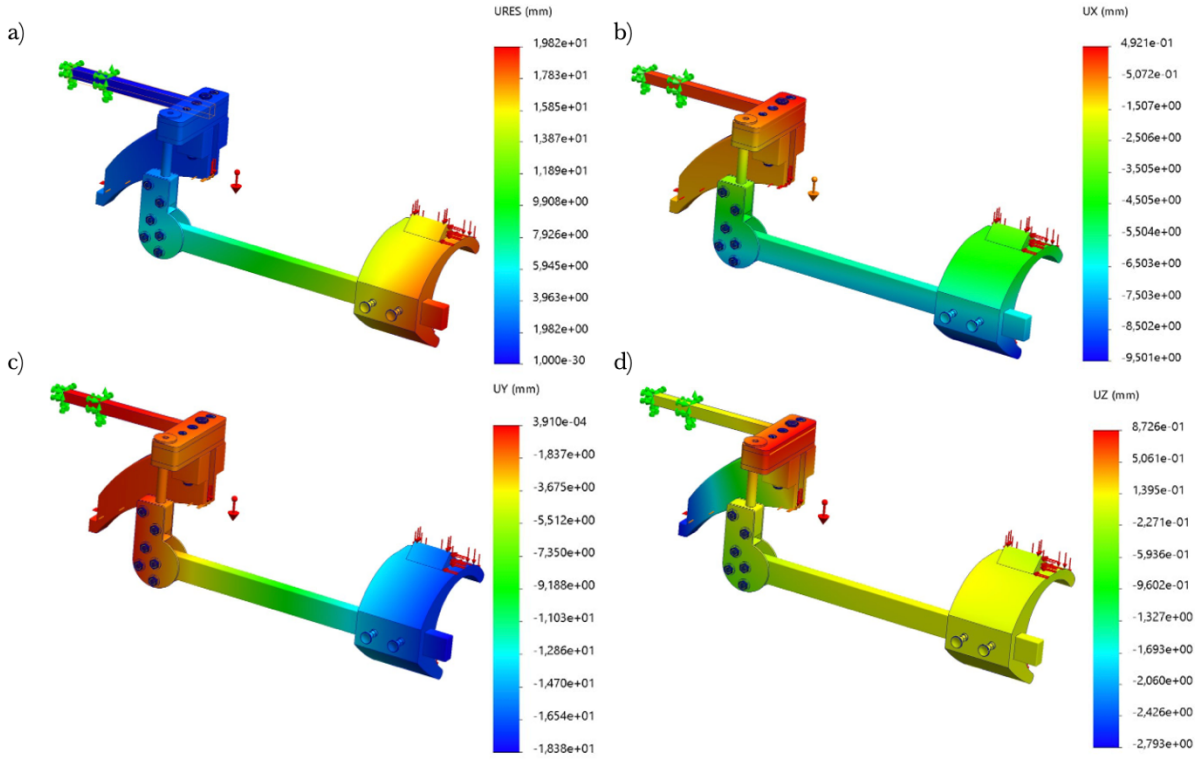

Figure 45: Displacement magnitudes: a) Resultant displacement; b) Displacement in the x-direction; c) Displacement in the y-direction; d) Displacement in the z-direction

5.4. Other exo arm structure modifications

5.4.1. Single indexing plunger

Since the indexing plunger has shown promising results, it has also been carried out an analysis to evaluate whether applying only one plunger to the bracelet would be sufficient and would not lead to an exceeding of the yield strength. Therefore, the CAD structure of the bracelet has been modified by placing only one hole for the plunger. This modification provides two improvements, firstly the sling can be placed in a greater number of configurations and can therefore be adapted more closely to the anthropometric measurements of the user because it can be centered in each of the six holes in the frame. Furthermore, in terms of usability, the single-plunger configuration makes it even easier for the user to change the position of the bracelet.
The results of the FEM analysis carried out on this new structure has shown promising results, as illustrated in Fig. 46.

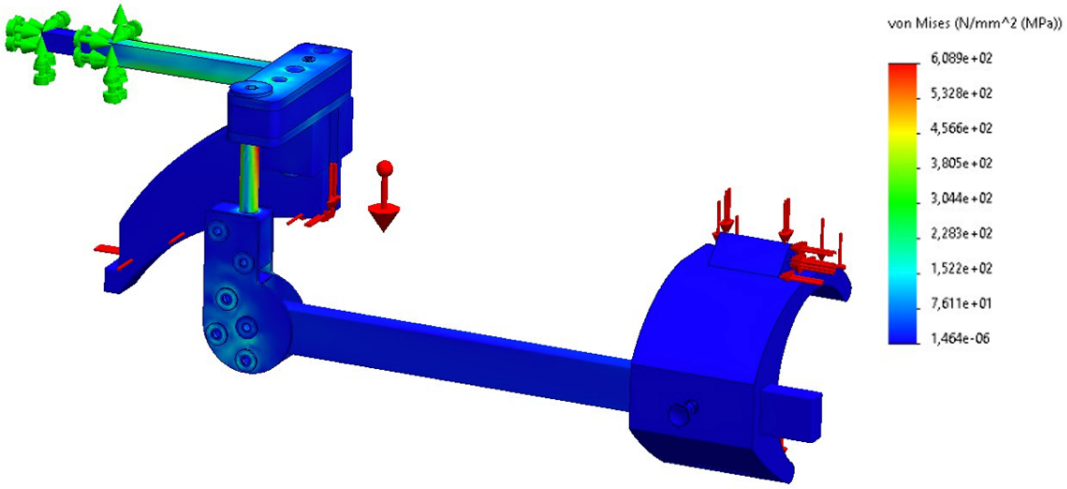

Figure 46: Exo-arm with single plunger Von Mises stresses

Examining the stress acting on the individual indexing plunger, Fig.47, the maximum Von Mises stress is slightly higher than in the previously analyzed configuration with two indexing plungers. Nevertheless, it remains significantly lower than the component's material yield strength.

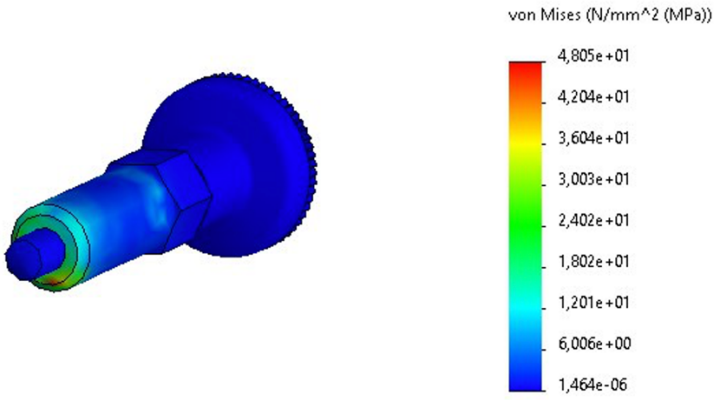

Figure 47: Single indexing plunger configuration Von Mises stresses

Considering the magnitude of displacements in the single indexing plunger configuration, Fig. 48, the values obtained from the simulation show only minor differences compared to the previous configuration. The maximum values for each direction are slightly higher. The biggest difference in absolute value is noticeable in the case of displacements in the x-direction but is still negligible.

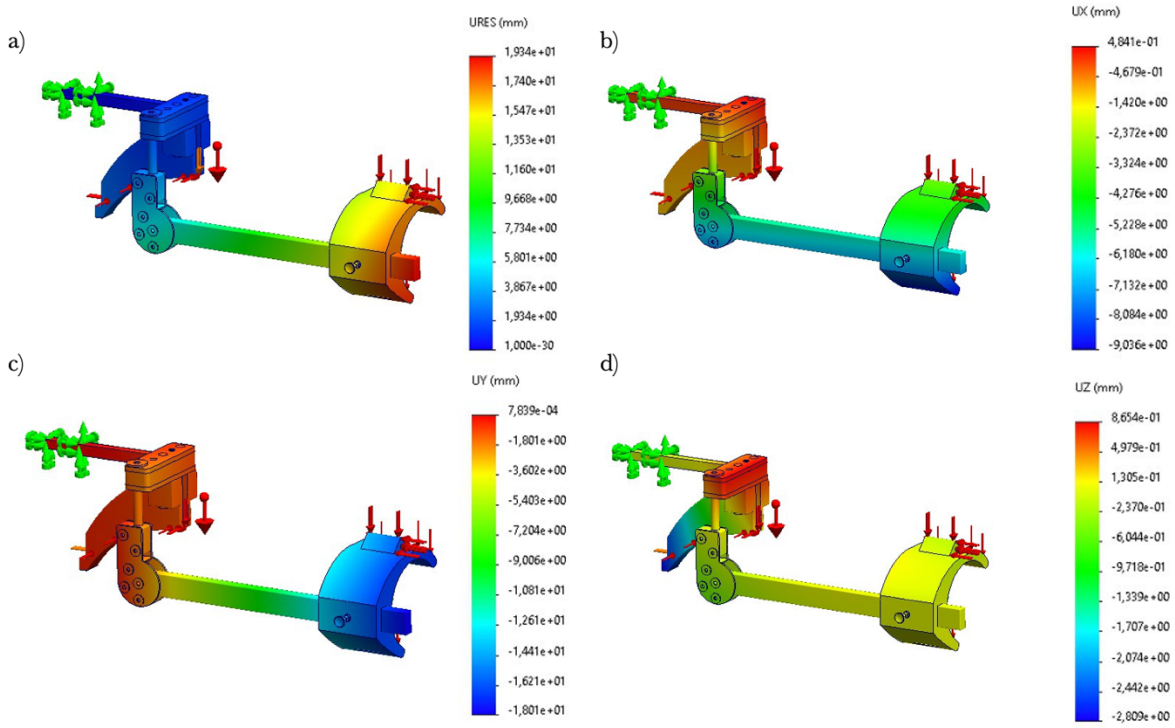

Figure 48: Displacement magnitudes for single indexing plunger configuration: a) Resultant displacement; b) displacement in the x-direction; c) displacement in the y-direction; d) displacement in the z-direction.

5.4.2. Different strut thickness

Another change in the prototype that has been examined regards the possibility to minimise the thickness of the strut since, previous analysis, has shown that the structure was a little too bulky. Therefore, it has been tried to modify the previous thickness of the strut that was equal to 12 mm in order to reduce it. Two cases have been analysed, the first one with a 10 mm thick rod and the second one with an 8 mm thick rod.
In Fig. 49, the distributions of Von Mises stresses obtained from the simulations of the rods with 10 mm and 8 mm thicknesses are shown. The maximum stress value obtained in the simulation of the thinner strut is higher than that of the medium-thickness strut and, as expected, higher than that of the strut with the initial thickness value. As expected, the most stressed area in these two cases also remains located in the M10 pin but, in both cases, the yield strength has not been exceeded.

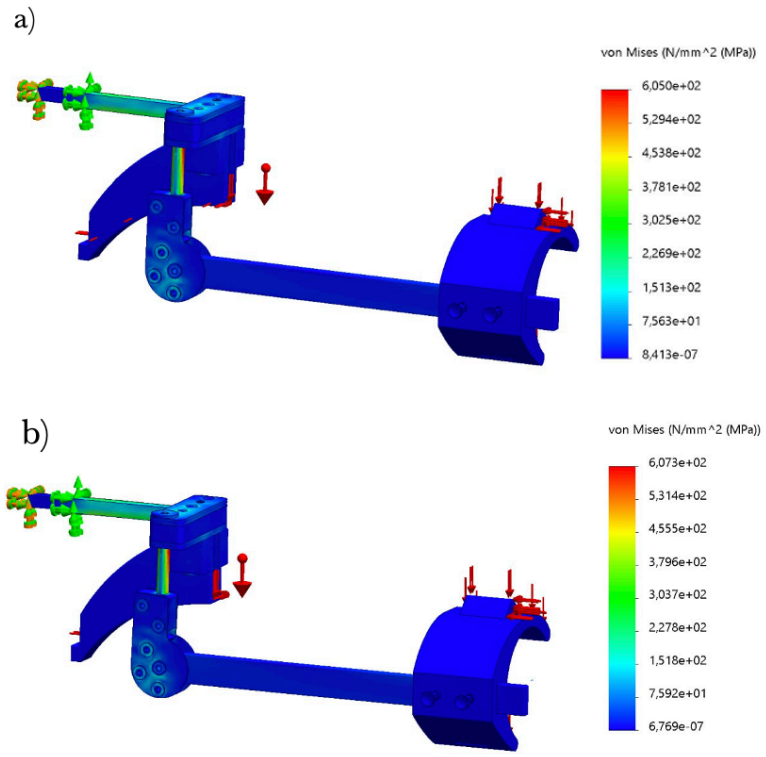

Figure 49: Von Mises stresses: a) 10mm-thick strut; b) 8mm-thick strut

In Fig. 50, a detailed view of the displacement magnitude that have been obtained by the simulation is shown.

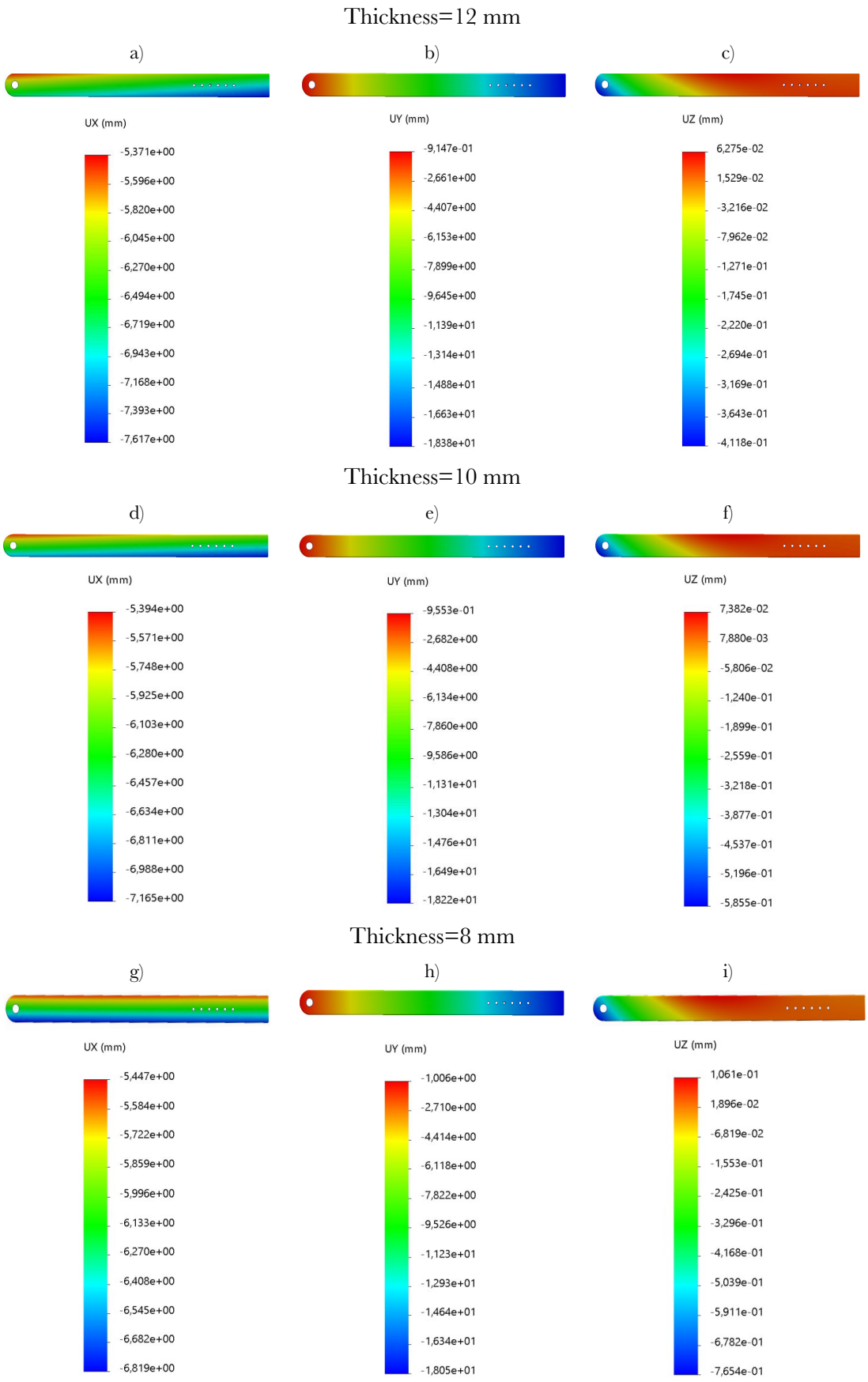

Figure 50: Detailed view of the displacement magnitudes on the three different struts in x, y and z directions

In particular the cases (a), (b), (c) refer to the strut with the initial thickness value equal to 12mm and are respectively the displacements in the x, y and z direction, similarly (d), (e), (f) are the displacements for the medium-thickness strut and (g), (h) and (i) are the displacements for the thinner strut.
For all three struts the minimum displacement values occur in the z-direction in which the entity of the displacement does not exceed the millimeter unit. This is likely due to the presence of the constraint located in the inner bracelet surface, which prevent the movement of the bracelet in the z-direction, simulating the force of the arm of the user acting on the bracelet. Regarding the displacement in the x-direction it noticeable that by comparing the figures (a), (d) and (g) in the (g) the magnitude of the displacement that affects the upper part of the strut in absolute value is higher than in the other two cases. Also, the distribution area of the maximum value of displacement is wider in the thinner strut and it is possible to see that by decreasing the thickness value in all three cases, the extent of the area gradually increases. The maximum absolute values of displacements are in y-direction for all three strut and the value is approximately equal to 18mm, thus showing no significant variation.

Chapter 6

Back frame modifications

With a view to facilitating the wearability and adjustment of the exoskeleton, an attempt has been made to modify the back frame adjustment mechanism and also to replace the harness currently in use. As far as the harness currently in use is concerned, the main problems relate to its weight, which is quite heavy and, considering that one of the limitations of the current structure is precisely its weight, surely trying to find a lighter harness could certainly allow for a substantial improvement. Furthermore, another problem with the exoskeleton's harness is related to the donning phase as the presence of the leg loops makes the operation more complex. Additionally, the adjustment system is not very quick. The aim of the research is to find a new commercial harness and, consequently, to redesign the CAD structure of the back frame in order to suit the new harness.

6.1. The new harness and back frame modifications

The new harness that has been chosen to replace the previous one is a harness manufactured by Festool and designed to be used with the TG-EXO-18 exoskeleton. The new harness, however, unlike the current one, has a different connection mechanism to the exoskeleton. It was therefore necessary to modify the back frame of the structure in order to adapt it to the requirements of the new harness. The new harness has three connections to the exoskeleton structure: the first connection, the upper one, has two perforated plastic tabs, the second connection is located centrally to the structure and consists of two fabric eyelets, and the third connection is located at the level of the lumbar belt. In order to adapt the structure, therefore, modifications have

been necessary, mainly related to the need to create a new central connection pivot to enable the structure to accommodate the fabric eyelets present in the harness.

For this reason, it was decided to replace the two telescopic tubes, which allow the modification of the exoskeleton's longitudinal length, with a new system featuring a single telescopic tube. Specifically, the system therefore consists of an outer telescopic tube with a rectangular cross-section inside which the inner tube with a square cross-section is inserted. Inside the rectangular tube there is a PLA structure that is specifically molded to act as a guide to allow the complete movement of the square tube in all possible configurations of use, Fig. 51(a). Two brackets have been attached to the sides of the outer telescopic tube, which use carabiners to connect the two fabric eyelets in the harness. In particular, the brackets have been connected by means of two M4 countersunk screws that screw into two specific PLA inserts that are, in turn, inserted into the PLA structure.

Again, with the aim of making the structure's adjustment mechanisms faster and easier, it was decided to replace the screws used for the previous telescopic system with a push-button spring. The hinges previously in use were also removed, as it was seen through FEM analysis that they constituted a stress concentration point and because they represented a non-fundamental part for the functioning of the structure. To connect the telescopic system to the upper part of the back frame, telescope tube terminals were used, which have a centrally threaded hole and thus allow the system to be linked to the exoskeleton via connectors. The detailed view of the connections between the new back-frame structure and the harness is shown in Fig.51(b).

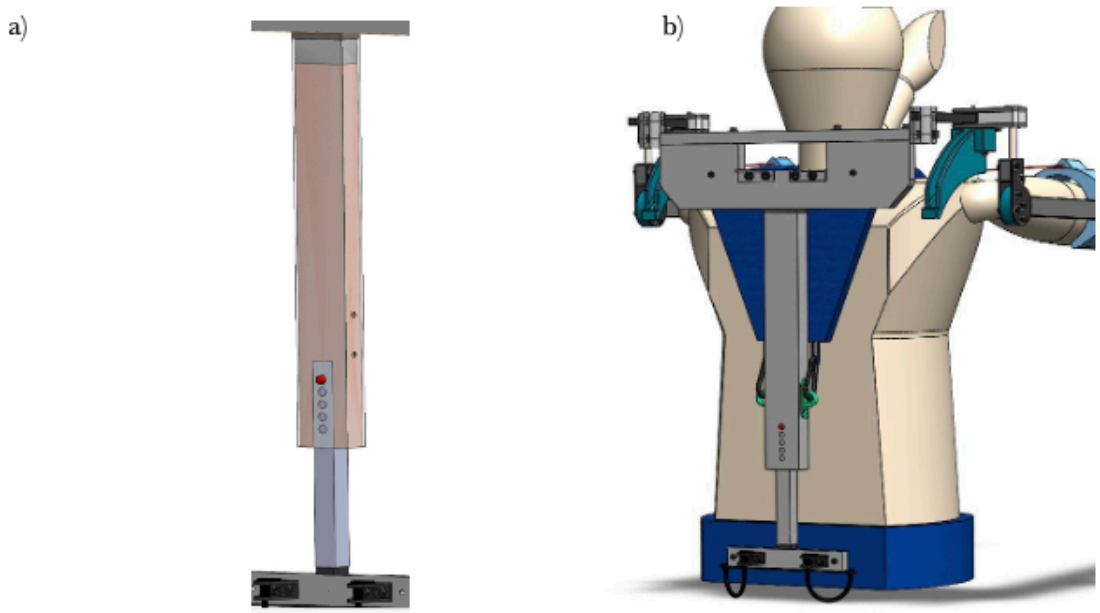

Figure 51: a) Detailed view of the inner part of the telescopic system; b) detailed view of the back-frame/harness connections.

Another change that became necessary has been to modify the upper part of the structure by eliminating the hollow boxes previously present in favor of a new solid structure that allows the plastic tabs of the housing to be screwed onto this new structure. It was also decided to replace the various components previously present in the upper part and design a single replacement in their place, which avoids the excessive number of superfluous connectors.

6.2. FEM Analysis

Even in this case a FEM Analysis has been carried out in order to evaluate the stresses and displacement to which the structure is subjected. The structure has been tested in the same conditions that have been described in the paragraph 5.2, namely, in the most binding working conditions.
As in the previous chapter, the materials, constraints, loads and connections that had to be set for the FEM analysis will now be analyzed.

6.2.1. FEM Materials

The materials that have been used for the back frame components, Fig.52, are respectively:

- PLA: used for the structure placed inside the two telescopic tubes;
- Stainless steel DIN.14301 X5CrNi18-10 (or AISI 304): used for the internal bar of the telescopic system (1), that allows the regulation of the transversal length of the exoskeleton, for the L-shaped plates both of the upper and of the lower part (2), to which the PAMs are connected, for the bracket (3) and, finally, used for the part connected with the two U-shaped cables (4);
- Aluminum EN AW-6060-T6: used for the external telescopic system that allows the regulation of the transversal length of the exoskeleton (5) and also for the tubes of the telescopic system for the regulation of the longitudinal length (6) , for the lower bar that connects to the lumbar belt (7) and also for the upper plate (8);
- Alloy steel 8.8: used for all the connectors;
- Brass: used for the insert for PLA;
- Alloy steel AISI 316: used for the push-button spring (9);
- Nylon 6/10: used for the terminals of the telescopic tubes (10).

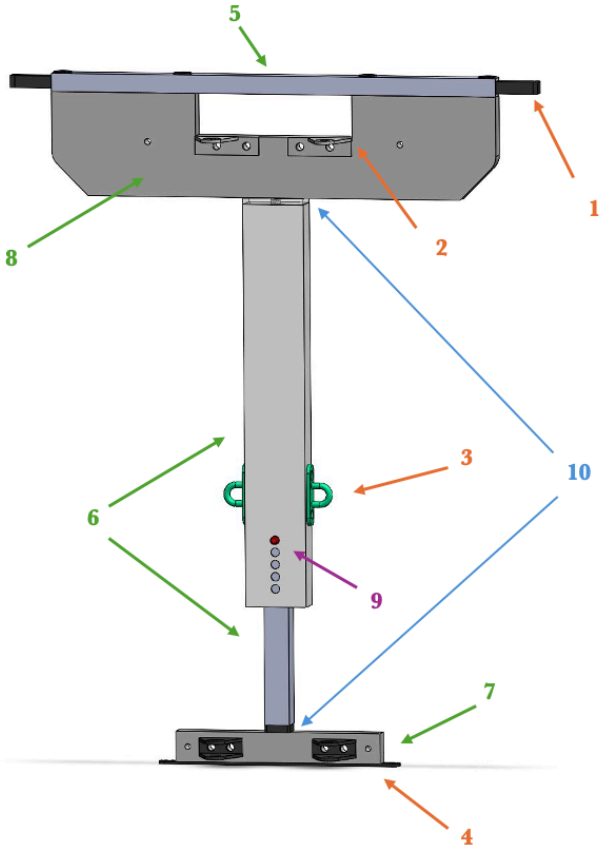

Figure 52: a) CAD structure of the new back frame telescopic system: : in orange the AISI 304 components; in green the aluminum components; in purple the AISI 316 component; in blue the Nylon 6/10 components.

For the materials above-mentioned have been made the same assumptions described in paragraph 5.2.1, and also the mechanical characteristics of the materials are the same that are reported in Tab.7.
In Tab.8 the mechanical the characteristics of materials not previously mentioned are listed.

Table 8: FEM materials mechanical characteristics

	E (MPa)	ν	G (MPa)	Sy (MPa)	Sut (MPa)
AISI 316	200000	0.3	77000	400	700
Nylon 6/10	26000	0.35	960	47	75

6.2.2. Loads, connectors and constraints

Subsequently, load and connectors have been applied to the structure and also the connector have been modelled, as can be seen in Fig.53.

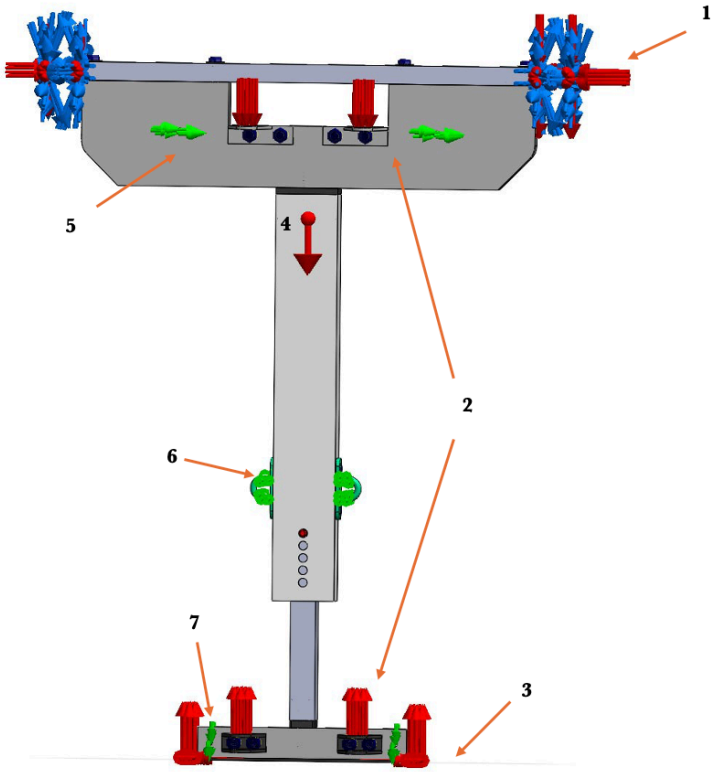

Figure 53: Back frame modelling with loads, torsions constraints and connectors

The reference axes are oriented with x-axis in the medio-lateral direction, y-axis in the craniocaudal direction and z-axis in the anteroposterior direction. The results of the forces obtained from the exo-arm simulations were applied to the inner rod of the telescopic system to adjust the biacromial distance. The load magnitudes have been evaluated considering the static equilibrium on the back frame in which have been also considered the reaction forces applied to the pelvic and the thorax belts.
Loads, that are represented in Fig.52 by the red arrows, were applied in the form of pressures.
The loads applied to the structure are located:

- On the right and left bars that connect the upper part of the back frame to the exo arms (1). The force simulates the load exchanged between the back frame and the exo arms.
  The values are equal to 0.11 MPa in x-direction, 0.52 MPa in y-direction and 0.02 MPa in z-direction for the right bar. While for the left bar the values are and

-0.051 MPa in x-direction, -0.25 MPa in y-direction and 0.013 MPa in z-direction;

- On the L-plates, that simulate the traction force of the MKMs (2). These are applied in the y direction and the value, in the right part, is equal to 4.33 MPa, while in the left is equal to 2.05 MPa. In both cases the loads have to be applied in the upper and in the lower structure with opposite verses;
- In the holes in which the cables pass after the two curves, that simulate the cable traction forces (3).
  The values for the right part are equal to 0.29 MPa in x-direction, -6.3 MPa in y-direction and 1.28 MPa in z-direction. While, for the left part the values are equal to 0.14 MPa in x-direction, -2.99 MPa in y-direction and 0.61 MPa in z-direction.

On the bars that connects the upper part of the back frame with the angular joints have also been applied the torsions, that are represented in Fig.52 by blue arrows, in the same locations of (1). Their values are equal to:

- On the right bar: M_x =-44.9 Nm; M_y =6.8 Nm and M_z = 13 Nm;
- On the left bar: M_x =-22.3 Nm; M_y =-3.3 Nm and M_z = 6.1 Nm.

It has also been applied the gravitational load that is applied to the center of gravity of the structure (4).

The constraints are represented by the green arrows in Fig.52. With regard to the constraints applied to the structure, in comparison to the previous case it must be considered that there is an additional constraint at the brackets level. In order to better evaluate the new configuration, three different cases of constraint setting were evaluated for the three connection zones: upper, the holes in which to screw plastic tabs of the harness (5), middle, the brackets in which to connect the fabric eyelets (6) and finally lower, the bar in which to start the lumbar belt (7).
The three cases analyzed are from the different directions of the constraints:

- 1st case: upper → mid-lateral, middle → antero-posterior, lower → cranio-caudal;
- 2nd case: upper → antero-posterior, middle → antero-posterior, lower → cranio-caudal + mid-lateral;
- 3rd case: upper → antero-posterior + medial-lateral, middle → antero-posterior, lower → cranio-caudal+ medial-lateral.

With regard to the connectors, they are all class 8.8, and for each has been defined a certain value of preload based on the dimension of the connector.

Finally, the structure has been discretized using a tetrahedral mesh, reported in Fig.54.

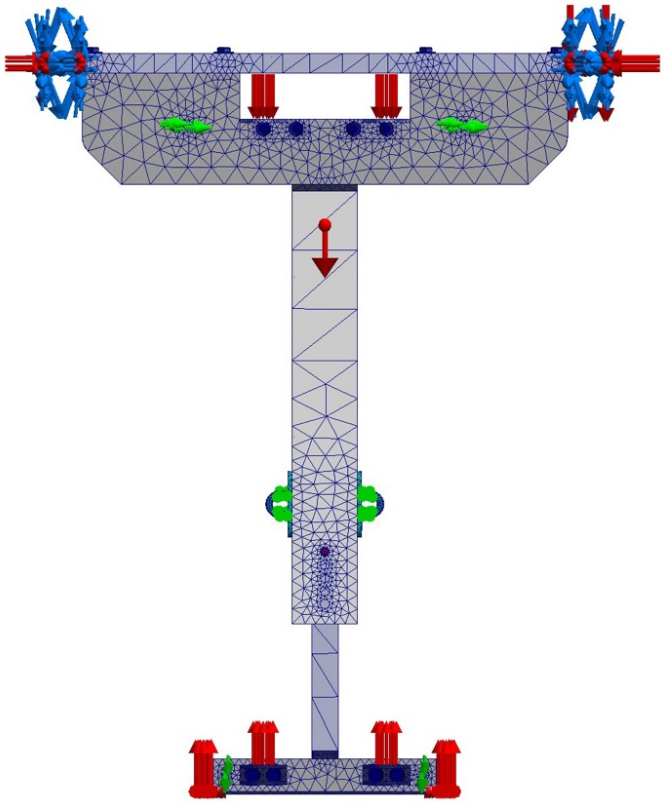

Figure 54: Back frame mesh

6.3. Simulation results

The result of the simulations that will be discussed regards the first constraints configuration since it has shown the most demanding conditions.
The results of the structure will be discussed in terms of stresses and displacements. The stresses that are applied to the back frame are shown in Fig.55(a) , the maximum value of the Von Mises stress is applied in the inner bar of the longitudinal telescopic system that allows the adjustment of the biacromial distance, Fig.55(c). This component is made of stainless steel, so its value of yield strength is equal to 640 MPa, while the maximum value of Von Mises stress is equal to 324.7 MPa so the yield strength has not been exceeded. Since the difference in the magnitude of yield strength between stainless steel and aluminum in Fig.55(b) are shown the entities of the stresses that act upon the aluminum components and, also in this case, the yield strength has not been exceeded.

As expected, the most stressed part of the structure is the right one since is the part in which the force values are bigger.

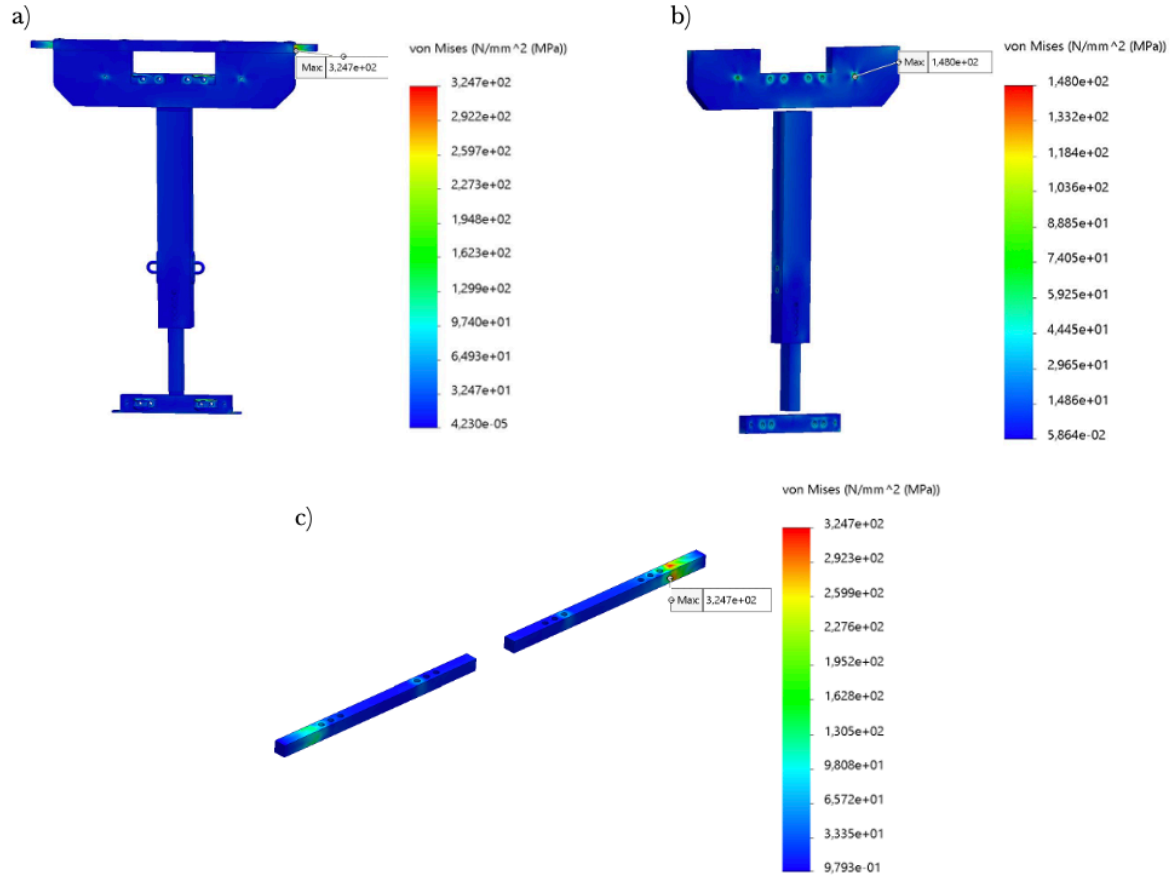

Figure 55: Von Mises stresses simulation results: a)complete structure; b) detailed views of the connecting holes in the aluminum components; c) detailed view of the inner bars of the telescopic system

The results of the displacements magnitudes obtained from the simulations are shown in Fig.56. As it is possible to see in the figure, the values of the displacements do not exceed the order of the millimetre for both the x and the y-direction. Only in the z-direction, the maximum value of displacement in absolute value reaches 1.658 mm, so the maximum displacement occurs in the anteroposterior direction in the upper part of the structure. Nevertheless, the entity of the displacement is, anyway, negligible.

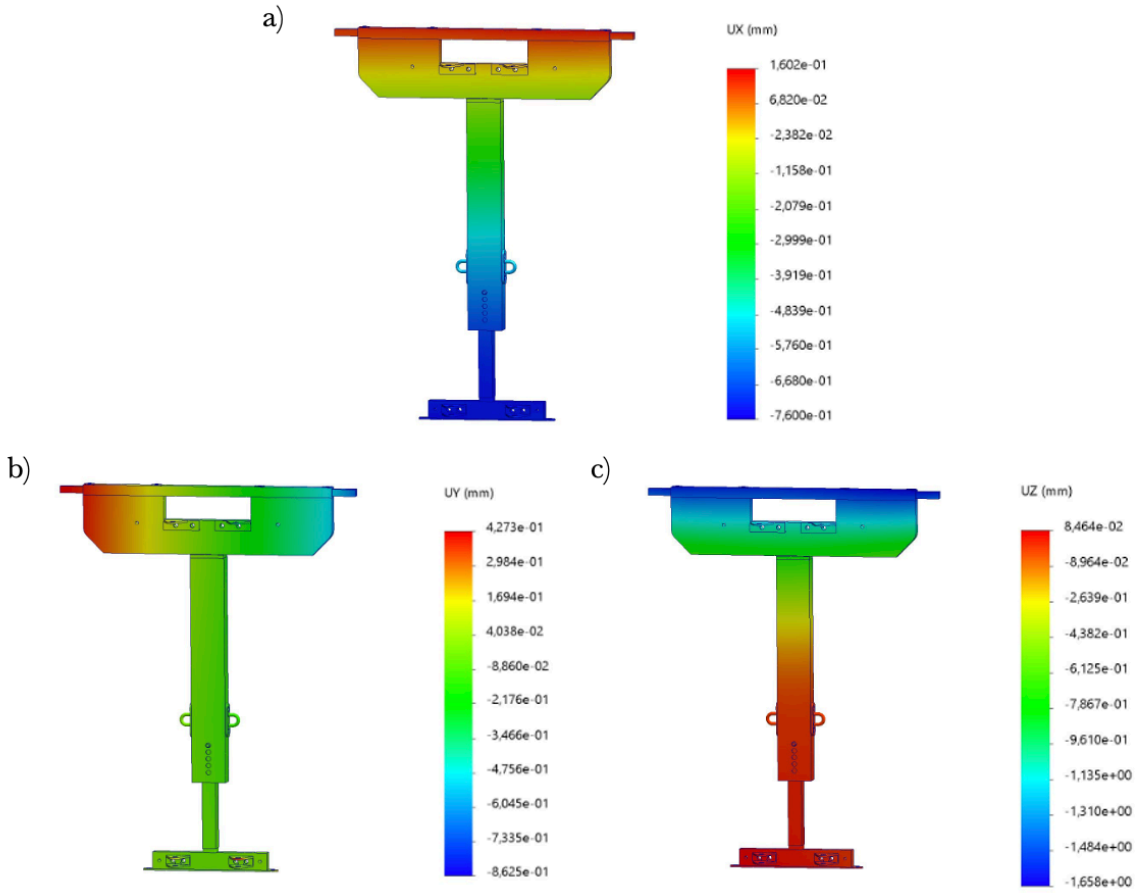

Figure 56: Displacement magnitudes in the Back frame: a) displacement in the x-direction; b) displacement in the y-direction; c) displacement in the z-direction.

Chapter 7

New Exo-design: supplementary analyses

7.1. New Exo-structure

The complete rendering of the CAD model of the redesigned structure is shown in Fig.57.

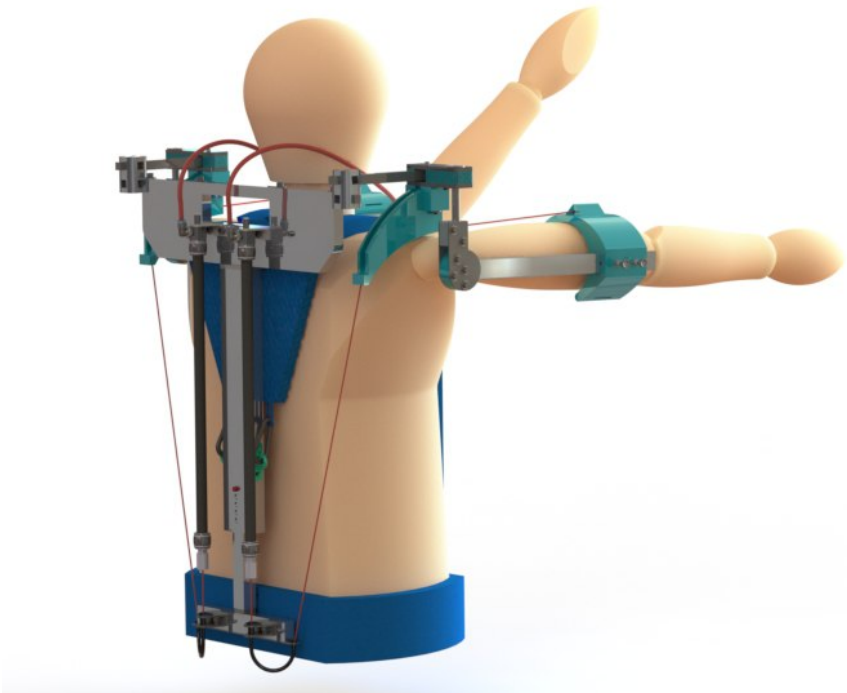

Figure 57: Final render CAD structure with all the previous discussed modifications

Since the tests carried out have been successful, work is underway to produce a prototype with all the modifications described in the previous chapters. The dimensioned technical drawings of the components to be built have been produced, Fig. 58, Fig.59 and Fig.60.

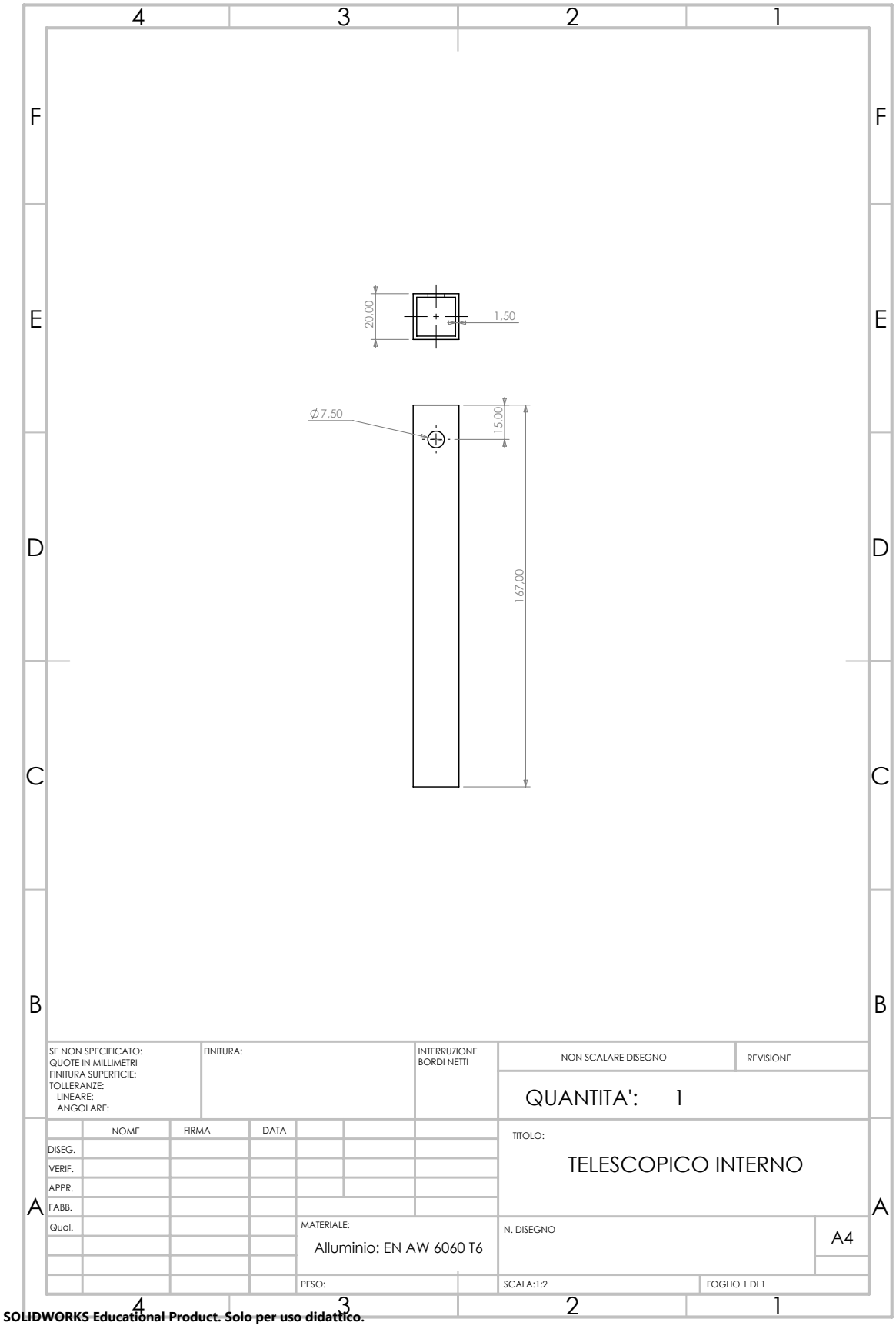

Figure 58: Dimensioned technical drawings of the inner telescopic tube

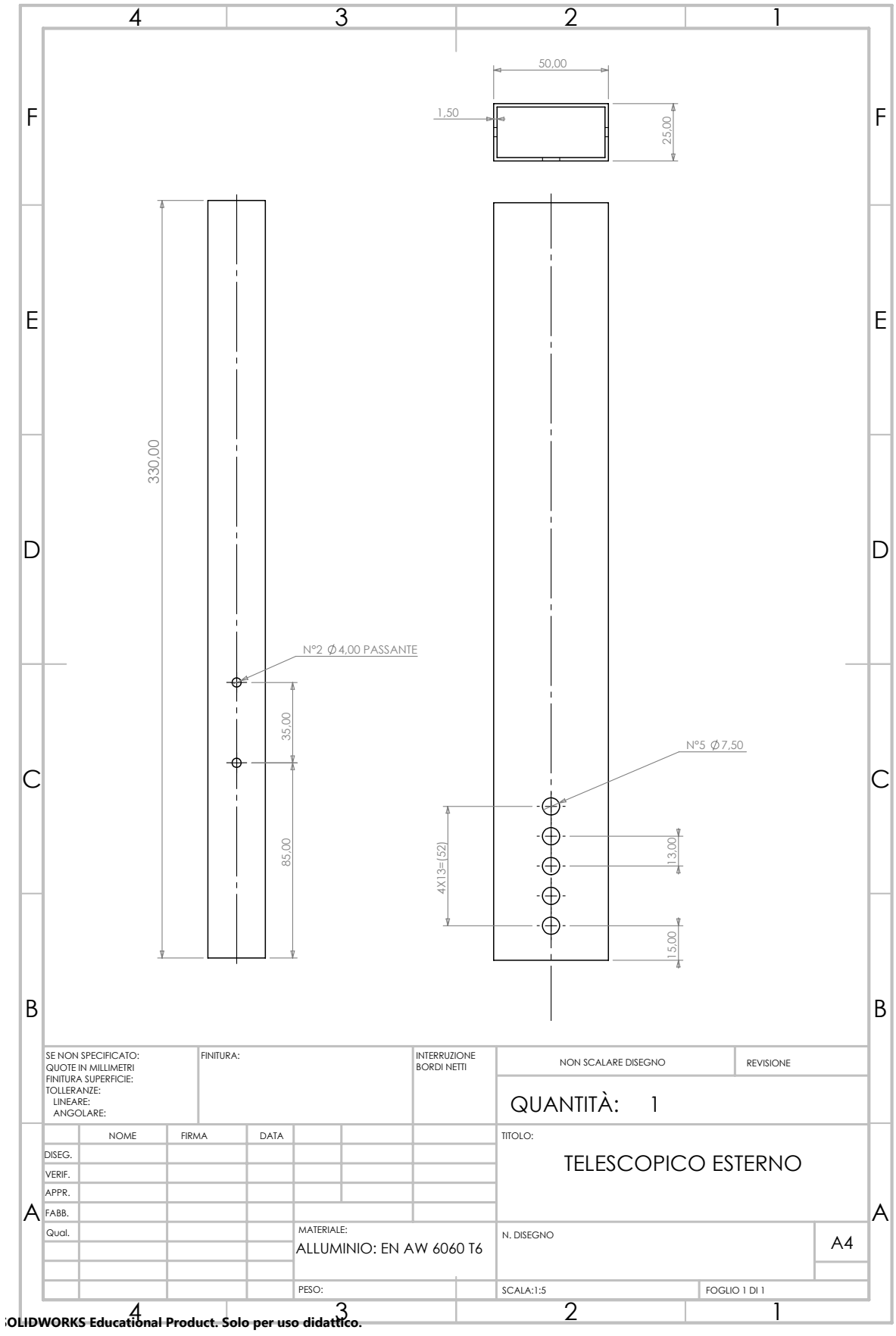

Figure 59: Dimensioned technical drawings of the outer telescopic tube

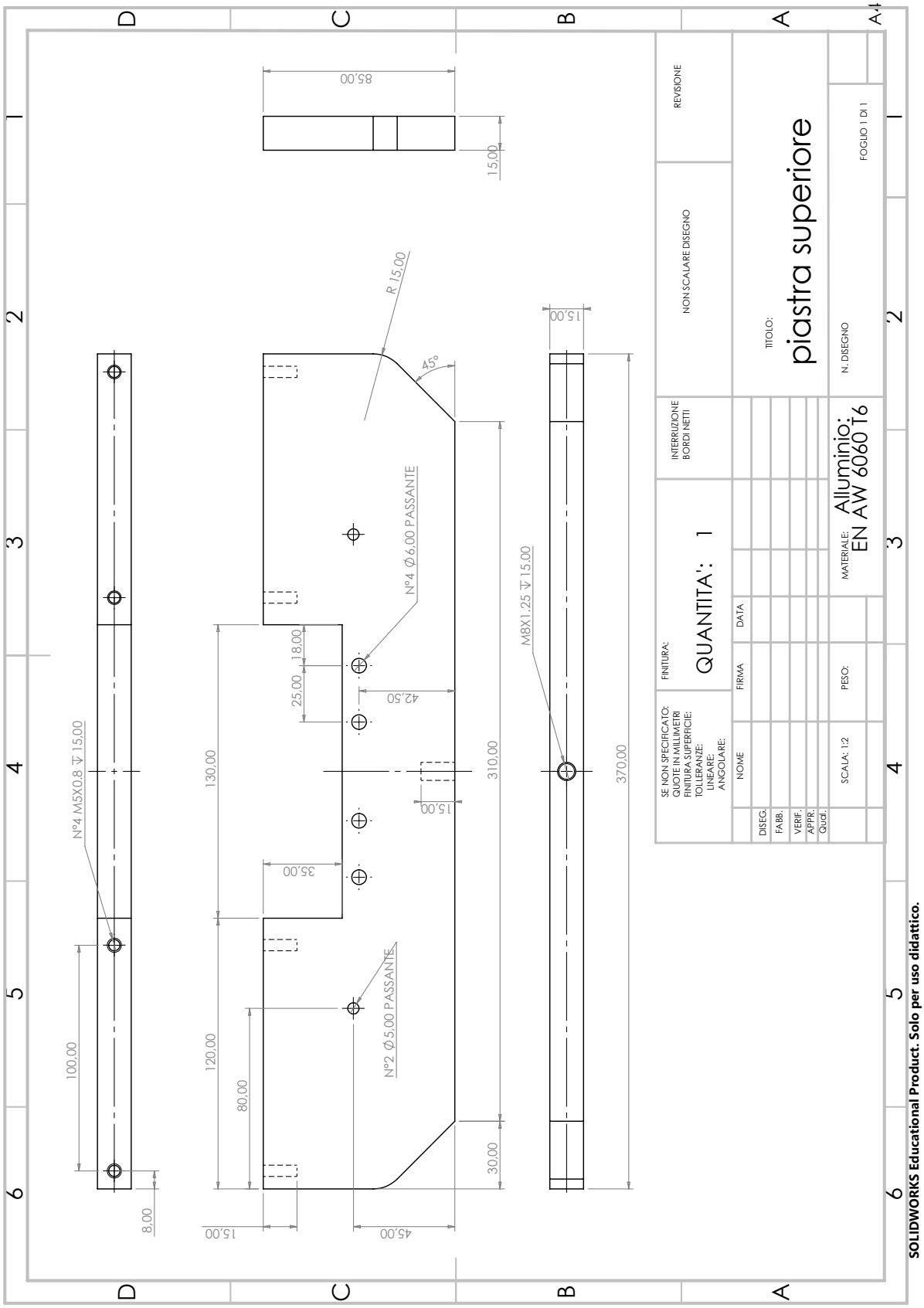

Figure 60: Dimensioned technical drawings of the upper plate of the back frame

In the following table are also reported all the commercial components that have been chosen for construction of the new prototype:

Table 9: List of commercial components and suppliers

Component	Quantity	Supplier	Product Code
Exo Arm			
Threaded inserts	4	Special Insert	850 0060.80
Spacer bushings	4	Elesa	GN.70201
Plungers	4	Elesa	GN.37309
Back Frame			
Rectangular end cap (50x25-M8)	1	ISC	00700800169
Square end cap (20x20-M8)	1	Misumi	320011
Mounting hook	1 pack (2 pcs)	Misumi	TPD-5
Quick spring plunger	1	Special Insert	QS02/22
Quick spring plunger	1	Special Insert	QS01/19
Threaded inserts	4	Special Insert	850 0040.80
Threaded inserts	4	Special Insert	604/C
Carabiners	2	Misumi	B-1135-5

7.2. Supplementary analyses

In order to appropriately assess the functioning of the structure, in addition to the FEM results discussed in the previous chapters, further analyses have been carried out. This is because FEM analyses show only the results of the stresses to which the structure is subjected and do not consider the effects on the user. Since the exoskeleton is a structure that, throughout its operation, comes into direct contact with the human body, it is also necessary to evaluate how the device and the subject reciprocally interact. For this purpose and considering that the main requirement for an exoskeleton is safety, the pressures to which the subject is subjected during use of the exoskeleton have been evaluated. Additionally, the response of the structure to misalignments of the shoulder joint center has also been analyzed.

7.2.1. Estimation of contact pressures on subject's body

As mentioned above, it is essential to assess the effects of the exoskeleton's presence on both the safety of the subject and the prevention of discomfort during use, especially considering that the exoskeleton must be worn for extended periods of operation. The evaluation of contact pressures has been performed through an analytical approach, in accordance with previous studies conducted in literature [68]. The three interfaces between the exoskeleton and the subject are, respectively, the bracelet, the pelvic belt and the thoracic belt. The aim of the investigation was, therefore, to compare the results of the stresses that occur on the subject with values obtained from the literature that define pain detection thresholds (PDTs) [69] [70]. To evaluate the magnitude of the pressures that act on the human body the contributions of both the gravitational and support torques have to be considered. With regard to the gravitational torque, both the contribution of the gravitational force due to the weight of the subject's own limb and the load resulting from the possible presence of tools in the hand must be considered. To calculate the gravitational force, the user's arm has been approximated to a rigid link with the mass centered at its center of mass. As far as the contribution given by the muscular effort is concerned, two contributions have been distinguished: the first related to the effort that the muscles make to maintain the appropriate flexion angle, θ_f, and thus correct the mismatch between gravitational force and support force, while, the second contribution, is related to the effort to maintain the ideal abduction angle, θ_a. The simulations have been evaluated through Matlab_R2024a, considering a 1.7 m tall subject, weighing 70 kg and in three different load conditions. In all the three cases the subject held a 2 kg load in the right hand but, in the first case, there is no tool in the left hand, in the second one, a 1 kg load is present in the left hand and finally, in the third case, a 2 kg load is present in both hands. In order to assess the contact pressures on the subject, it was necessary to define the anthropometric measurements in order to determine the length of the various body segments and their weights. From this information, the overall resultant of the gravitational torque, determined by the weights of the various body districts, have been calculated. The possible presence of a tool has also been considered in the calculation, so as to analyze how the contact pressures vary according to the different applied loads. Subsequently, the contribution of the forces generated by McKibben's pneumatic muscles has been assessed. For each side of the body, the force exerted by the PAMs has been calculated, taking into account that the weight applied to the arms could be different. Then, the contribution of the forces exchanged between the arm and the cuff has been analyzed, considering in the sagittal plane both the distribution of the applied weight forces and the action of the user's

muscles, which compensated for the mismatch between gravitational torque and support torque. For the calculation of the contact pressure application surfaces at arm level, the measurements of the CAD model of the cuff were used.

Finally, the static equilibrium at the structure has been calculated to estimate the forces at the level of the back frame. After the dimensions of the interface surfaces between the harness and the user have been measured, the contact pressures on the pelvis and thorax have been evaluated.

To evaluate whether the stresses acting on the subject are excessive, the pressure values have been compared to the PDTs of each area analyzed. In Fig.61 the results for each case are shown. Obviously, as can be seen in the figure, increasing the load in each hand consequently the pressure levels applied to the subject also increase. This is also because, as the load in the hands increases, the pressure level at which each PAM must be pressurized also increases, leading to higher pressures applied on the user.

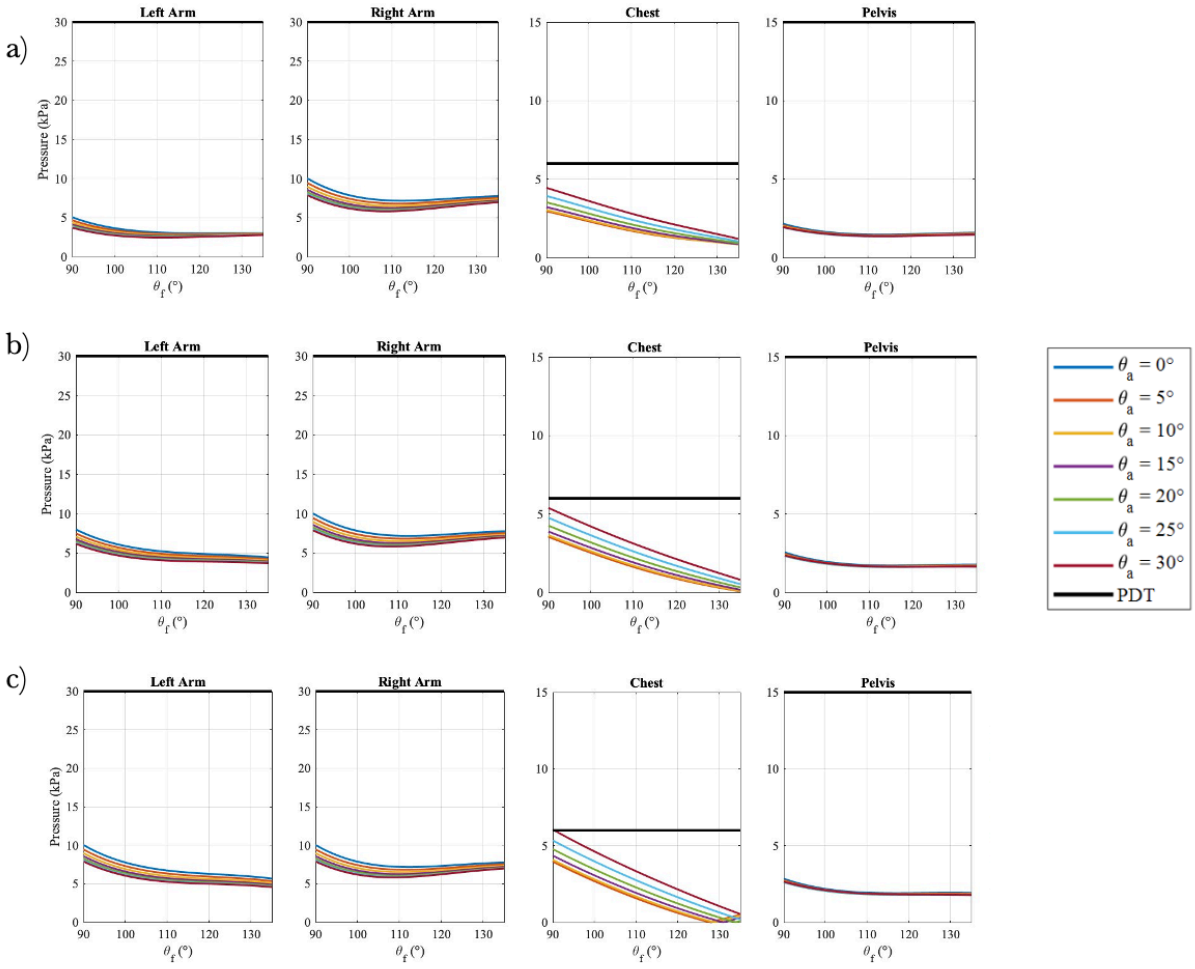

Figure 61: Pressure magnitude on the subject: a) 2kg in the right hand – 0kg in the left hand; b) 2kg in the right hand – 1kg in the left hand; c) 2kg in both hands.

The results reflect the previous findings obtained from the preceding prototype study [68], there are no particularly significant differences.
In all three cases, the pressure levels do not exceed the PDT, so it can be concluded that the structure under consideration is safe and does not generate discomfort for the user.

7.2.2. Impact of misalignments between SJC and EXOJC on performance

As previously discussed in section 1.2.1, one of the most significant challenges in upper-limb exoskeleton design is related to the SJC movement. This occurs because the movement of the SJC causes misalignments between the center of the shoulders and the joint center of the exoskeleton and these can result in discomfort, pain and, in the worst cases, may lead to dislocations and fractures. In particular, the prototype under consideration is a 2 DOFs exoskeleton, meaning that the structure is less bulky but, at the same time, is more susceptible to misalignment issues. Within the considered working range, the magnitude of the displacement of the SJC is equal to 2.8 cm upwards and 0.3 cm in the mediolateral direction, so the latter can be neglected [26], [68]. The analysis and quantification of misalignments have been performed following the methodology outlined in [71]. Specifically, the evaluation considers the impact of misalignments in terms of the effectiveness of the support torque in compensating for the gravitational torque. The ratio of gravitational torque to support torque was evaluated by varying the shoulder elevation angle, θ_1, and the elbow flexion angle, θ_2. Since the exact position of the SJC is unknown, eight initial positions of the ExoJC have been considered. The initial positions are scattered around a circumference in which the SJC is centered as shown in Fig.62.

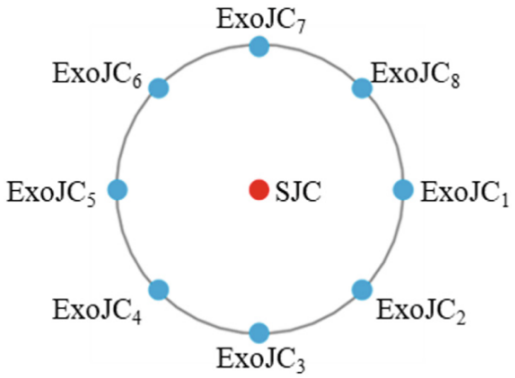

Figure 62: Locations of the ExoJC initial positions [71]

The aim of the analysis is to understand in which cases the exoskeleton adequately supports the work of the user.

The simulation has been performed using Matlab. To conduct the analysis, first, the movement of the SJC has been evaluated by examining the abduction movement of the shoulder between 0 and 180°. Both the gravitational moment and the support torque generated by the exoskeleton have been calculated. The moment exerted by the exoskeleton has then been assessed considering the misalignment between ExoJC and SJC. Finally, the magnitude of the misalignment effects, expressed as the ratio of support torque to gravitational torque, has been estimated. In Fig.63, the results of the analysis are shown.

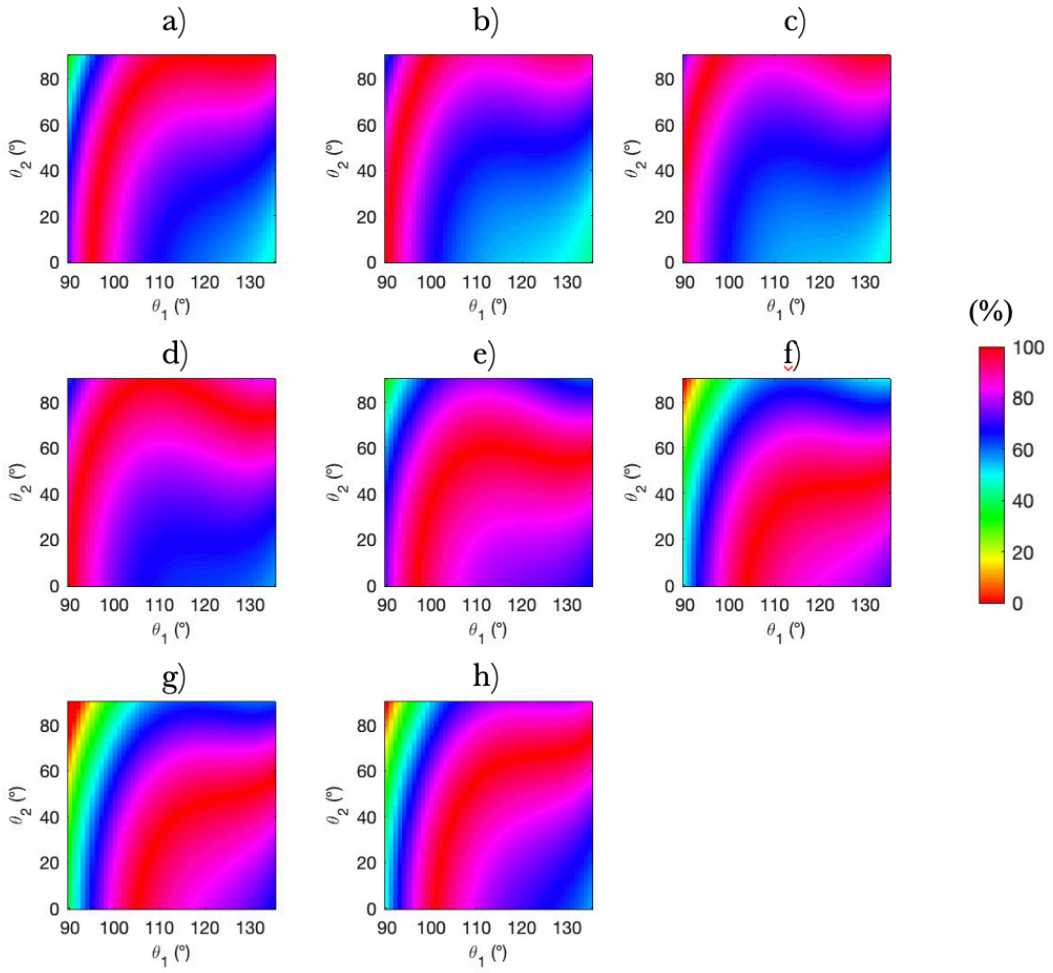

Figure 63:Percentage of support given by the assistive torque with respect to the gravitational torque in the previous described initial positions: a) ExoJC$_1$; b) ExoJC$_2$; c) ExoJC$_3$; d) ExoJC$_4$; e) ExoJC$_5$; g) ExoJC$_6$; f) ExoJC$_7$; g) ExoJC$_8$.

As shown in the previous figure, the optimal configuration, in which the ratio between gravitational and support torque is closest to 100%, indicates that the assistive torque effectively compensates for all the gravitational torque. These optimal positions occur when the initial ExoJC is below the SJC, considering the positions shown in Fig.62. In the cases where the assistive torque is lower than the gravitational torque, the support

provided is insufficient, requiring the user to exert additional effort to perform the movement. Conversely, if the assistive torque exceeds the gravitational torque, the user must exert force to push the arm downward to maintain a specific position, increasing the load on the shoulder flexor muscles. This situation is as ineffective as the previous one since requiring the user to exert effort to either raise or lower the arm leads to fatigue. Therefore, in both cases, the support provided by the exoskeleton is not adequate for its intended purpose. This situation is shown in the cases (f), (g) and (h) where the ExoJC is positioned above the SJC. In these cases, in fact, when both θ_1 and θ_2 are equal to 90° the percentage of the ratio is much greater that 100%.

Comparing the results of the current study on misalignment effects with previous analyses conducted on the previous structure [71], it can be seen that the differences are not particularly pronounced. In general, it can be said that the areas where the gravitational and support pairs are equal, are shifted to smaller values of θ_2 , and this trend is visible in all graphs. Also, the results obtained on this prototype in the cases (f), (g) and (h) have shown the same behaviour of once obtained in the previous structural analyses.

Chapter 8

Conclusions and future developments

The problem related to WMSDs has yet to be solved, as it has been observed how frequently it afflicts industrial workers and the damage it can cause to their health. Given that a major cause of WMSDs is related to overhead work, it is imperative to find a solution that supports the worker so that no shoulder discomfort occurs.
The last decade has seen a significant momentum towards the development and modernization of exoskeletons, which one possible application is the industrial sector. These are wearable devices that can help the worker by decreasing the muscular effort required to perform a procedure or even eliminating it altogether. In particular, exoskeletons for upper limbs are particularly suitable when the objective is to prevent shoulder disorders. For industrial use, the best alternative is passive exoskeletons, as they usually have a less bulky structure, use simple mechanical elements, do not require an actuator, are more flexible, and can operate in remote locations for long hours.
The main subject of this thesis is a passive upper limb exoskeleton that operates using two McKibben muscles, i.e., artificial pneumatic muscles that generate a support torque counteracting the gravitational torque produced by both the weight of the user's limb and the possible presence of tools. In order to improve some of the problems that emerged in previous studies of the prototype under consideration, several tests were carried out with the final aim of improving the usability of the device. Primarily, the possibility of inserting a pneumatic circuit allowing the pressurization of the McKibben muscles by the user himself was evaluated, granting more autonomy to the user. The functioning of this structure was validated by means of a leakage test, which ascertained that there were no significant leaks in the circuit that could affect the functioning of the structure.
Subsequently, the focus was placed on the position adjustment mechanism located on the exo-arm cuff. The previous mechanism was replaced with a new one based on the

use of indexing plungers that make the mechanism easier to adjust. Other possible modifications to the exo-arm were also evaluated, such as thinning the strut and using only one indexing plunger to make the structure less bulky. Additionally, with the aim of making the structure lighter, the previous harness was also modified in favour of a new one that is lighter and easier to adjust. To make this change, it was necessary to modify the attachment mechanism and thus the interface between the harness and the back frame. To evaluate the function of the structures that were modified, FEM analyses were carried out using SolidWorks software, firstly the CAD models of the structures were made and then, using SolidWorks Simulation, static analyses were conducted. The analyses showed that the yield strengths of each material were not exceeded in any case. Of course, there are other aspects of the structure that could be improved, such as modifying it to allow the user to lower the arms more easily by implementing a disengagement mechanism, reducing the overall weight by selecting new materials with the same mechanical properties but lower weight, or modifying the structure to minimize the misalignment between the SJC and the ExoJC. Since the new prototype, incorporating all the modifications discussed in this thesis, is already in development, with components being sourced and customized parts being manufactured, future work will focus on constructing the structure properly to enable experimental testing. This would allow an applied evaluation of all the advantages that have been analysed for improving the usability of the device.

References

[1] J. Nassour, G. Zhao, and M. Grimmer, “Soft pneumatic elbow exoskeleton reduces the muscle activity, metabolic cost and fatigue during holding and carrying of loads,” *Sci Rep*, vol. 11, no. 1, p. 12556, Jun. 2021, doi: 10.1038/s41598-021-91702-5.

[2] M. K. Constand and J. C. MacDermid, “Effects of neck pain on reaching overhead and reading: a case–control study of long and short neck flexion,” *Sports Medicine, Arthroscopy, Rehabilitation, Therapy & Technology*, vol. 5, no. 1, p. 21, Dec. 2013, doi: 10.1186/2052-1847-5-21.

[3] M. R. Islam, C. Spiewak, M. H. Rahman, and R. Fareh, “A Brief Review on Robotic Exoskeletons for Upper Extremity Rehabilitation to Find the Gap between Research Porotype and Commercial Type,” *Advances in Robotics & Automation*, vol. 06, no. 03, 2017, doi: 10.4172/2168-9695.1000177.

[4] N. Jia *et al.*, “Epidemiological Data of Work-Related Musculoskeletal Disorders — China, 2018–2020,” *China CDC Wkly*, vol. 3, no. 18, pp. 383–389, 2021, doi: 10.46234/ccdcw2021.104.

[5] J. Liang *et al.*, “Shoulder work-related musculoskeletal disorders and related factors of workers in 15 industries of China: a cross-sectional study,” *BMC Musculoskelet Disord*, vol. 23, no. 1, Dec. 2022, doi: 10.1186/s12891-022-05917-2.

[6] S. T. Bennett *et al.*, “Usability and Biomechanical Testing of Passive Exoskeletons for Construction Workers: A Field-Based Pilot Study,” *Buildings*, vol. 13, no. 3, p. 822, Mar. 2023, doi: 10.3390/buildings13030822.

[7] R. Govaerts *et al.*, “Prevalence and incidence of work-related musculoskeletal disorders in secondary industries of 21st century Europe: a systematic review and meta-analysis,” *BMC Musculoskelet Disord*, vol. 22, no. 1, Dec. 2021, doi: 10.1186/s12891-021-04615-9.

[8] M. Cenciarini and A. M. Dollar, “Biomechanical considerations in the design of lower limb exoskeletons,” in *2011 IEEE International Conference on Rehabilitation Robotics*, IEEE, Jun. 2011, pp. 1–6. doi: 10.1109/ICORR.2011.5975366.

[9] J. L. Pons, Ed., *Wearable Robots*. Wiley, 2008. doi: 10.1002/9780470987667.

[10] J. A. de la Tejera, R. Bustamante-Bello, R. A. Ramirez-Mendoza, and J. Izquierdo-Reyes, “Systematic Review of Exoskeletons towards a General Categorization Model Proposal,” *Applied Sciences*, vol. 11, no. 1, p. 76, Dec. 2020, doi: 10.3390/app11010076.

[11] S. Christensen and S. Bai, “Kinematic Analysis and Design of a Novel Shoulder Exoskeleton Using a Double Parallelogram Linkage,” *J Mech Robot*, vol. 10, no. 4, Aug. 2018, doi: 10.1115/1.4040132.

[12] B. Kim and A. D. Deshpande, “An upper-body rehabilitation exoskeleton Harmony with an anatomical shoulder mechanism: Design, modeling, control, and performance evaluation,” *Int J Rob Res*, vol. 36, no. 4, pp. 414–435, Apr. 2017, doi: 10.1177/0278364917706743.

[13] E. Carmeli, S. Peleg, G. Bartur, E. Elbo, and J. Vatine, “HandTutor enhanced hand rehabilitation after stroke — a pilot study,” *Physiotherapy Research International*, vol. 16, no. 4, pp. 191–200, Dec. 2011, doi: 10.1002/pri.485.

[14] S. Kim, M. A. Nussbaum, M. I. Mokhlespour Esfahani, M. M. Alemi, B. Jia, and E. Rashedi, “Assessing the influence of a passive, upper extremity exoskeletal vest for

tasks requiring arm elevation: Part II – 'Unexpected' effects on shoulder motion, balance, and spine loading," *Appl Ergon*, vol. 70, pp. 323–330, Jul. 2018, doi: 10.1016/j.apergo.2018.02.024.
[15] S. Christensen, S. Rafique, and S. Bai, "Design of a powered full-body exoskeleton for physical assistance of elderly people," *Int J Adv Robot Syst*, vol. 18, no. 6, Nov. 2021, doi: 10.1177/17298814211053534.
[16] M. A. Gull, S. Bai, and T. Bak, "A Review on Design of Upper Limb Exoskeletons," *Robotics*, vol. 9, no. 1, p. 16, Mar. 2020, doi: 10.3390/robotics9010016.
[17] S. J. Hall, *BASIC BIOMECHANICS*, 7th ed. McGraw-Hill Education, 2015.
[18] M. A. Williamson, "A review of the coracoclavicular joint: Description, etiology, and clinical significance," *Clinical Anatomy*, vol. 36, no. 5, pp. 715–725, Jul. 2023, doi: 10.1002/ca.24040.
[19] C. McCausland, E. Sawyer, B. J. Eovaldi, and M. Varacallo, *Anatomy, Shoulder and Upper Limb, Shoulder Muscles*. 2024.
[20] Ł. Jaworski, R. Karpiński, and A. Dobrowolska, "BIOMECHANICS OF THE UPPER LIMB," *Journal of Technology and Exploitation in Mechanical Engineering*, vol. 2, no. 1, pp. 56–59, Dec. 2016, doi: 10.35784/jteme.517.
[21] W. Bakhsh and G. Nicandri, "Anatomy and Physical Examination of the Shoulder.," *Sports Med Arthrosc Rev*, vol. 26, no. 3, pp. e10–e22, Sep. 2018, doi: 10.1097/JSA.0000000000000202.
[22] F. H. Netter, *NETTER ATLAS of HUMAN ANATOMY*, 8th ed. 2022.
[23] "Anatomy & Physiology, Connexions Web site."
[24] A. Blanco Ortega *et al.*, "Biomechanics of the Upper Limbs: A Review in the Sports Combat Ambit Highlighting Wearable Sensors," *Sensors*, vol. 22, no. 13, p. 4905, Jun. 2022, doi: 10.3390/s22134905.
[25] U. K. Latif, Z. Gong, V. Nanjappan, and G. V. Georgiev, "DESIGNING FOR REHABILITATION MOVEMENT RECOGNITION AND MEASUREMENT IN VIRTUAL REALITY," *Proceedings of the Design Society*, vol. 3, pp. 1387–1396, Jul. 2023, doi: 10.1017/pds.2023.139.
[26] T. Nef and R. Riener, "Shoulder actuation mechanisms for arm rehabilitation exoskeletons," in *2008 2nd IEEE RAS & EMBS International Conference on Biomedical Robotics and Biomechatronics*, IEEE, Oct. 2008, pp. 862–868. doi: 10.1109/BIOROB.2008.4762794.
[27] A. M. Hill, A. M. J. Bull, A. L. Wallace, and G. R. Johnson, "Qualitative and quantitative descriptions of glenohumeral motion," *Gait Posture*, vol. 27, no. 2, pp. 177–188, Feb. 2008, doi: 10.1016/j.gaitpost.2007.04.008.
[28] W. Sahara, K. Sugamoto, M. Murai, H. Tanaka, and H. Yoshikawa, "The three-dimensional motions of glenohumeral joint under semi-loaded condition during arm abduction using vertically open MRI," *Clinical Biomechanics*, vol. 22, no. 3, pp. 304–312, Mar. 2007, doi: 10.1016/j.clinbiomech.2006.04.012.
[29] A. El Habachi, S. Duprey, L. Cheze, and R. Dumas, "A parallel mechanism of the shoulder—application to multi-body optimisation," *Multibody Syst Dyn*, vol. 33, no. 4, pp. 439–451, Apr. 2015, doi: 10.1007/s11044-014-9418-7.
[30] H. E. J. Veeger and F. C. T. van der Helm, "Shoulder function: The perfect compromise between mobility and stability," *J Biomech*, vol. 40, no. 10, pp. 2119–2129, Jan. 2007, doi: 10.1016/j.jbiomech.2006.10.016.
[31] C. Carignan, J. Tang, S. Roderick, and M. Naylor, "A Configuration-Space Approach to Controlling a Rehabilitation Arm Exoskeleton," in *2007 IEEE 10th International Conference on Rehabilitation Robotics*, IEEE, Jun. 2007, pp. 179–187. doi: 10.1109/ICORR.2007.4428425.

[32] Z. Li, Z. Huang, W. He, and C.-Y. Su, “Adaptive Impedance Control for an Upper Limb Robotic Exoskeleton Using Biological Signals,” *IEEE Transactions on Industrial Electronics*, vol. 64, no. 2, pp. 1664–1674, Feb. 2017, doi: 10.1109/TIE.2016.2538741.
[33] T. Nef, M. Guidali, and R. Riener, “ARMin III – Arm Therapy Exoskeleton with an Ergonomic Shoulder Actuation,” *Appl Bionics Biomech*, vol. 6, no. 2, pp. 127–142, Jan. 2009, doi: 10.1080/11762320902840179.
[34] E. Pennestrì, R. Stefanelli, P. P. Valentini, and L. Vita, “Virtual musculo-skeletal model for the biomechanical analysis of the upper limb,” *J Biomech*, vol. 40, no. 6, pp. 1350–1361, Jan. 2007, doi: 10.1016/j.jbiomech.2006.05.013.
[35] Y. Chen, G. Li, Y. Zhu, J. Zhao, and H. Cai, “Design of a 6-DOF upper limb rehabilitation exoskeleton with parallel actuated joints,” *Biomed Mater Eng*, vol. 24, no. 6, pp. 2527–2535, 2014, doi: 10.3233/BME-141067.
[36] P. Groshaw, “Hardiman | Arm Test, Hardiman | Prototype Project,” 1969.
[37] A. Voilque, J. Masood, JC. Fauroux, L. Sabourin, and O. Guezet, “Industrial Exoskeleton Technology: Classification, Structural Analysis, and Structural Complexity Indicator,” in *2019 Wearable Robotics Association Conference (WearRAcon)*, IEEE, Mar. 2019, pp. 13–20. doi: 10.1109/WEARRACON.2019.8719395.
[38] Siciliano and Khatib, Eds., *Springer Handbook of Robotics*. Springer.
[39] H. Kazerooni, “Human/robot interaction via the transfer of power and information signals,” in *Images of the Twenty-First Century. Proceedings of the Annual International Engineering in Medicine and Biology Society*, IEEE, 1989, pp. 908–909. doi: 10.1109/IEMBS.1989.96042.
[40] R. A. R. C. Gopura, D. S. V. Bandara, K. Kiguchi, and G. K. I. Mann, “Developments in hardware systems of active upper-limb exoskeleton robots: A review,” *Rob Auton Syst*, vol. 75, pp. 203–220, Jan. 2016, doi: 10.1016/j.robot.2015.10.001.
[41] V. S. Huang and J. W. Krakauer, “Robotic neurorehabilitation: a computational motor learning perspective,” *J Neuroeng Rehabil*, vol. 6, no. 1, p. 5, Dec. 2009, doi: 10.1186/1743-0003-6-5.
[42] “https://wearable-robotics.com.”
[43] E. Galofaro, E. D’Antonio, F. Patané, M. Casadio, and L. Masia, “Three-Dimensional Assessment of Upper Limb Proprioception via a Wearable Exoskeleton,” *Applied Sciences*, vol. 11, no. 6, p. 2615, Mar. 2021, doi: 10.3390/app11062615.
[44] M. P. de Looze, T. Bosch, F. Krause, K. S. Stadler, and L. W. O’Sullivan, “Exoskeletons for industrial application and their potential effects on physical work load,” *Ergonomics*, vol. 59, no. 5, pp. 671–681, May 2016, doi: 10.1080/00140139.2015.1081988.
[45] “agade-exoskeletons.com.”
[46] F. Casolo, S. Cinquemani, and M. Cocetta, “On active lower limb exoskeletons actuators,” in *2008 5th International Symposium on Mechatronics and Its Applications*, IEEE, May 2008, pp. 1–6. doi: 10.1109/ISMA.2008.4648796.
[47] M. A. Gull, S. Bai, and T. Bak, “A Review on Design of Upper Limb Exoskeletons,” *Robotics*, vol. 9, no. 1, p. 16, Mar. 2020, doi: 10.3390/robotics9010016.
[48] A. D. D. R. Carvalho, N. Karanth P, and V. Desai, “Characterization of pneumatic muscle actuators and their implementation on an elbow exoskeleton with a novel hinge design,” *Sensors and Actuators Reports*, vol. 4, p. 100109, Nov. 2022, doi: 10.1016/j.snr.2022.100109.
[49] Z. Li and S. Bai, “A novel revolute joint of variable stiffness with reconfigurability,” *Mech Mach Theory*, vol. 133, pp. 720–736, Mar. 2019, doi: 10.1016/j.mechmachtheory.2018.12.011.

[50] Z. Li, H. Xie, W. Li, and Z. Yao, “Proceeding of human exoskeleton technology and discussions on future research,” *Chinese Journal of Mechanical Engineering*, vol. 27, no. 3, pp. 437–447, May 2014, doi: 10.3901/CJME.2014.03.437.
[51] D. M. G. Preethichandra *et al.*, “Passive and Active Exoskeleton Solutions: Sensors, Actuators, Applications, and Recent Trends,” *Sensors*, vol. 24, no. 21, p. 7095, Nov. 2024, doi: 10.3390/s24217095.
[52] J. Theurel, K. Desbrosses, T. Roux, and A. Savescu, “Physiological consequences of using an upper limb exoskeleton during manual handling tasks,” *Appl Ergon*, vol. 67, pp. 211–217, Feb. 2018, doi: 10.1016/j.apergo.2017.10.008.
[53] D. J. Hyun, K. Bae, K. Kim, S. Nam, and D. Lee, “A light-weight passive upper arm assistive exoskeleton based on multi-linkage spring-energy dissipation mechanism for overhead tasks,” *Rob Auton Syst*, vol. 122, p. 103309, Dec. 2019, doi: 10.1016/j.robot.2019.103309.
[54] F. Daerden and D. Lefeber, “Pneumatic Artificial Muscles: actuators for robotics and automation,” 2002.
[55] A. L. Visan and N. Alexandrescu, “A Survey on the Evolution of Nonconventional Pneumatic Actuators,” *Adv Mat Res*, vol. 463–464, pp. 1069–1072, Feb. 2012, doi: 10.4028/www.scientific.net/AMR.463-464.1069.
[56] G. Andrikopoulos, G. Nikolakopoulos, and S. Manesis, “A Survey on Applications of Pneumatic Artificial Muscles,” 2011.
[57] D. G. Caldwell, G. A. Medrano-Cerda, and M. Goodwin, “Control of pneumatic muscle actuators,” *IEEE Control Syst*, vol. 15, no. 1, pp. 40–48, Feb. 1995, doi: 10.1109/37.341863.
[58] P. de Leva, “Adjustments to Zatsiorsky-Seluyanov’s segment inertia parameters,” *J Biomech*, vol. 29, no. 9, pp. 1223–1230, Sep. 1996, doi: 10.1016/0021-9290(95)00178-6.
[59] C.-P. Chou and B. Hannaford, “Measurement and modeling of McKibben Pneumatic Artificial Muscles,” 1996.
[60] B. Tondu and P. Lopez, “Modeling and control of McKibben artificial muscle robot actuators,” *IEEE Control Syst*, vol. 20, no. 2, pp. 15–38, Apr. 2000, doi: 10.1109/37.833638.
[61] M. Tóthová and J. Piteľ, “Numerical Approximation of Static Characteristics of McKibben Pneumatic Artificial Muscle,” *INTERNATIONAL JOURNAL OF MATHEMATICS AND COMPUTERS IN SIMULATION*, 2015.
[62] J. Sarosi, I. Biro, J. Nemeth, and L. Cveticanin, “Dynamic modeling of a pneumatic muscle actuator with two-direction motion,” *Mech Mach Theory*, vol. 85, pp. 25–34, Mar. 2015, doi: 10.1016/j.mechmachtheory.2014.11.006.
[63] J. SÁROSI and Z. FABULYA, “NEW FUNCTION APPROXIMATION FOR THE FORCE GENERATED BY FLUIDIC MUSCLE.”
[64] J. Sárosi, Z. Fabulya, -János Gyeviki, G. Keszthelyi-Szabó, and -Péter Szendrő, “INVESTIGATION OF ACCURACY OF THE NEWEST FUNCTION APPROXIMATION FOR THE FORCE GENERATED BY PNEUMATIC ARTIFICIAL MUSCLE.”
[65] J. Sárosi and Z. Fabulya, “MATHEMATICAL ANALYSIS OF THE FUNCTION APPROXIMATION FOR THE FORCE GENERATED BY PNEUMATIC ARTIFICIAL MUSCLE,” 2012.
[66] J. Piteľ and M. Tóthová, “Modelling of pneumatic muscle actuator using Hill’s model with different approximations of static characteristics of artificial muscle,” *MATEC Web of Conferences*, vol. 76, p. 02015, Oct. 2016, doi: 10.1051/matecconf/20167602015.

[67] “FESTO - DMSP Operating instructions.”
[68] M. Paterna, C. De Benedictis, and C. Ferraresi, “Preliminary Testing of a Passive Exoskeleton Prototype Based on McKibben Muscles,” *Machines*, vol. 12, no. 6, p. 388, Jun. 2024, doi: 10.3390/machines12060388.
[69] T. Graven-Nielsen, H. B. Vaegter, S. Finocchietti, G. Handberg, and L. Arendt-Nielsen, “Assessment of musculoskeletal pain sensitivity and temporal summation by cuff pressure algometry,” *Pain*, vol. 156, no. 11, pp. 2193–2202, Nov. 2015, doi: 10.1097/j.pain.0000000000000294.
[70] Ž. Kozinc, J. Babič, and N. Šarabon, “Human pressure tolerance and effects of different padding materials with implications for development of exoskeletons and similar devices,” *Appl Ergon*, vol. 93, p. 103379, May 2021, doi: 10.1016/j.apergo.2021.103379.
[71] M. Paterna, C. De Benedictis, and C. Ferraresi, “Effect of Joint Misalignment in Upper Limb Exoskeleton Based on McKibben Muscles,” in *Mechanisms and Machine Science*, Springer Science and Business Media B.V., 2024, pp. 35–42. doi: 10.1007/978-3-031-64569-3_5.